PNNL-12192
UC-2000

# Anoxic Plume Attenuation in a Fluctuating Water Table System: Impact of 100-D Area In Situ Redox Manipulation on Downgradient Dissolved Oxygen Concentrations

M. D. Williams
V. R. Vermeul
M. Oostrom
J. C. Evans
J. S. Fruchter
J. D. Istok[a]
M. D. Humphrey[a]
D. C. Lanigan
J. E. Szecsody
M.D. White
T. W. Wietsma
C. R. Cole

May 1999

Prepared for
the U.S. Department of Energy
under Contract DE-AC06-76RLO 1830

Pacific Northwest National Laboratory
Richland, Washington 99352

(a) Oregon State University, Corvallis, Oregon

## DISCLAIMER

# Summary

A treatability study is underway at the 100-D Area of the Hanford Site, 160 m from the Columbia River. The target contaminant for the treatability test is chromate (hexavalent chromium) in excess of 1,000 μg/L in groundwater. In Situ Redox Manipulation (ISRM) is an innovative treatment technology that establishes reducing conditions in an aquifer to treat redox-sensitive contaminants (e.g., hexavalent chromium, uranium, technetium, and chlorinated solvents) in groundwater. As a side effect, an anoxic plume is formed downgradient from the treatment zone. This report describes the results of a study on the fate of an anoxic groundwater plume in an unconfined oxidizing aquifer with a fluctuating water table.

The objective of the study is to predict dissolved oxygen concentrations in the groundwater near the Columbia River to assess the potential impact on aquatic organisms. The primary concern is the impact of the discharge of anoxic groundwater on these organisms. Because adequate time has not elapsed for sufficient monitoring since the start of the ISRM treatability study at 100-D Area, this study uses a combination of applied laboratory experiments and numerical modeling to predict downgradient dissolved oxygen concentrations from the site.

The intermediate-scale laboratory experiments on reoxygenation in a fluctuating water table such as that which exists in the ISRM treatment zone showed that anoxic water can be reoxygenated rapidly from water table fluctuations due to the entrapment of air bubbles containing atmospheric concentrations of oxygen. These rates were much greater than oxygen diffusion alone. The water within the zone of fluctuation was significantly reoxygenated within one week of daily water table raising and lowering.

The numerical model incorporated a fluctuating water table induced by the Columbia River along with air entrapment in the zone of fluctuation. The model also incorporated the effects of the groundwater mixing with river water (bank storage) near the river's edge. This model predicted 75 to 95 percent oxygen saturation at the river. Of those tested, air entrapment caused by water table fluctuations had the greatest impact on the attenuation of the dissolved oxygen concentrations discharging from the aquifer and should be reliable over a wide range of river stage fluctuations. Mixing processes in the riverbed (within 1 m of the river bottom) will further increase the oxygen saturation.

A newly installed well in the spring of 1999 will provide an additional downgradient well for water quality monitoring (including dissolved oxygen) and water table between the ISRM site and the Columbia River fluctuations to test some of the predictions, parameters, and assumptions in these simulations. Columbia River substrate porewater sampling tubes installed along the river shoreline downgradient of the site will also provide additional monitoring data in the future with the predicted arrival of groundwater from the ISRM site later in 1999 and 2000.

# Acknowledgments

This work was prepared with the support of the following contributors:

| | |
|---|---|
| DOE Headquarters: | Office of Science and Technology<br>Skip Chamberlain |
| Focus Area/Program: | Subsurface Contaminants Focus Area<br>James Wright |
| DOE Operations Office: | Richland Operations Office<br>Science and Technology Programs Division<br>John P. Neath, Technical Program Officer |
| Contractor: | Pacific Northwest National Laboratory<br>Environmental Science and Technology Environmental Technology Division<br>Rod K. Quinn, Manager |

# Contents

# Figures

## Tables

# 1.0 Introduction

This report describes the results of a study on the fate of an anoxic groundwater plume in an unconfined oxidizing aquifer with a fluctuating water table. An innovative remediation technology, In Situ Redox Manipulation (ISRM), which establishes reducing conditions in an aquifer to treat redox-sensitive contaminants (e.g., hexavalent chromium, uranium, technetium, and chlorinated solvents) in groundwater, has been applied at the 100-D Area at the Hanford Site. A side effect of the ISRM-established barrier is an anoxic plume that forms downgradient from the site. A treatability study is underway at the 100 D Area ISRM site (Williams et al. 1999), 160 m (525 ft) from the Columbia River, for the remediation of groundwater contaminated with hexavalent chromium in excess of 1,000 µg/L (see Figures 1.1 and 1.2).

The objective of this study is to predict dissolved oxygen concentrations in the groundwater near the Columbia River for assessing the potential impact on aquatic organisms. The primary concern is the effect of the discharge of anoxic groundwater on aquatic organisms in the river. Salmon redds have not been identified in the Columbia River downgradient of the current ISRM site (see Figure 1.2); a study has concluded that this portion of the Hanford Reach has low potential for fall Chinook to spawn, with less than 1 percent of the area suitable habitat based on measurements of depth, velocity, and substrate (Mueller and Geist 1998). So while the current site does not pose any potential threat to salmon habitat, gathering this information will help guide deployment of this remediation approach to other areas that may be sensitive.

## 1.1 Treatability Study Background

This study was conducted to support the ISRM treatability test (Williams et al. 1999; Fruchter et al. 1994, 1995, 1996, 1997) for chromate contamination in the aquifer on the west side of 100-D Area (100-HR-3 Operable Unit) of the Hanford Site (see Figures 1.1 and 1.2). ISRM is an innovative permeable barrier technology for treatment of redox-sensitive groundwater contaminants. The technology involves injecting into the aquifer a chemical reducing reagent, sodium dithionite, which reduces the naturally occurring Fe(III) in the aquifer sediments to Fe(II). Following a short reaction period (days), the reaction products and residual chemicals are pumped out of the aquifer, leaving behind a fixed zone of Fe(II) for treating redox-sensitive contaminants (e.g., chromate, chlorinated solvents, uranium, and technetium) that migrate through the zone. In addition to removing the redox-sensitive contaminants from the groundwater, the Fe(II) in the treatment zone can also react with other oxidizing species in the groundwater, notably, dissolved oxygen. In most sites considered for application of the ISRM technology in oxidizing aquifers, the oxidizing capacity of the dissolved oxygen greatly exceeds the Fe(II) consumed in the treatment for the target contaminant, thus primarily determining the longevity of the reduced zone.

A 56-m (150-ft)-long ISRM zone was installed at the 100-D Area in 1998 (Figure 1.2) to determine the feasibility and performance of ISRM for remediating chromate-contaminated groundwater. The site is 160 m (525 ft) from the Columbia River. Prior to the test (and upgradient of the test site), the groundwater was generally saturated with dissolved oxygen (7 to 9 mg/L at approximately 20°C). Following the test, dissolved oxygen concentrations in the wells within the treatment zone were 0.0 mg/L. Nearby wells downgradient from the ISRM zone

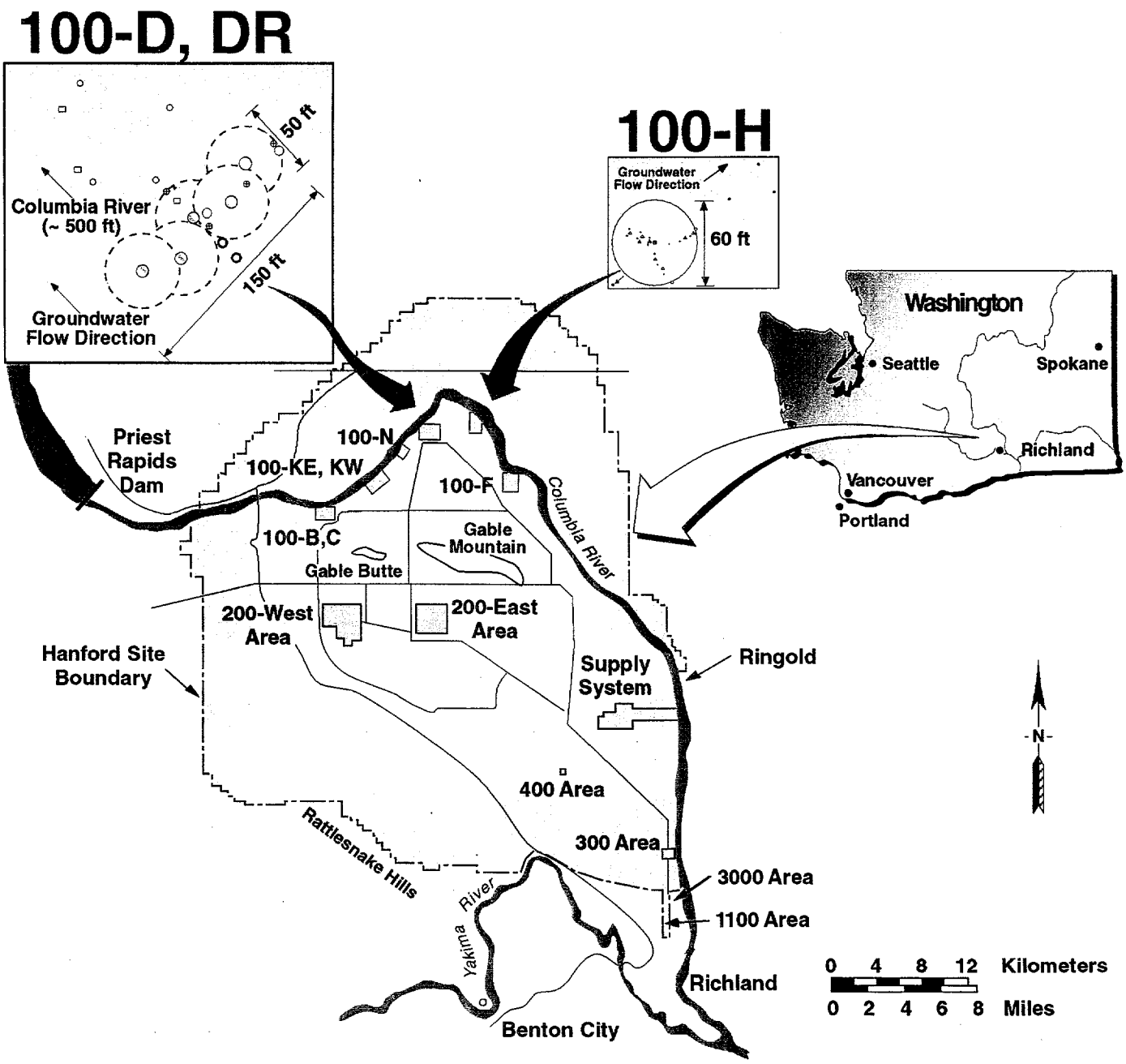


**Figure 1.1.** Location of the In Situ Redox Manipulation 100-H Area Proof-of-Principle Test Site and 100-D Area Treatability Test Site

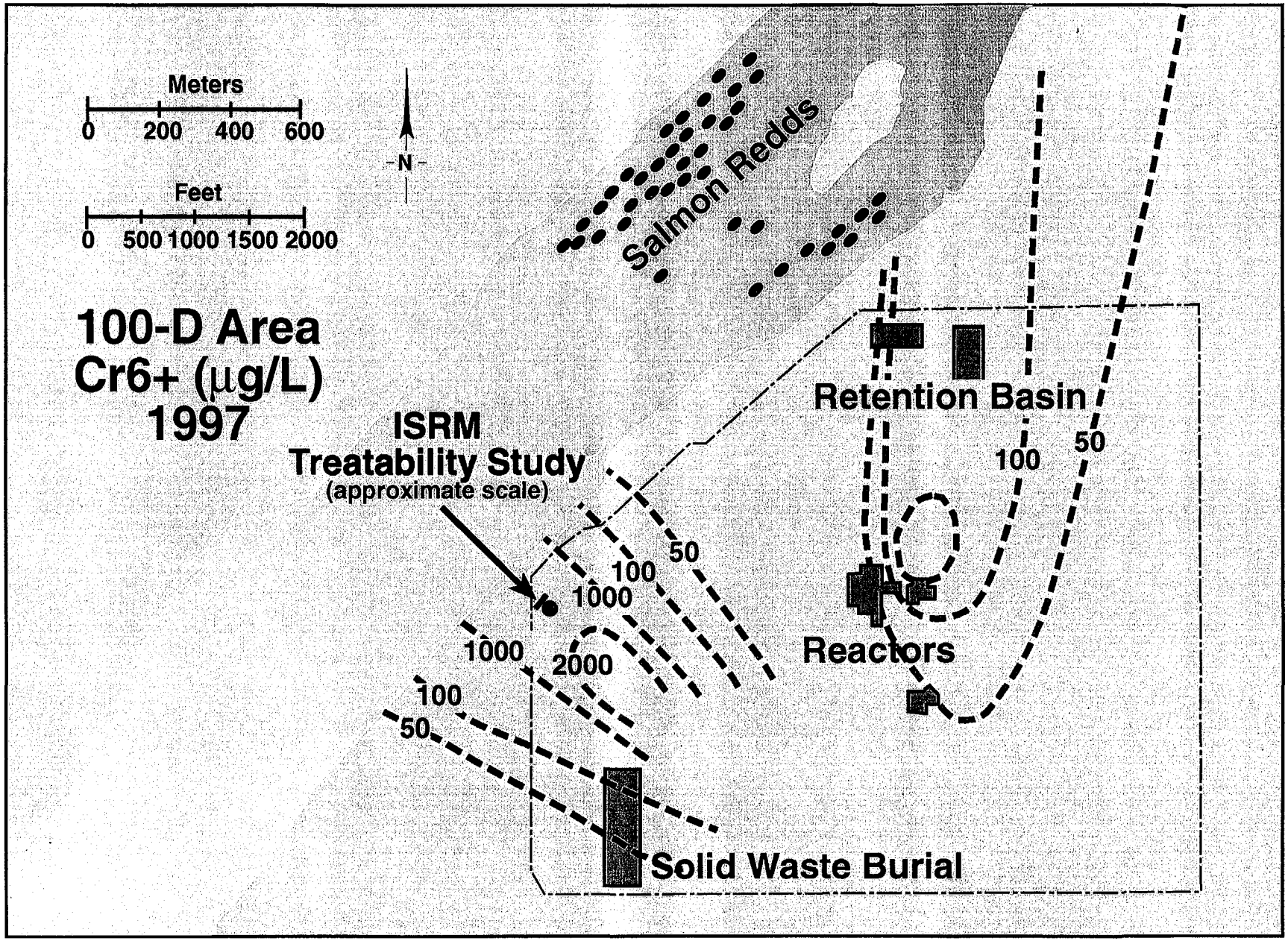


**Figure 1.2.** 100-D Area $Cr^{6+}$ Groundwater Concentrations (µg/L) for 1997

(within 27 m [100 ft]) have shown significant reductions in dissolved oxygen concentrations. Section 2 contains a more detailed description of the ISRM site and the dissolved oxygen monitoring results at the test site.
\

## 1.2 Processes Important in Re-Oxygenation

The conceptual diagram in Figure 1.3 illustrates the processes that may be important in the attenuation of an anoxic plume in the hydrogeologic setting of the 100-D Area ISRM treatability test site. These processes include the following:

- oxygen diffusion from the vadose zone above the unconfined aquifer and the aquitard below
- recharge of oxygenated water
- air entrapment from within the zone of the fluctuating water table
- trapped air bubbles below the water table
- creation of a mixing zone from bank storage (e.g., oxygenated river water entering the aquifer during periods of relatively high river stage).

One of the most important factors controlling the hydrology of the unconfined aquifer of the Hanford Site near the Columbia River (within ~305 m [1000 ft]) is the large variation in river stage from the operation of hydroelectric dams. These result in large daily, weekly, and seasonal variations in river stage (up to 2 m daily and 4 m seasonally) for meeting power demands, flood control, irrigation, and salmon management. Figure 1.4, a cross-section through the site to the Columbia River, depicts the connection between the upper unconfined aquifer and the river. The water table elevation and thickness increased by 1.5 m (5 ft), and the hydraulic gradient direction was reversed (moving away from the river) during an extreme flood event in the spring of 1997. Water table variations at the site during a more normal year (e.g., 1998) were +/-0.03 m (0.1 ft).

Processes within the river and in the uppermost portion of the river bottom (1 m), although important in understanding the ultimate concentrations aquatic organisms are exposed to, were outside the scope of this study. These processes include mixing of discharging groundwater within the river, turbulent mixing of river water at the bottom of the river channel, and the down-stream flow of river water within the riverbed (Hyporheic Zone). In addition, the shallowest river substrate porewater samplers that were installed were 1 m below the river bottom. The results of the modeling and analysis presented here could be coupled with a river model to quantify these processes that occur closer to the river channel.

## 1.3 Study Approach and Scope

With the ISRM 150-ft permeable treatment zone installed, direct measurements of dissolved oxygen in the aquifer downgradient of the site along the path toward the Columbia River can provide the most direct measure of attenuation of the anoxic plume. Due to the distances and groundwater velocities (~1 ft/day) involved, the full impact of the test on the river will not occur until late 1999 or 2000. In addition, the longevity of the ISRM zone at the site (23 +/- 6 years) may result in impacts not seen in the initial arrival times. Therefore, we developed a predictive model to investigate this issue at this time.

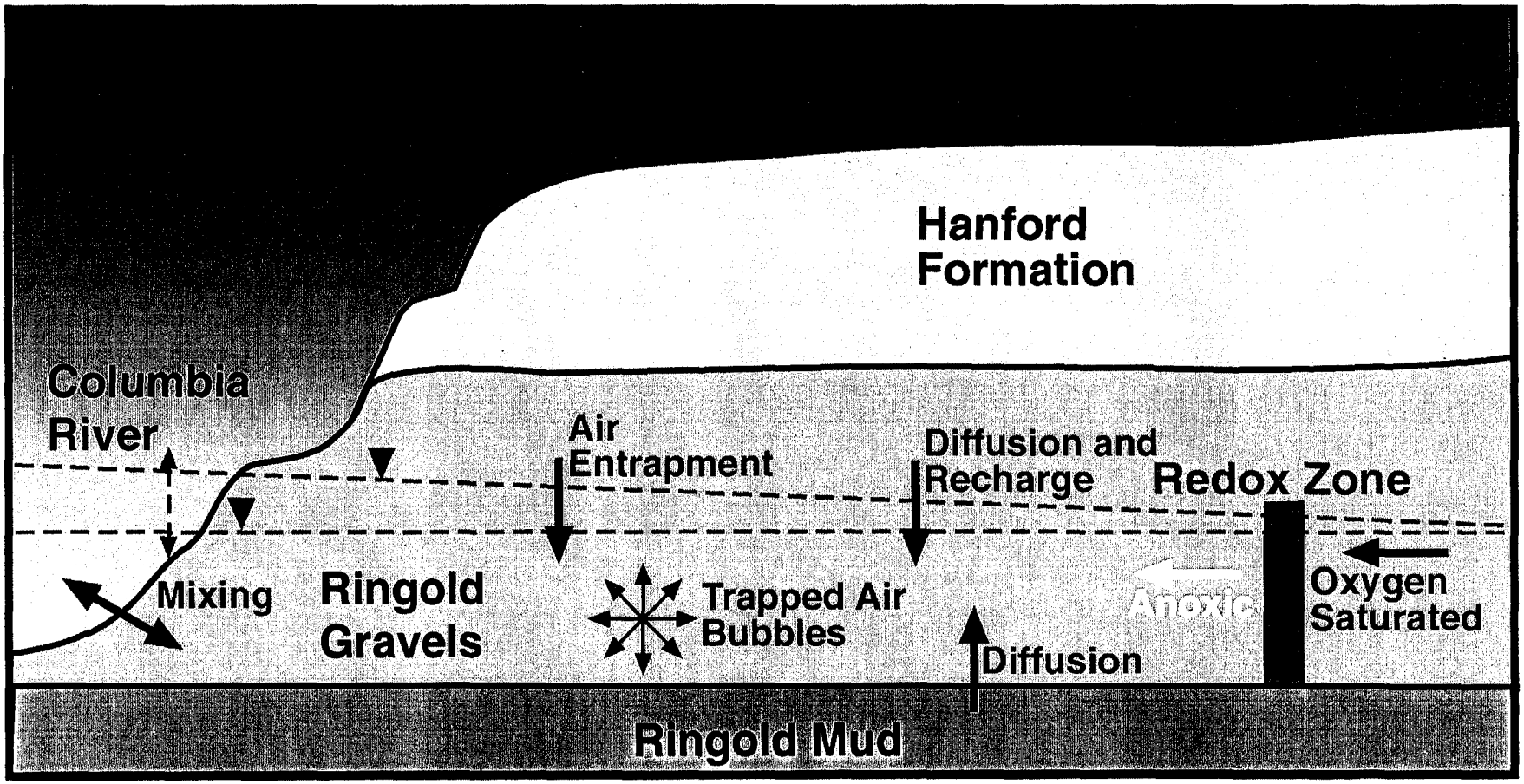


**Figure 1.3.** Conceptual Diagram of Reoxygenation Processes

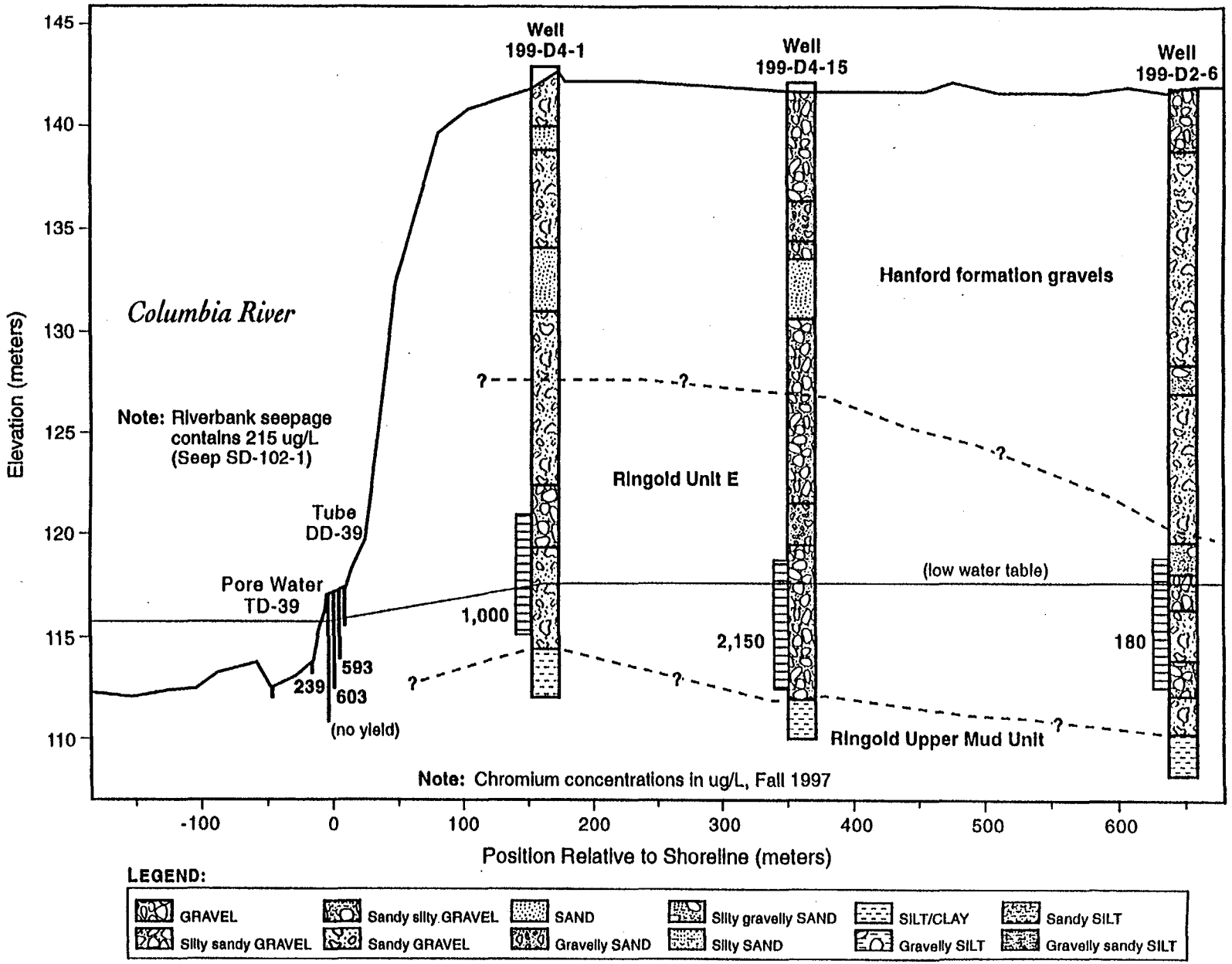


**Figure 1.4.** Geologic Cross-Section and Hexavalent Chromium Concentrations on the West Side of 100-D Area (from Peterson et al. 1998). The ISRM Treatability Site is at Well 199-D4-1.

Groundwater sampling tubes were installed in the substrate of the river downgradient of the site for measuring the effect of the site on water quality. An additional downgradient monitoring well will be installed between the ISRM site and the river in June 1999 to determine water quality at distances farther downgradient from the test than the existing monitoring wells.

The objective of this study is to investigate and quantify the processes identified for reoxygenation (Figure 1.3). The data will be incorporated into a predictive numerical model to determine their impact on the anoxic plume under the conditions at the site. Two areas were identified that required additional information, the determination of trapped air bubbles below the water table and the influence of air entrapment from a fluctuating water table. A dissolved gas tracer test was conducted at the site to help determine the existence and amount of trapped air bubbles in the aquifer (below the water table). Laboratory experiments were conducted to investigate the influence of air entrapment from a fluctuating water table.

This report contains the following:

- Site description and results of the current groundwater monitoring of dissolved oxygen at the 100-D Area ISRM site and from a set of Columbia River substrate porewater sampling tubes (Section 2)
- Description and results of intermediate-scale experiments to study the mechanism of air entrapment and subsequent reoxygenation from a fluctuating water table (Section 3)
- Description and results of dissolved gas tracer tests for characterization of trapped air bubbles below the water table (Section 4)
- Development and results of numerical models used for prediction (Section 5)
- Summary and conclusions (Section 6)
- Cited references (Section 7).

# 2.0 Site Description and Dissolved Oxygen Monitoring

The specific locations of the 100-D Area ISRM treatability test site and surveyed wells, at various scales, are shown in Figures 2.1 to 2.3. For this treatability study, a series of wells at the site (see Figure 2.4) was used to inject and withdraw a chemical reagent consisting of sodium dithionite and potassium carbonate/bicarbonate pH buffers to reduce the Fe(III) to Fe(II) in the aquifer sediments. The Fe(II) in the aquifer sediments then treats the redox-sensitive groundwater contaminants (e.g., chromate) migrating through this reduced zone. The six injection wells shown in Figure 2.4 created overlapping cylindrical reduced zones approximately 56 m (150 ft) long and 15 m (50 ft) wide to intercept a portion of the chromate-contaminated groundwater. The site is 160 m (525 ft) from the Columbia River. The dithionite injection/withdrawal operations were started in September 1997 and completed in July 1998.

Other wells at the site, shown in Figures 2.3 and 2.4, were installed for monitoring the performance of the treatment zone and to assess its downgradient effects on groundwater chemistry. Prior to the test, groundwater at the site had concentrations of hexavalent chromium ($Cr^{6+}$) exceeding 1000 µg/L. Following the ISRM test, concentrations of $Cr^{6+}$ were below the detection limit (7 µg/L) in the injection wells with concentrations in the downgradient wells continuing to drop as the treated groundwater migrates downgradient from the injection area.

To assess the impact of the ISRM treatment zone on the groundwater quality, groundwater in the wells at the site are monitored for chromate, dissolved oxygen, pH, electrical conductivity, anions (e.g., sulfate and nitrate), and trace metals. The farthest downgradient well from the ISRM reduced zone is D4-6, at a distance of 27 meters (90 ft). An additional monitoring well will be installed in June 1999 between the site and the Columbia River along the mean groundwater flow direction (see location on Figure 2.2), 91 m (300 ft) downgradient from the site and 73 m (240 ft) feet from the river. This well was installed specifically for monitoring dissolved oxygen concentrations farther downgradient of the ISRM site and closer to the river.

In addition to the monitoring wells, multilevel Columbia River substrate porewater sampling tubes (CRSPST) have also been installed along the river downgradient of the ISRM site (see Figure 2.2 for locations) at depths 1 to 5 m below the river bottom. Water samples collected from these tubes are analyzed for chromate, dissolved oxygen, pH, electrical conductivity, and anions. A full description of the results of this monitoring is provided in Williams et al. (1999).

## 2.1 Hydrogeologic Setting

This section focuses on the hydrogeologic description of the site, dissolved oxygen monitoring, and the impact on water levels at the site from the Columbia River. The general hydrogeologic setting of the 100-HR-3 Operable Unit (encompassing the 100-D and 100-H Areas) is described in Lindsey and Jaeger (1993). Characterization activities of the uppermost unconfined aquifer performed during drilling of the wells at the ISRM site conform to the generalized setting for the 100-D and were similar to the cross-section shown in Figure 1.4. Specifically, the unconfined aquifer at the ISRM test site is within the E-gravel unit of the Ringold Formation. The bottom

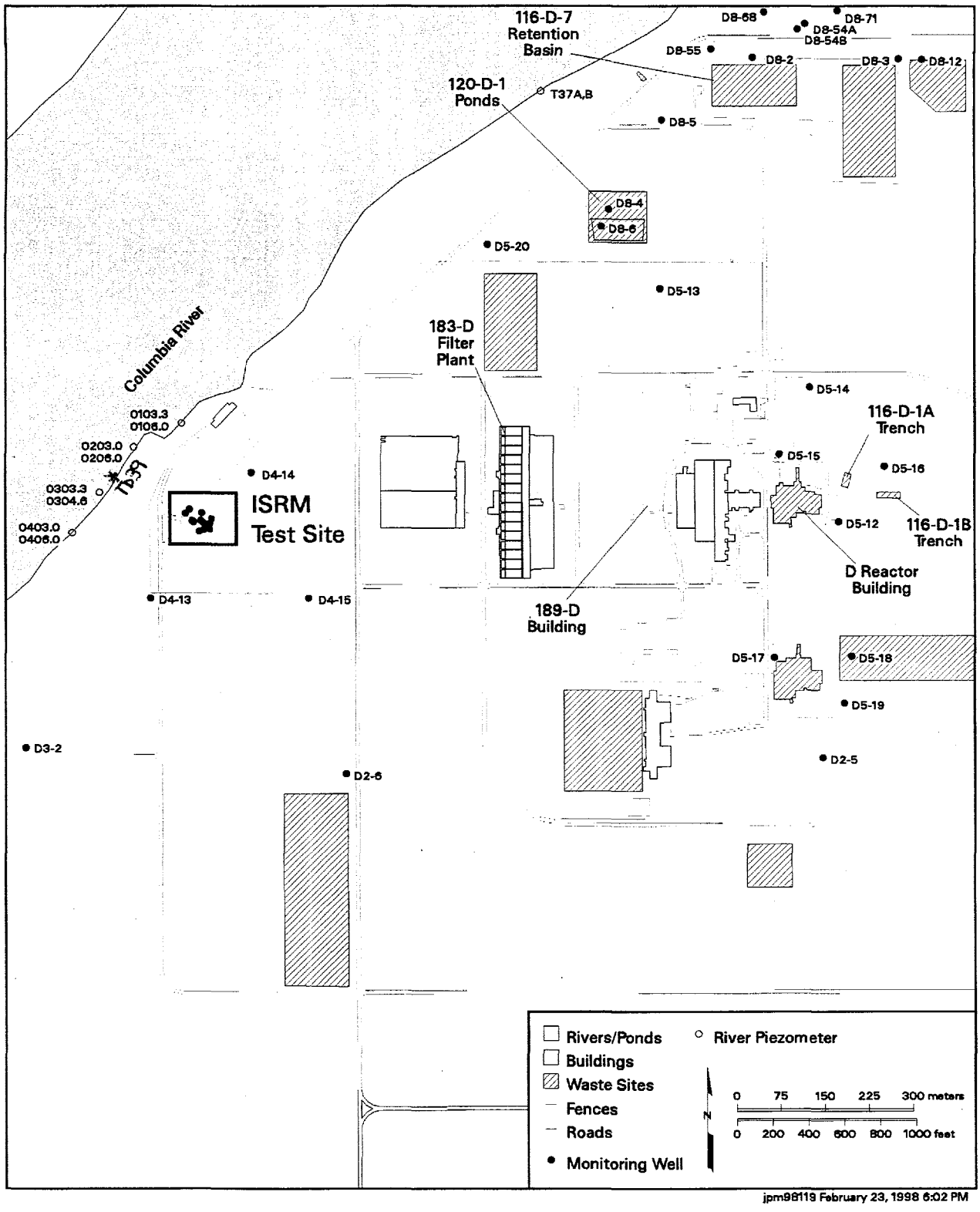


**Figure 2.1.** Location of ISRM Test Site and Wells at 100-D Area

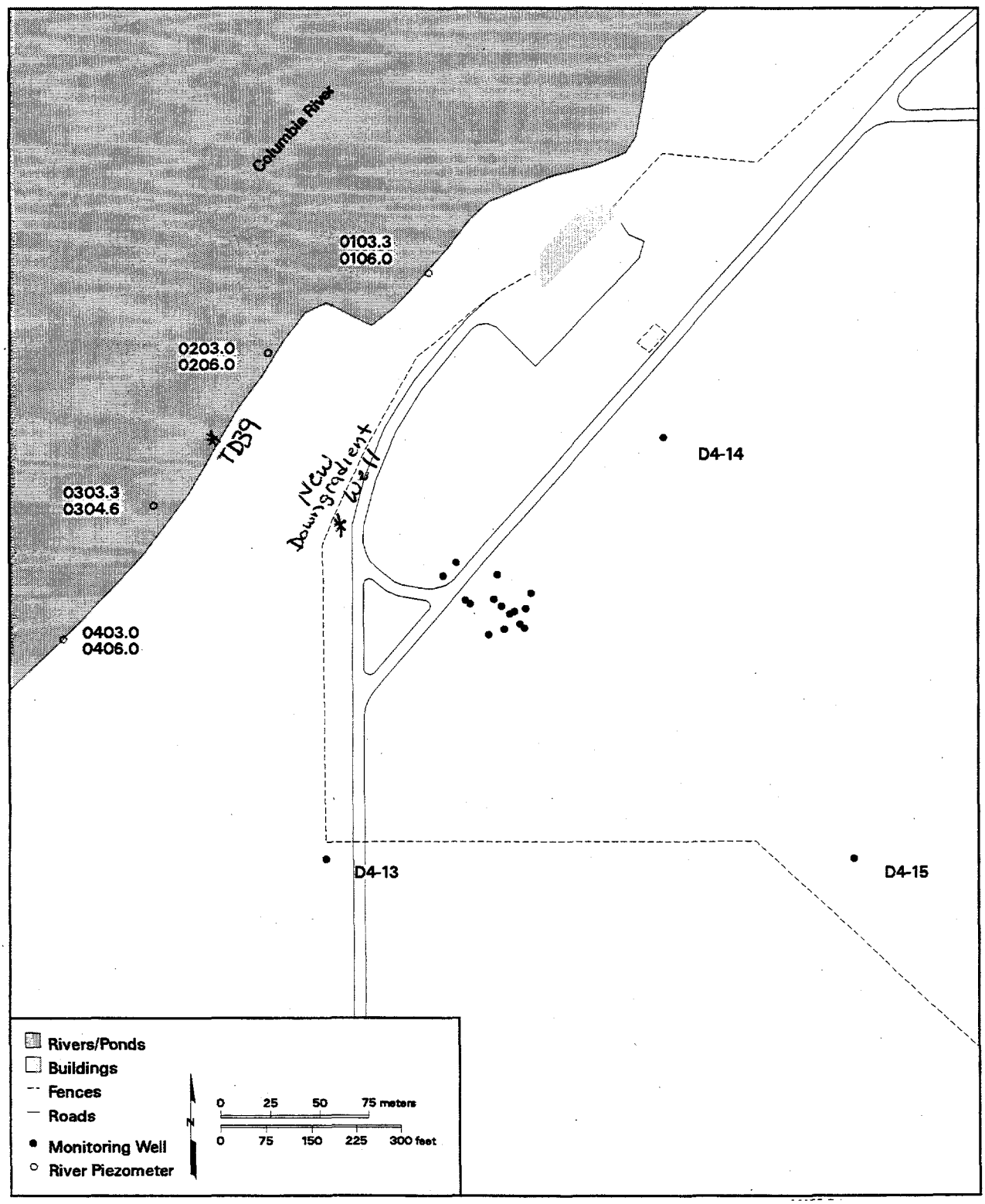


**Figure 2.2.** Location of Wells and Columbia River Substrate Porewater Samplers Surrounding the ISRM Site at 100-D Area

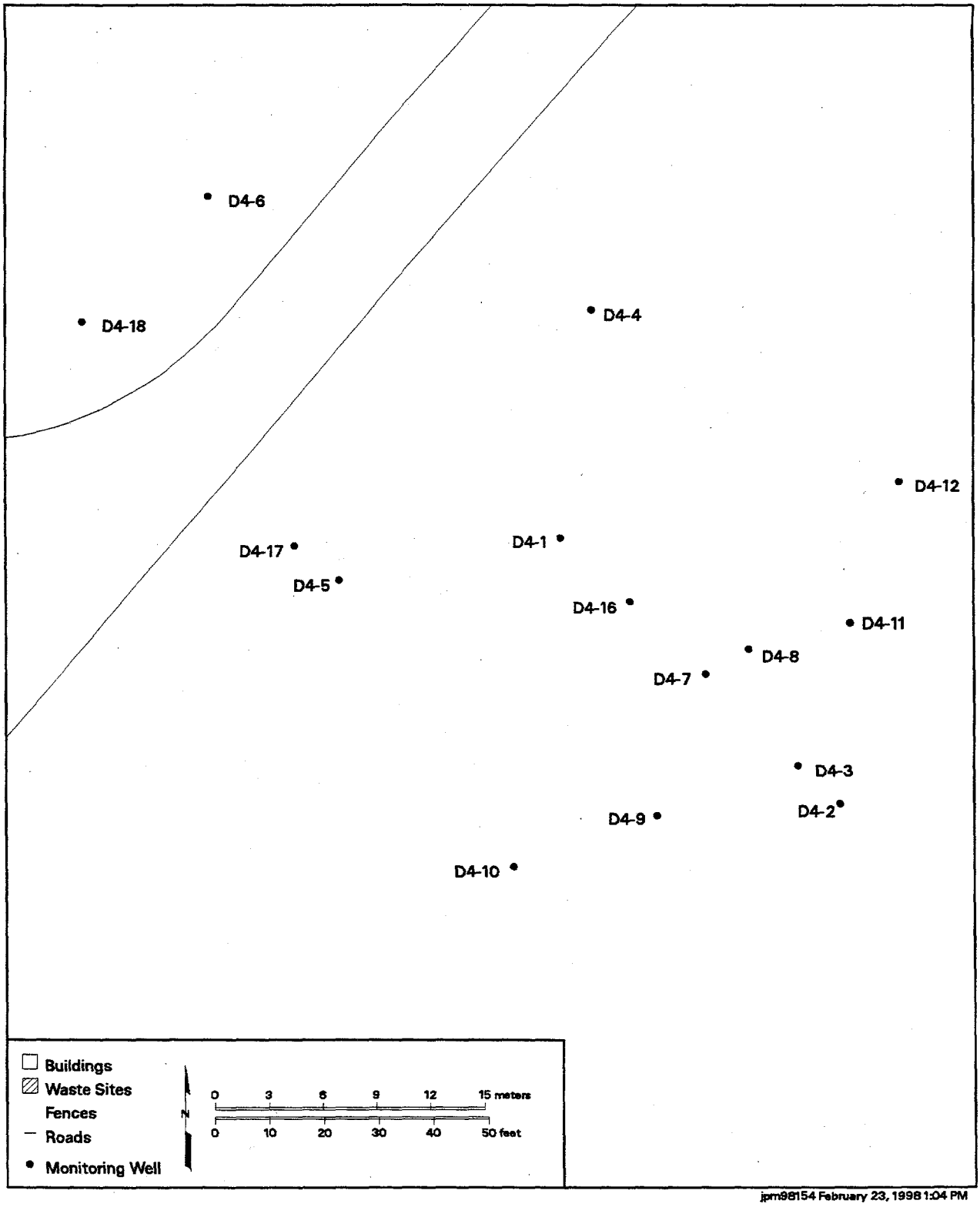


**Figure 2.3.** Wells (from survey data) at 100-D Area ISRM Treatability Test Site

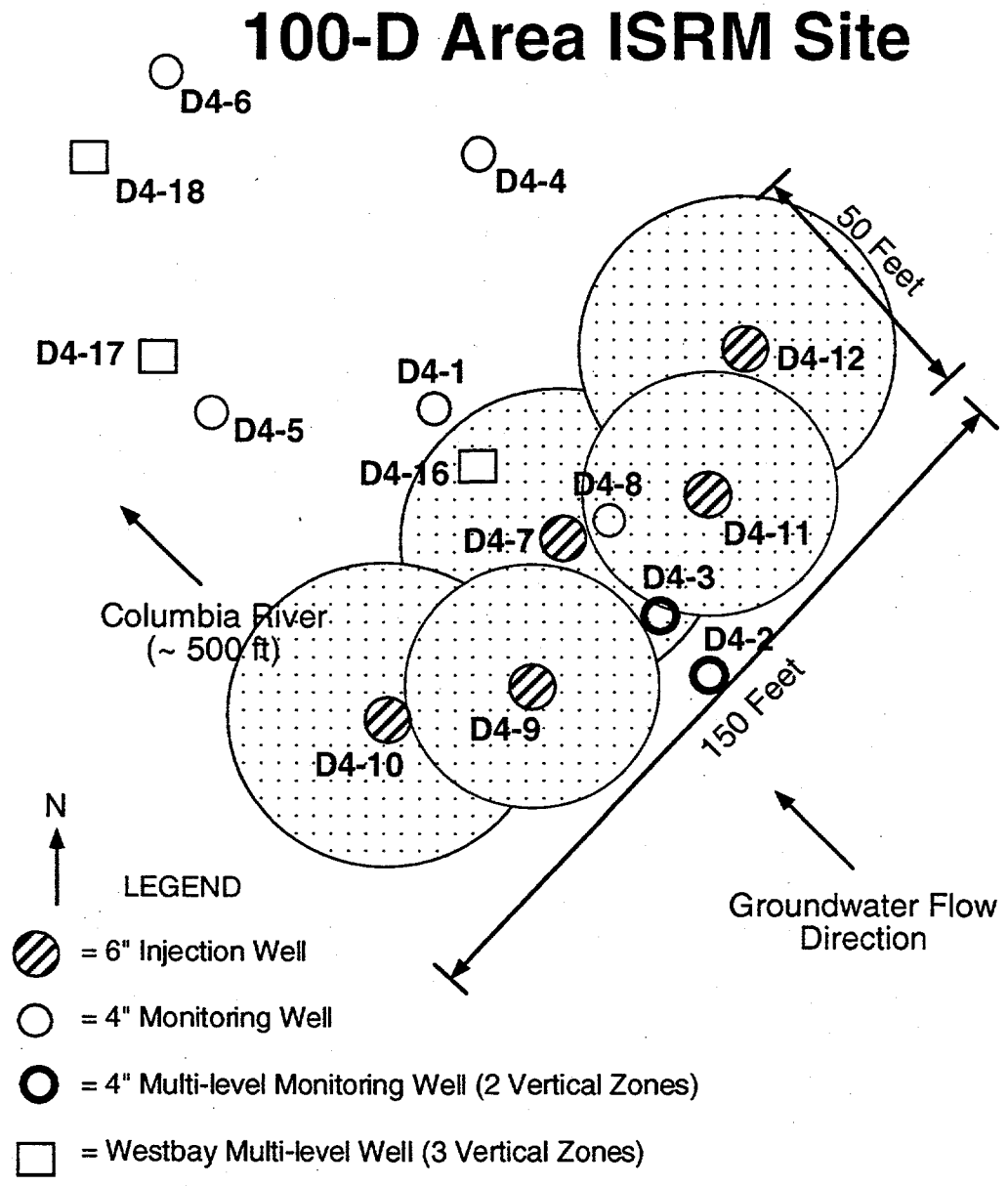


**Figure 2.4.** Emplacement Strategy and Well Diagram for the 100-D Area In Situ Redox Manipulation Treatability Test

of the unconfined aquifer is composed of a Ringold mud unit (overbank deposits and paleosols). Deviations in the elevation of the confining unit bounding the bottom of the unconfined aquifer were less than two feet during the drilling of the 15 wells at the site. The elevation of the mud unit also corresponds to the low permeability unit at the river inferred by the "no-yield" zone at a 20-ft depth for the river substrate porewater sampling tube (TD-39 shown in Figure 1.4). The unconfined aquifer thickness at the test site is 4.6 m (15 ft) during normal river stage of the Columbia River.

## 2.2 Groundwater Flow Direction

Since field activities at the ISRM treatability test site were initiated in the spring of 1997, water levels in site monitoring wells have been routinely monitored to determine the hydraulic gradient, groundwater flow direction, and the variability in these parameters over the time scale of the treatability test. Water-level measurements, along with horizontal and vertical survey data for each well site location, were used to estimate the local hydraulic gradient and flow direction.

The estimated groundwater flow velocities shown in Figure 2.5 are based on measured hydraulic gradients, average hydraulic conductivity of 54 ft/day obtained from hydraulic tests conducted in site monitoring wells, and average sediment porosity of 0.14 obtained from analysis of sediment core collected while installing monitoring wells. As indicated, groundwater typically flows to the west-northwest at about 1 ft/day. The deviation from this typical flow direction during the first three monitoring events (June 4, August 21, and September 8, 1997) is associated with recovery from historically high Columbia River flows during the spring of 1997. Water levels in the wells dropped approximately 5 ft from the time of installation (spring/ summer 1997) to the fall of 1997, resulting in a change in aquifer thickness from 20 to 15 ft.

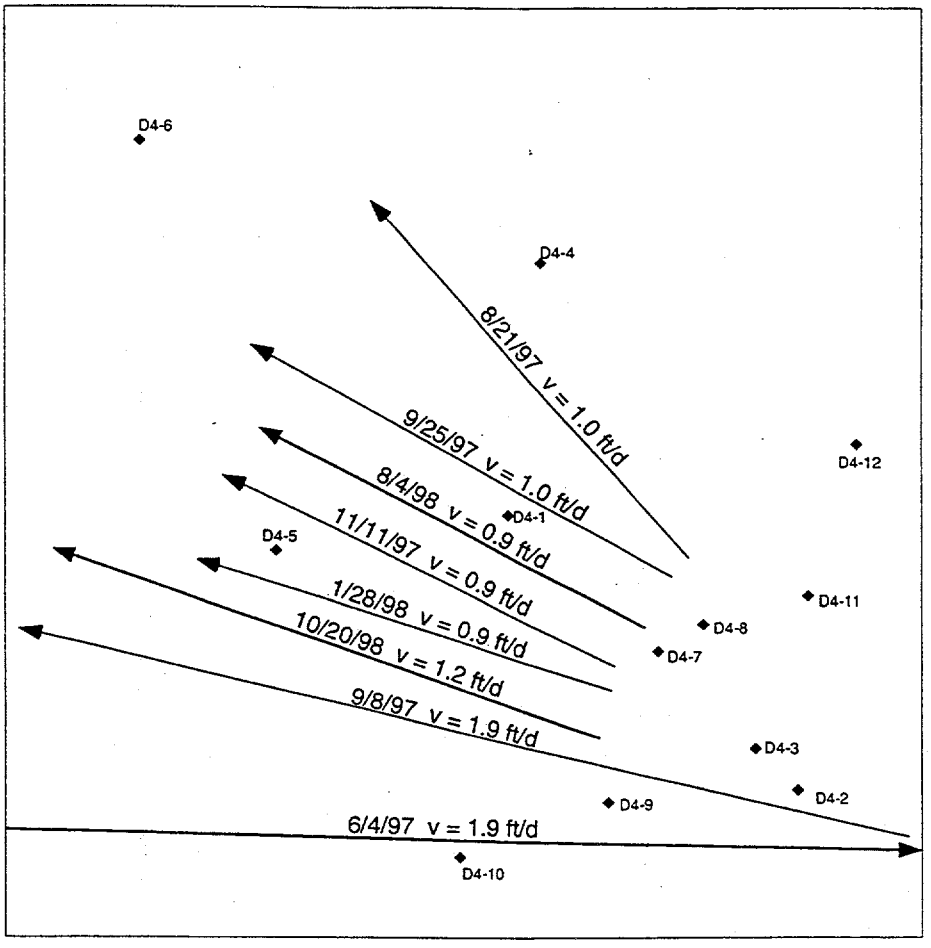


**Figure 2.5.** Groundwater Flow Magnitude and Direction from Water Level Measurements. Groundwater velocity calculation assumes K = 54 ft/d and n = 0.14.

## 2.3 Dissolved Oxygen Monitoring

Baseline dissolved oxygen measurements at the site are shown in Figure 2.6. Although variability exists, groundwater in the standard wells at the site prior to the test can be considered saturated (relative to atmospheric concentrations of oxygen) with an average dissolved oxygen concentration of 8.23 mg/L and a range of 7.14 to 9.03 mg/L. Dissolved oxygen concentrations are temperature dependent, as shown in Table 2.1. Although all sample tubing running between the wellhead and the field trailer was insulated, some of the temperature variations may have been caused by differences in heat gain associated with variable surface sample tubing lengths. Temperature measurements during the baseline data shown in Figure 2.6 ranged from 17.3 to 22.6°C. During winter months, groundwater sampling temperatures range from 16 to 17°C.

**Table 2.1.** Solubility of Oxygen in Water

| Temperature (°C) | Dissolved Oxygen Concentration (mg/L) (Yellowstone Instruments, Inc.) |
|---|---|
| 15 | 10.2 |
| 17 | 9.7 |
| 20 | 9.2 |
| 25 | 8.4 |

The one multilevel Westbay well (D4-16) shown in Figure 2.4 had significantly lower dissolved oxygen concentrations that were related to the small volume of water purged from this well during its development (it was installed less than two months before taking the sampling data shown in Figure 2.6). Hexavalent chromium concentrations were also low. These effects have been noticed in groundwater samples collected from newly installed wells. Crushing and exposing of fresh mineral surfaces during drilling creates a temporary negative Eh condition near the wellbore, which reacts with dissolved oxygen and hexavalent chromium in the groundwater. Elevated manganese levels have also been detected in newly installed wells at the 100-H Area ISRM site. Development and purging of Westbay wells is limited due to the low volume groundwater samplers (1-L bottles). Two additional Westbay wells (D4-17 and D4-18) were installed at the site following the first dithionite injection/withdrawal test for additional downgradient monitoring, as shown in Figures 2.3 and 2.4. Dissolved oxygen measurements from the Westbay wells are also influenced by a small headspace in the Westbay sampler, which contains air that biases the measurements. Dissolved oxygen measurements from the Westbay wells are difficult to compare with dissolved oxygen measurements made from the standard wells, which have variable-speed submersible pumps.

Figures 2.7, 2.8, and 2.9 show post-emplacement dissolved oxygen concentrations at the site; the groundwater is anoxic within the treatment zone. Dissolved oxygen concentrations in the downgradient wells dropped significantly by September 1998 and continued to show a drop in the December 1998 and April 1999 sampling events. D4-6, the farthest downgradient well, was at approximately 40 percent of the average baseline concentrations by the December sampling event and 20 percent by April 1999. Relatively high dissolved oxygen concentrations in well

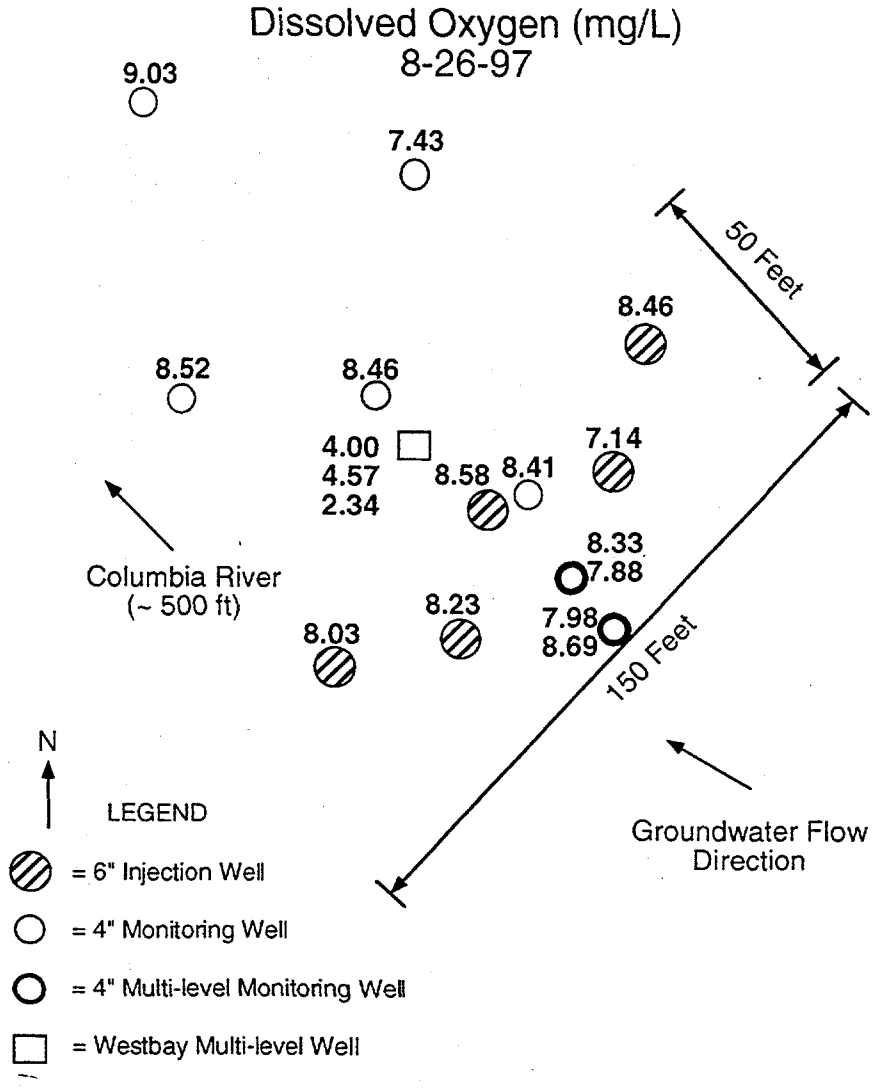


**Figure 2.6.** Baseline Dissolved Oxygen Concentrations at the 100-D Area ISRM Site

D4-4 are related to changes in groundwater flow direction. D4-4 is not directly downgradient of the 56-m (150 ft)-wide reduced zone based on the average groundwater flow directions of the site, although it may be influenced by some end effects (hexavalent chromium concentrations at this well are also relatively high compared with the other downgradient wells).

## 2.3 Columbia River Porewater Sampling Tubes

A series of sampling tubes was installed in the substrate of the Columbia River (see Figures 2.1 and 2.2) to monitor the groundwater entering the river and determine any impact from the test on the water quality. Four pairs of sampling tubes were installed about 300 ft apart in the river. Each pair includes a shallow (~1-m [3-ft] depth) and a deep (~2-m [6-ft] depth) monitoring interval. In addition to the sampling tubes installed for the ISRM test, an existing set of multilevel sampling tubes (TD-39, located between 0203.0 and 0303.3) is monitored as part of this test. Details on the installation of sampling tubes are described in Peterson et al. (1998).

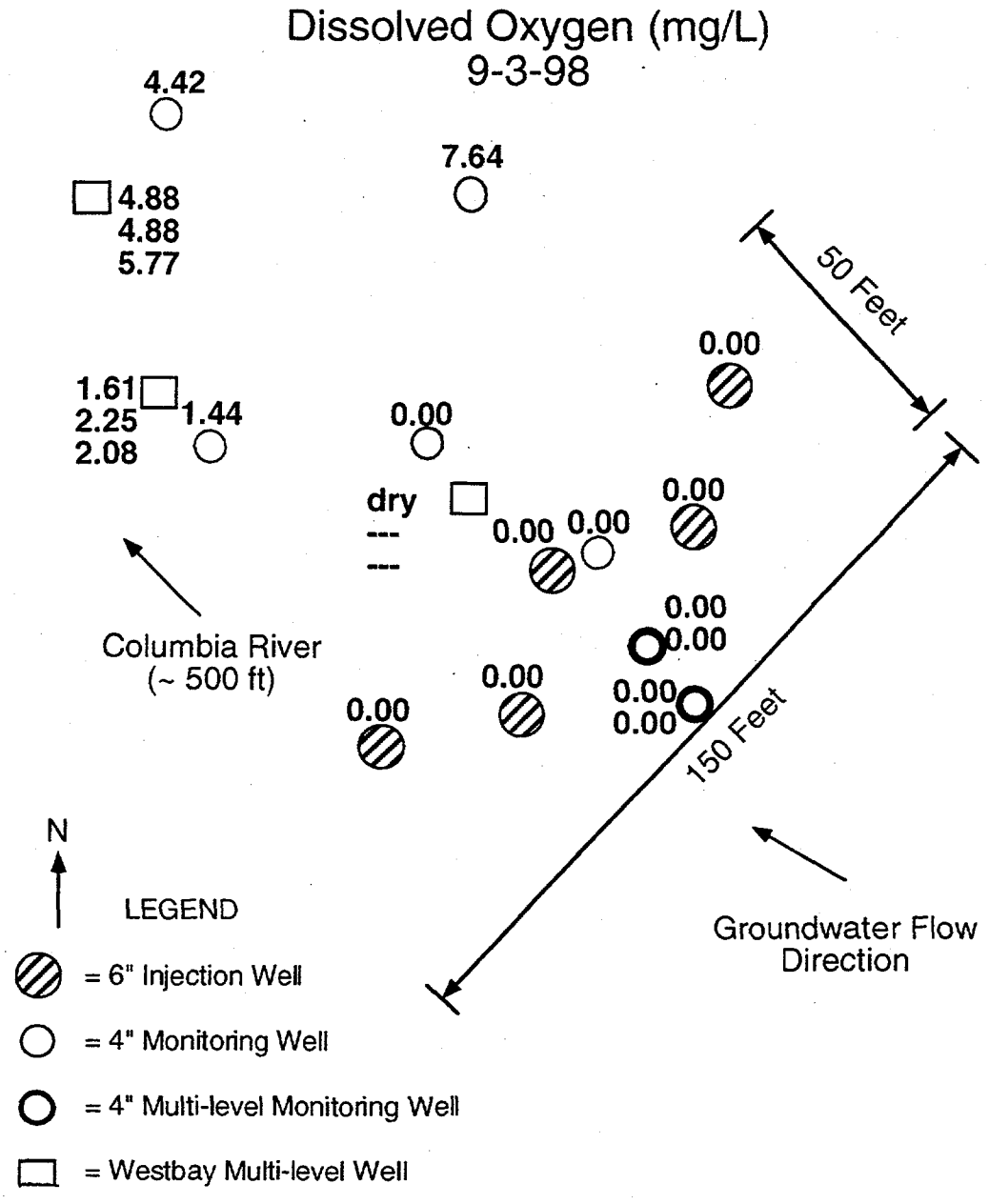


**Figure 2.7.** Post-Emplacement Dissolved Oxygen Concentrations at 100-D ISRM Site, September 3, 1998

A portable peristaltic pump is used to collect water samples from the sampling tubes. Electrical conductivity (EC), pH, and dissolved oxygen are measured in the field using electrodes during purging of the tubes. Water samples are collected for chromate and anion analysis once the electrode values are stabilized and recorded (purge time varied from five to 15 minutes based on length of tubing).

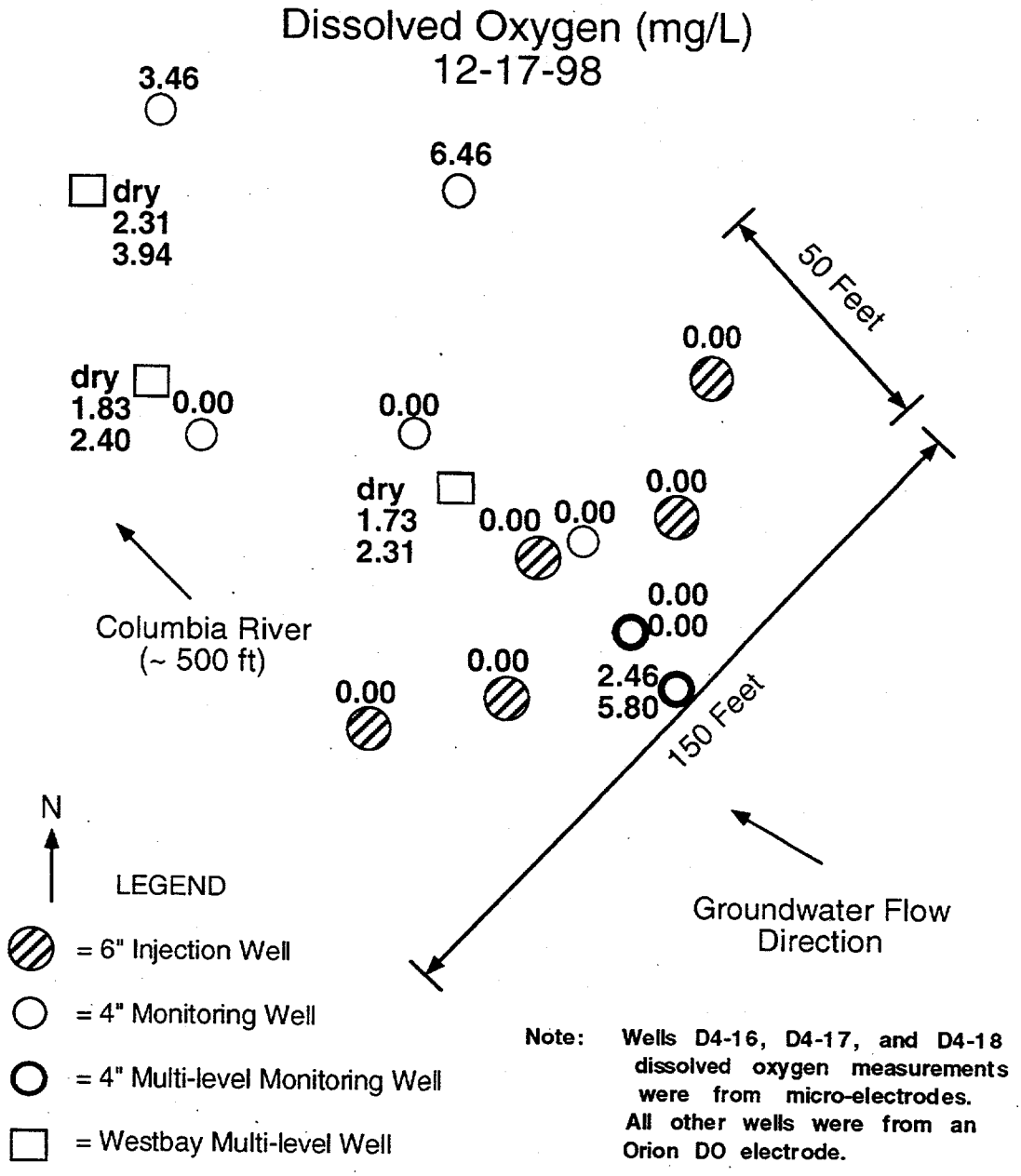


**Figure 2.8.** Post-Emplacement Dissolved Oxygen Concentrations at the 100-D ISRM Site, December 17, 1998

The electrical conductivity, $Cr^{6+}$, and dissolved oxygen measurements from sampling of the 100-D Area ISRM Columbia River porewater sampling tubes are plotted in Figure 2.10. ISRM porewater sampling tubes (Redox-0103.3, 0106.0, 0203.0, 0206.0, 0303.3, 0304.6, 0403.0, and 0406.0) were installed in November and December 1997, after the D4-7 dithionite injection/ withdrawal test. Four pairs of sampling tubes were installed at four locations along the river

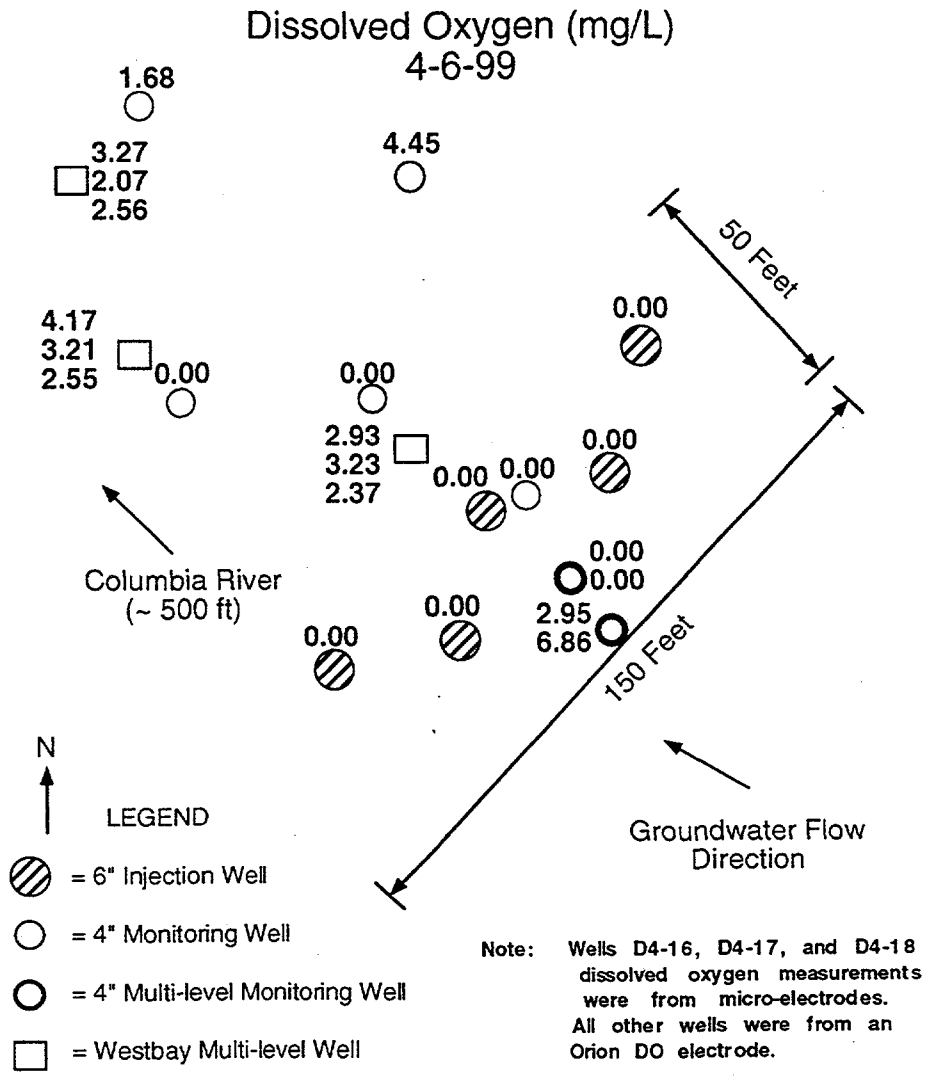


**Figure 2.9**. Post-Emplacement Dissolved Oxygen Concentrations at 100-D ISRM Site, April 6, 1999

downgradient from the ISRM site with two sampling depths each (the last two digits of the ID are the sampling depths). The TD-39 sampling tubes were installed prior to the ISRM emplacement (Peterson et al. 1998).

Water samples collected from the sampling tubes are a mixture of both river water and groundwater. The contribution of each source to the sample is related to the river stage and aquifer pressures at the time of sampling. Samples collected at high river stage are dominated by river water. Because the river water and groundwater have distinct ranges of electrical conductivity (river water ~150 microS/cm$^2$ and groundwater ~600 microS/cm$^2$), the electrical conductivity can be used to distinguish the relative contribution of each (see mixing curves in Peterson

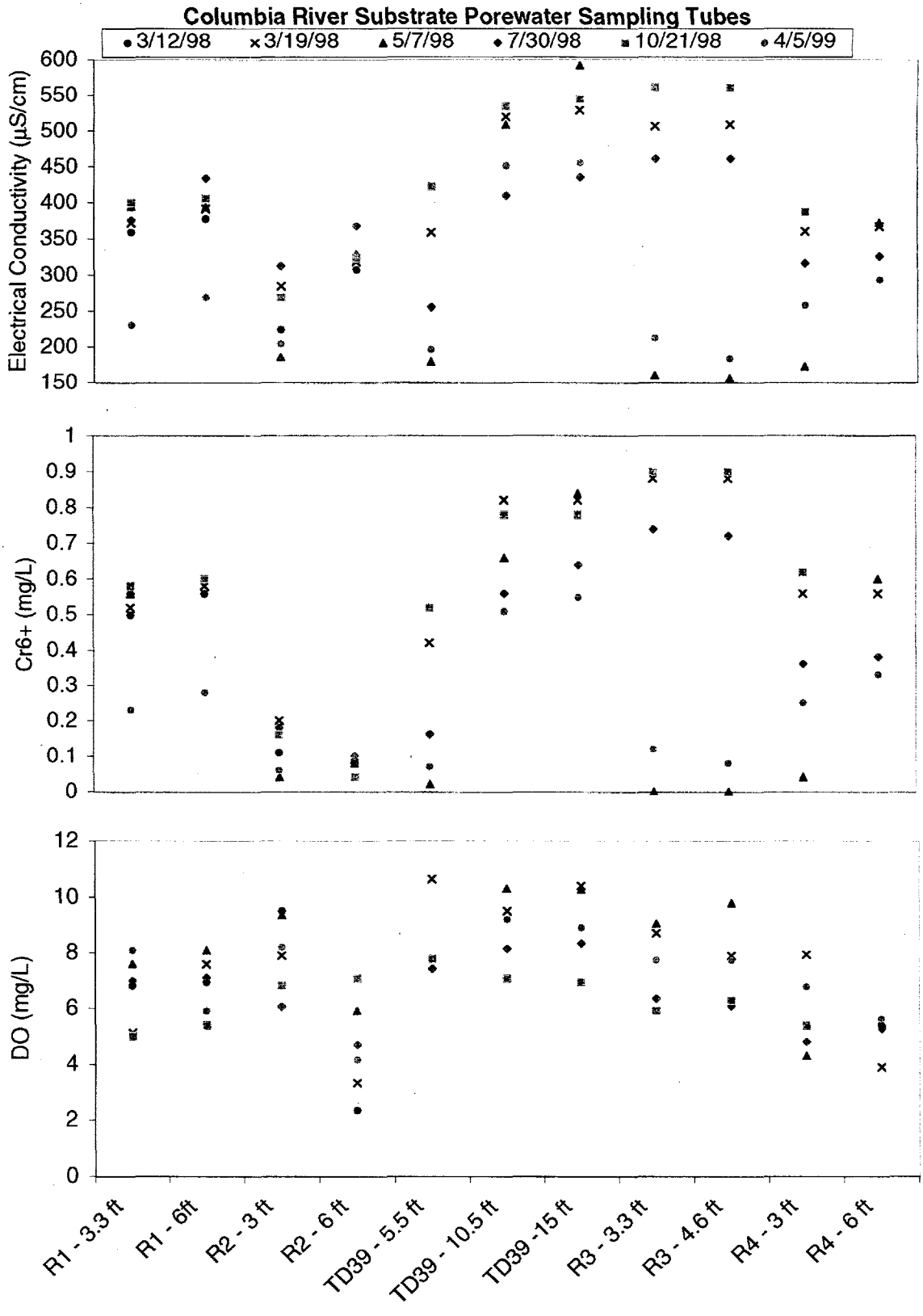


**Figure 2.10**. Columbia River Substrate Porewater Sampling Tubes Downgradient from the 100-D Area ISRM Site. Locations are shown in Figures 2.1 and .2.2.

et al.1998; Hope and Peterson 1996). Hexavalent chromium has not been detected in the river water. It is important to consider the electrical conductivity measurements of the samples to establish the relative river water dilution when interpreting the hexavalent chromium measurements. Concentrations of $Cr^{6+}$ in the aquifer in this area (prior to the ISRM test) were 1.0 mg/L. $Cr^{6+}$ has not been detected in the water samples collected from the Columbia River at 100-D Area. The field analysis method used for $Cr^{6+}$ has a detection limit of 7 μg/L (0.007 mg/L).

Considering both the $Cr^{6+}$ and EC, most of the variability in the measurements shown in Figure 2.9 can be explained by river water mixing (e.g., when EC is low, $Cr^{6+}$ is also low). No clear trend can be determined from the dissolved oxygen data (i.e., DO concentration versus EC) in this figure. Based on the data shown in Figure 2.10, mixing and dilution of river water within the aquifer can result in concentrations ranging from 0 to 90 percent of the baseline (i.e., pre-ISRM test) aquifer concentrations determined farther away (e.g., 130 m).

One tube, Redox02 at a 6-ft depth, appears to be consistently low in $Cr^{6+}$ while maintaining relatively high EC. The dissolved oxygen at Redox02-6 ft is also lower (on average) than other tubes, but the recent values are within the ranges of dissolved oxygen measured in the other tubes at other times. The trend of increasing dissolved oxygen concentration seems to suggest that the water quality in this tube may be influenced from its installation (e.g., negative Eh from crushing minerals) as seen in monitoring wells after installation and without sufficient development. Although $Cr^{6+}$ concentrations in the Redox02-6 ft tube are lower than baseline aquifer concentrations (even when accounting for river water dilution), it cannot be concluded that this reduction in chromate is a downgradient effect of the ISRM treatability study. In addition, the groundwater velocities required to move this distance (160 m) before the first sampling event of this tube in December 1997 (these data are not shown on Figure 2.10 because the samples measured for EC were collected at a different times than for $Cr^{6+}$ measurements) is outside the range of current estimates on the travel time to the river—1.5 to 2.5 years.

## 2.4 Influence of the Columbia River

Groundwater typically flows to the west-northwest at approximately 1 ft/day. Deviations from this typical flow direction occurred during the first few months following well installation (June to September 1997) and was associated with recovery from historically high Columbia River flows during the spring and summer of 1997 (see Figure 2.5). The initial water table at the site (June 1997) indicated groundwater flow directions were 180 degrees away from the typical groundwater flow direction (i.e., away from the river). Water levels in the wells dropped approximately 5 ft from the time of well installation (spring/ summer of 1997) to the fall of 1997, resulting in a change in aquifer thickness from 20 to 15 ft.

Pressure transducers were installed in some of the wells during the summer and fall of 1997. Well D4-4 showed a typical daily range of fluctuation of 0.03 m (with a few 0.06-m peaks) in response to Columbia River stage fluctuations. In the mid-1990s, an array of wells in the 100-N Area (upriver from the D-Area ISRM site, as shown in Figure 1.1) were equipped with pressure transducers and a telemetry system to log hourly water level measurements. The system ran continuously until 1997. Figure 2.11 shows the Columbia River stage at N-Area along with water levels for a few wells at different distances from the river over a one-week period. For a 1.6-m change in the Columbia River, as shown in the figure, the well 25 m from the river had a

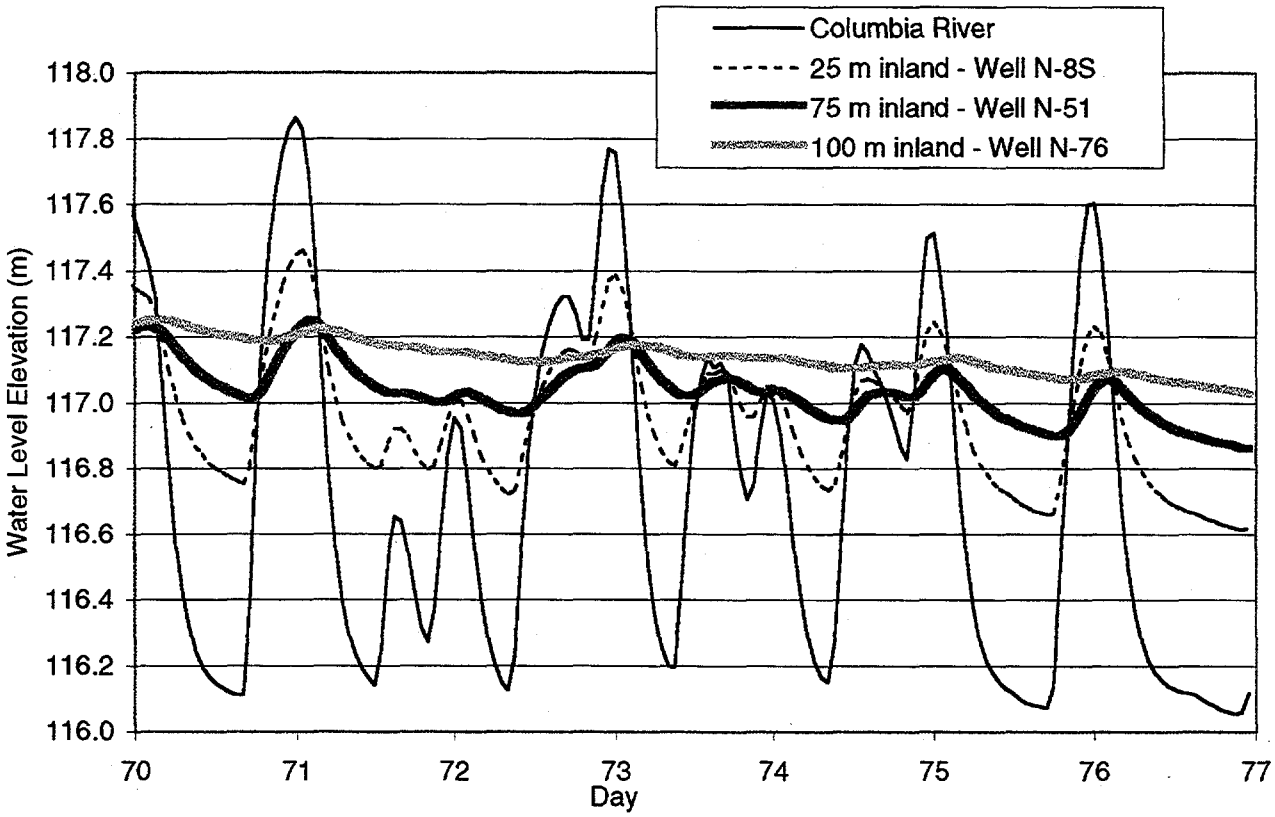


**Figure 2.11.** Columbia River and Monitoring Well Water Elevations, March 1995

0.6-m response. A well 75 m from the river had a 0.2-m response, and at 100 m the well had a 0.05 m response. The additional downgradient monitoring well to be installed at the 100-D Area ISRM test site, as mentioned previously, will provide information on the magnitude of water table fluctuations closer to the river than the existing wells.

The Columbia River stage for 1998 at the D-Area is shown in Figure 2.12. The river stage is controlled by the hydroelectric dams operated along the river for power production, flood control, irrigation, and salmon habitat management. During 1998, the river stage at 100-D Area ranged from a low of 115.9 m in the fall to a high of 120.4 m in the spring, with a mean of 117.9 m. Average daily river stage fluctuations during 1998 were approximately 1.5 m with maximum fluctuations of 2.5 m. River stage is generally highest in the spring and can vary widely from year to year based on the magnitude of the freshet. These data (Figure 2.12) are also provided to show the basis for selecting the river stage period used in numerical simulations discussed in Section 5. The first quarter of 1998 was chosen for predictive modeling to provide a conservative estimate (e.g., no extremes of fluctuation or river stage elevation).

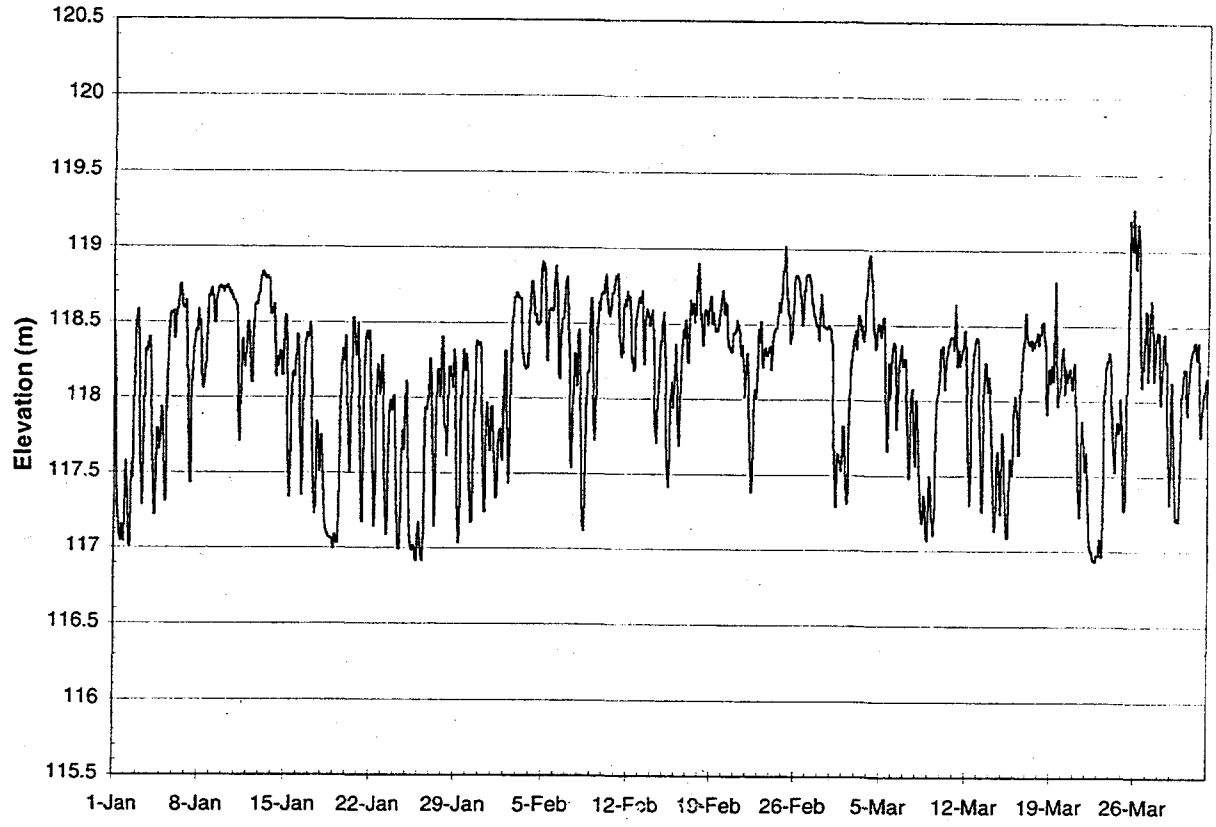


**Figure 2.12 (a).** Columbia River Stage, First Quarter 1998

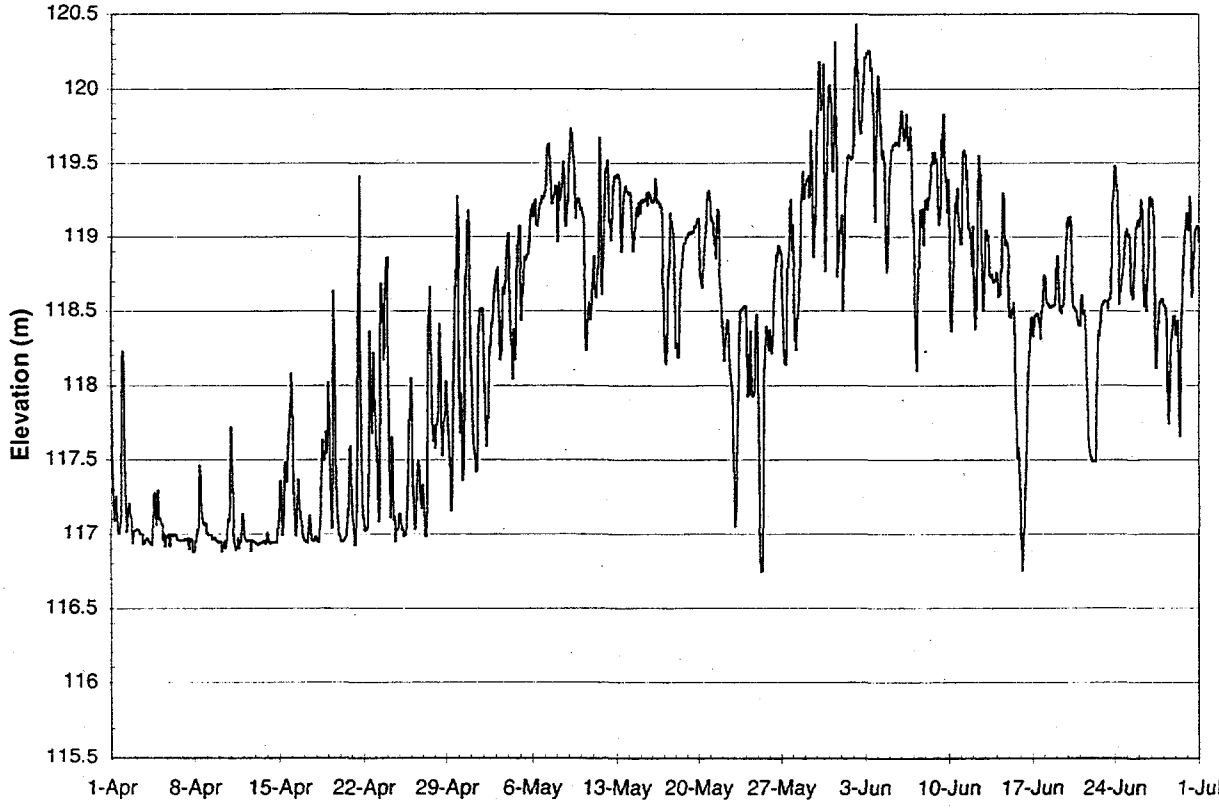


**Figure 2.12 (b).** Columbia River Stage, Second Quarter 1998

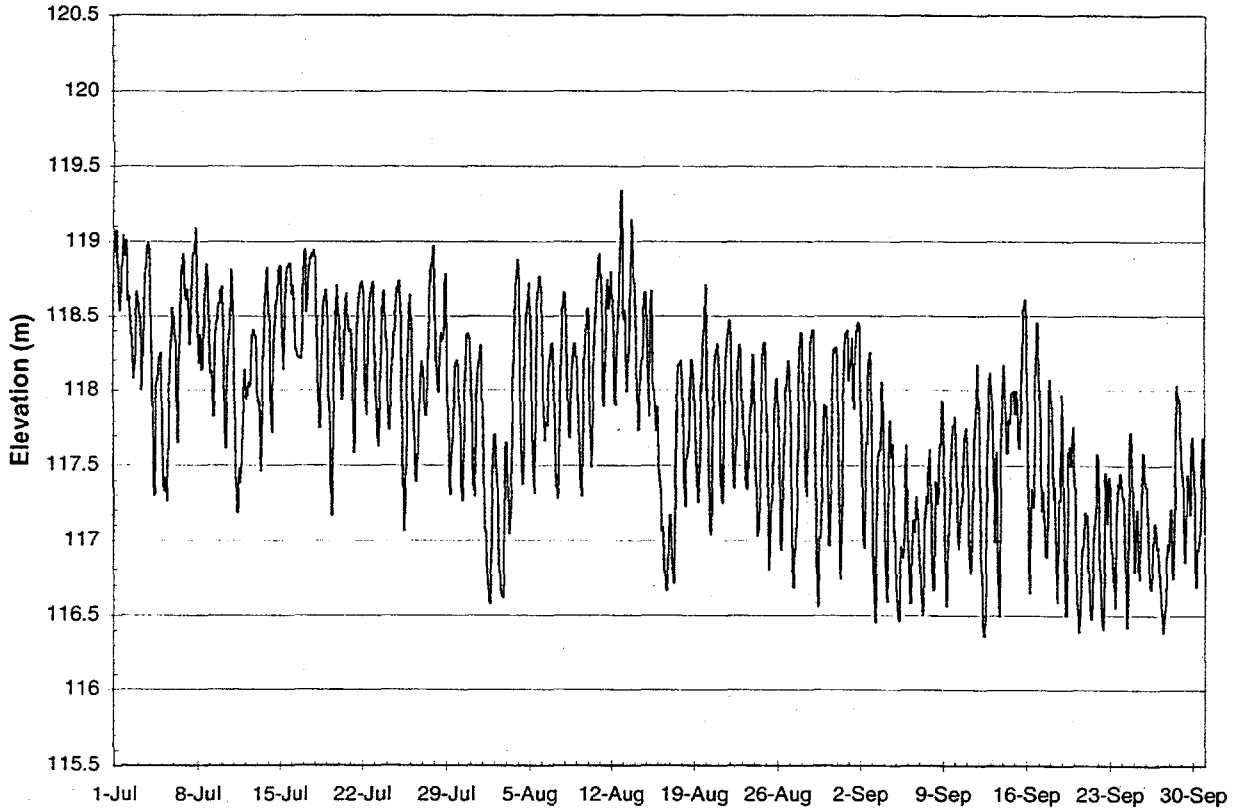


**Figure 2.12 (c).** Columbia River Stage, Third Quarter 1998

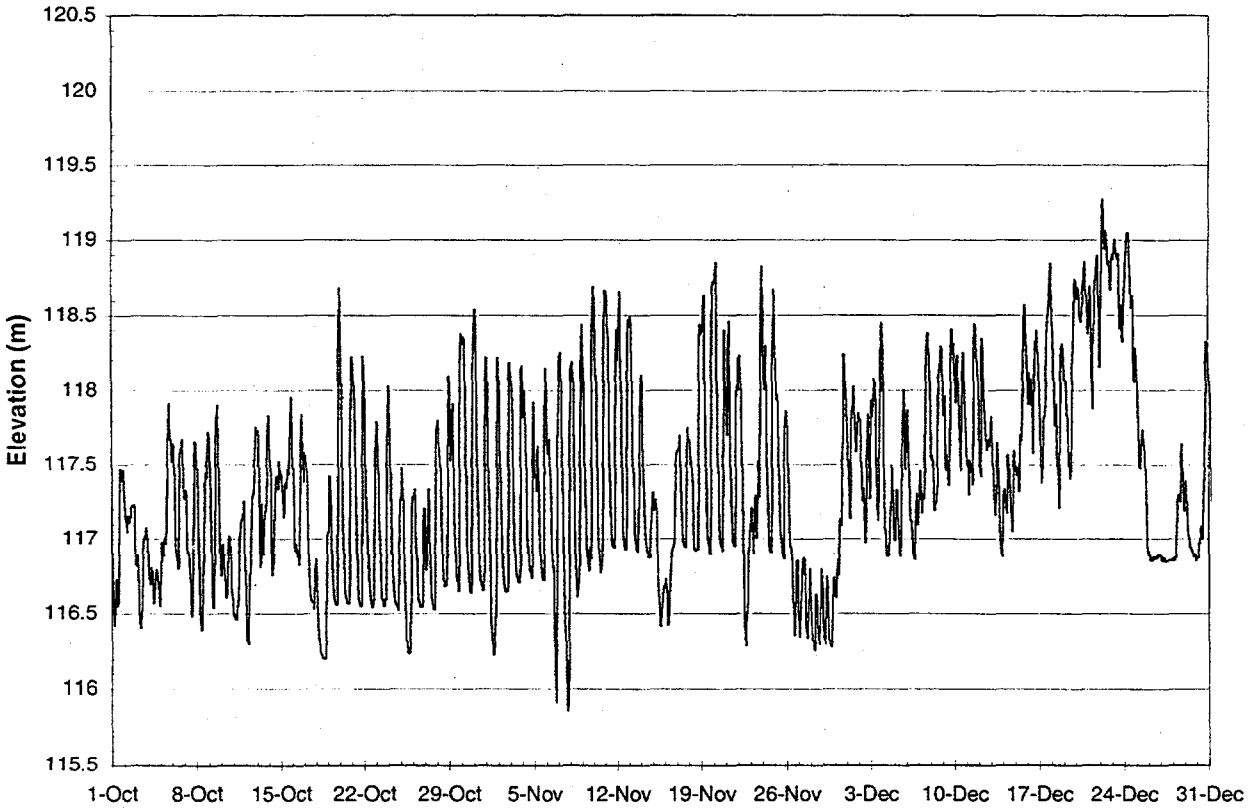


**Figure 2.12(d).** Columbia River Stage, Fourth Quarter 1998

# 3.0 Fluctuating Water Table Experiments

The main objective of this work was to conduct an intermediate-scale flow cell experiment with a fluctuating water table to study the effect of air entrapment on dissolved oxygen (DO) transfer and transport. A second objective was to evaluate whether the multifluid simulator STOMP (White and Oostrom 1999) would be able to accurately simulate the observed water movement and air entrapment as well as the measured DO concentrations. The simulator employs routines for hysteretic air entrapment and assumes equilibrium partitioning between the gas and aqueous phases. Good agreement between measured and simulated DO concentrations would mean that the partitioning of oxygen is an equilibrium process. However, consistent overpredicting of measured concentrations would mean that the partitioning is rate limited, as observed by Fry et al. (1995, 1996) and Donaldson et al. (1997, 1998) in experiments using greater pore water velocities.

## 3.1 Flow-Cell Description and Instrumentation

The experiment was conducted in a Plexiglas flow cell with internal dimensions of 30.5-cm-long by 7-cm-wide by 90-cm-high (Figure 3.1). A schematic of the flow cell with the locations of the DO probes and the gamma-radiation measurements is shown in Figure 3.2. The flow cell was packed under saturated conditions with a fine-grained 30/40 mesh sand (Unimin Corp., Le Sueur, Minn., USA). The sand was obtained prewashed (with water) and presieved and has a high chemical purity and very low organic matter content (Schroth et al. 1996). Pertinent information on the sand properties, including saturated hydraulic conductivity and water retention parameters, is listed in Table 3.1. The saturated hydraulic conductivity was determined in a 1-m-long column using the constant head method (Dirksen and Klute 1986). The Brooks and Corey (1964) water retention parameters and the maximum entrapped gas saturation were obtained using a saturation-capillary pressure cell as described by Lenhard (1992). A manometer was connected to the bottom of the flow cell to determine the approximate location of the water table during water-table fluctuations.

A fully automated, nondestructive, and nonintrusive dual-energy gamma radiation system was used to determine water saturation at 39 calibrated locations. The gamma locations (GL) are numbered 1 through 39 (Figure 3.2). The gamma system, equipped with a 280-μCi Americium and a 100-μCi cesium source, was calibrated according to procedures outlined by Oostrom and Dane (1990) and Oostrom et al. (1998). The calibration procedure yielded porosity and dry bulk density values at each location. The average values are listed in Table 3.1. The low standard deviations in these data indicate that the packing procedure resulted in a fairly homogenous system.

Aqueous samples for dissolved oxygen (DO) concentration measurements were obtained at 10 locations. The DO ports are labeled A–J (Figure 3.2). The ports were connected to a 12-way distribution valve with 1/16-in. OD stainless steel tubing. In addition to the 10 ports, reservoirs with anoxic and oxygen-saturated water were also connected to the distribution value to obtain reference concentrations. A syringe pump was used to extract 2-mL samples from the flow cell and the two standard solutions and inject the sample through three micro flow-through oxygen electrodes (Microelectrodes Inc., Bedford, New Hampshire).

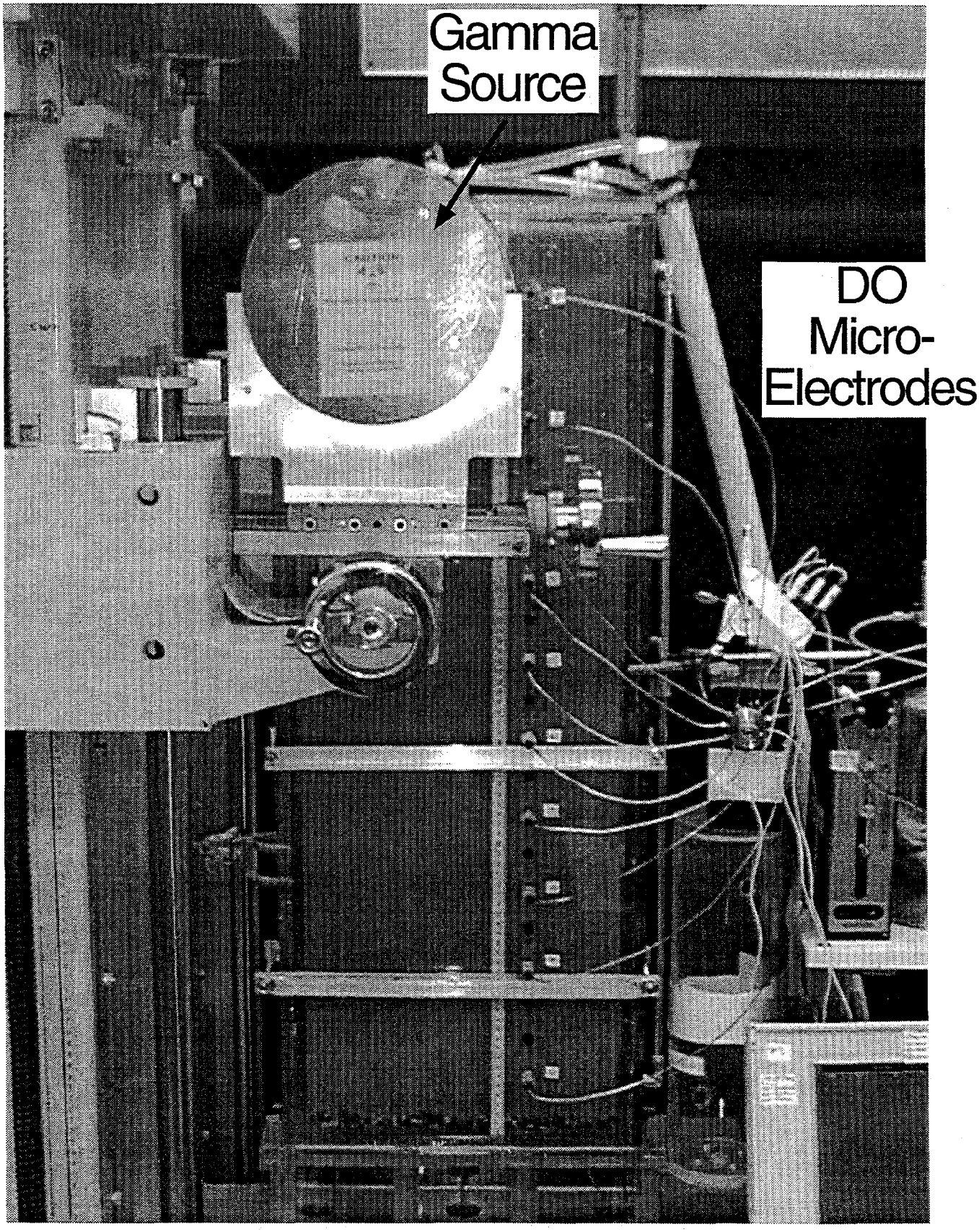


**Figure 3.1.** Flow Cell Showing Dual-Energy Gamma (Cs, Am) System for Fluid Saturation Measurements and Microelectrodes for Measuring Dissolved Oxygen

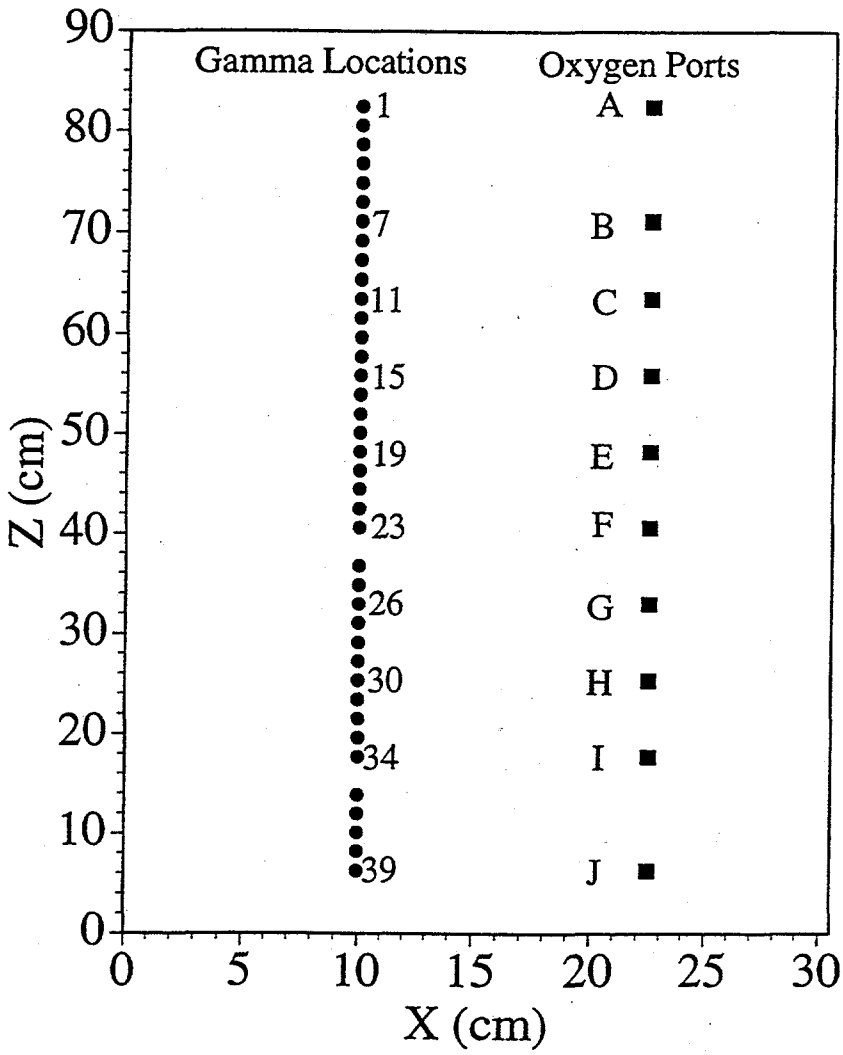


**Figure 3.2.** Dimensions of Flow Cell with Locations of Dual-Gamma Measurements for Water Saturation (GL1 to GL39) and Dissolved Oxygen Sampling Ports (A to J)

The syringe pump provided a consistent flow rate through the three oxygen electrodes for increased precision in these measurements. The oxygen electrodes were calibrated before and after each sampling round with oxygen-saturated and anoxic water standards.

**Table 3.1.** Porous Medium Properties and STOMP Input Parameters

| | |
|---|---|
| Uniformity ($d_{60}/d_{10}$) | 1.23[(a)] |
| Sphericity | 0.9 [(a)] |
| Brooks-Corey air-entry pressure head, $h_d$ (cm $H_2O$) | 13.0 |
| Brooks-Corey $\lambda$ | 5.0 |
| Irreducible water saturation, $S_m$ | 0.01 |
| Maximum entrapped gas saturation, | 0.155 |
| Permeability ($10^{-10}$ $m^2$) | 1.24 |
| Standard deviation ($10^{-10}$ $m^2$) | 0.11 |
| Porosity | 0.325 |
| Bulk density (kg $m^{-3}$) | 1789 |
| Oxygen - Henry's Law Coefficient (dimensionless) | 30.5 |
| Oxygen - Aqueous Phase Diffusion Coefficient ($m^2/s$) | $2 \times 10^{-9}$ |
| Oxygen - Gas Phase Diffusion Coefficient ($m^2/s$) | $2 \times 10^{-5}$ |
| Effective Gas Phase Diffusion Coefficient ($m^2/s$) [(b)] | $5 \times 10^{-7}$ |
| Dispersivity - Longitudinal (cm) | 0.5 cm |

(a) Schroth et al. (1996)

(b) The gas-phase diffusion coefficient was reduced to account for gas-phase diffusive fluxes in partially saturated soils where water films bridging the pore spaces can limit the gas diffusive transfer rate (see text for discussion).

## 3.2 Experiment Description

At the start of the fluctuating water table experiment, the flow cell was fully saturated. The packed flow cell was flushed upward with anoxic water until no dissolved oxygen was detected at any of the sampling locations (approximately four pore volumes) prior to the start of the main drainage of the experiment. During the experiment, water was extracted from and injected into the flow cell using a Masterflex pump with a flow rate of approximately 2 mL/min through three connections at the bottom. The extracted water was pumped into a reservoir that was continuously sparged with ultrapure nitrogen and helium gas. Oxygen-free water was pumped into the flow cell from this reservoir. The fluctuating water table experiment consisted of six 24-hour drainage/imbibition cycles (Figures 3.3 and 3.4). The drainage and imbibition parts each lasted 12 hours. The experiment was concluded by a seventh drainage period in which we attempted to pump out as much water as possible. During the second drainage period, we encountered difficulties with the pump for approximately two hours, during which the water table was kept at a constant level. The pump failure is reflected by the horizontal segments in the locations of the water table and the top of the capillary fringe in Figure 3.4.

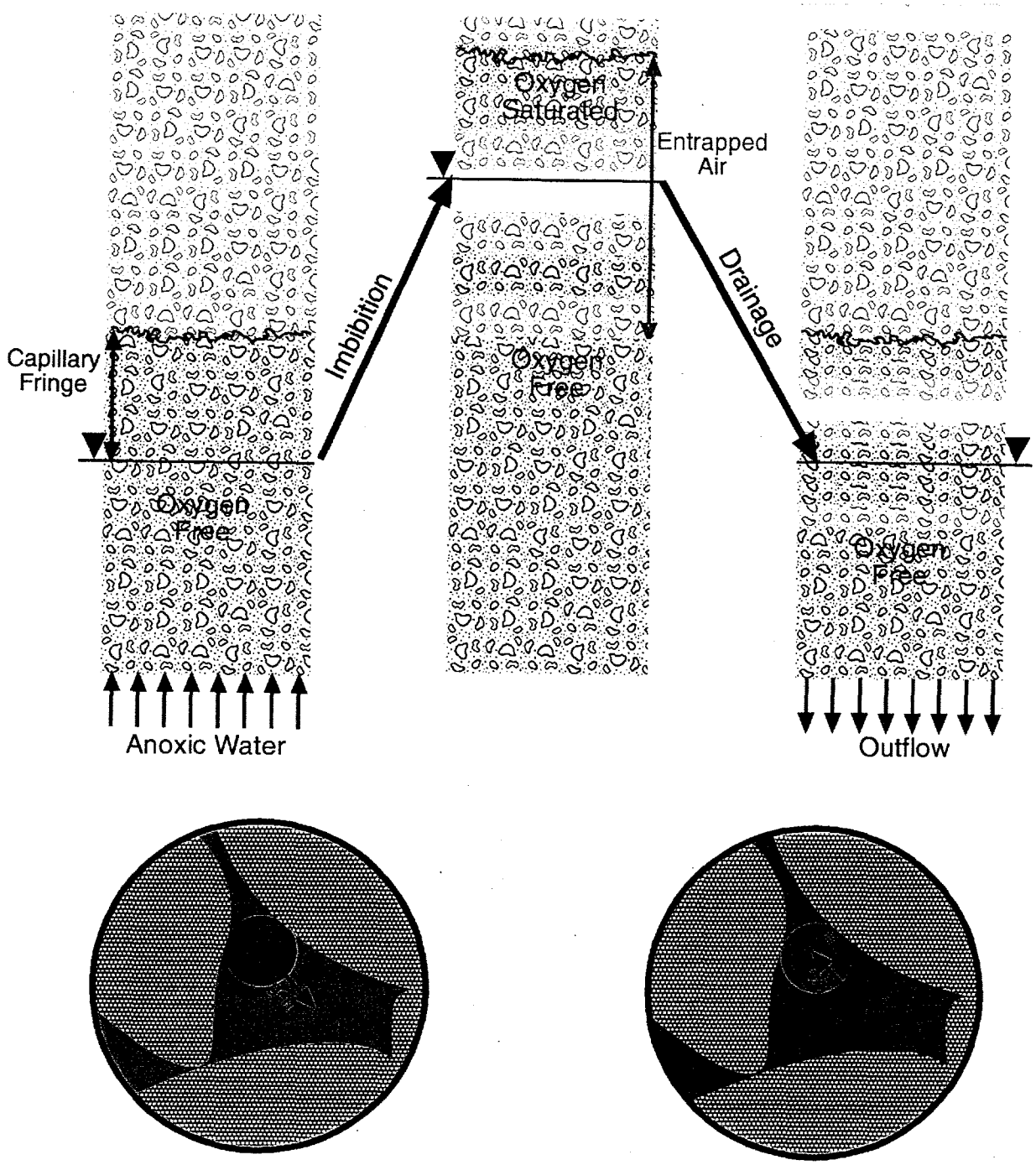


**Figure 3.3.** Experimental Schematic Illustrating Water-Level Dynamics and Oxygen Exchange Between Aqueous and Gas Phases

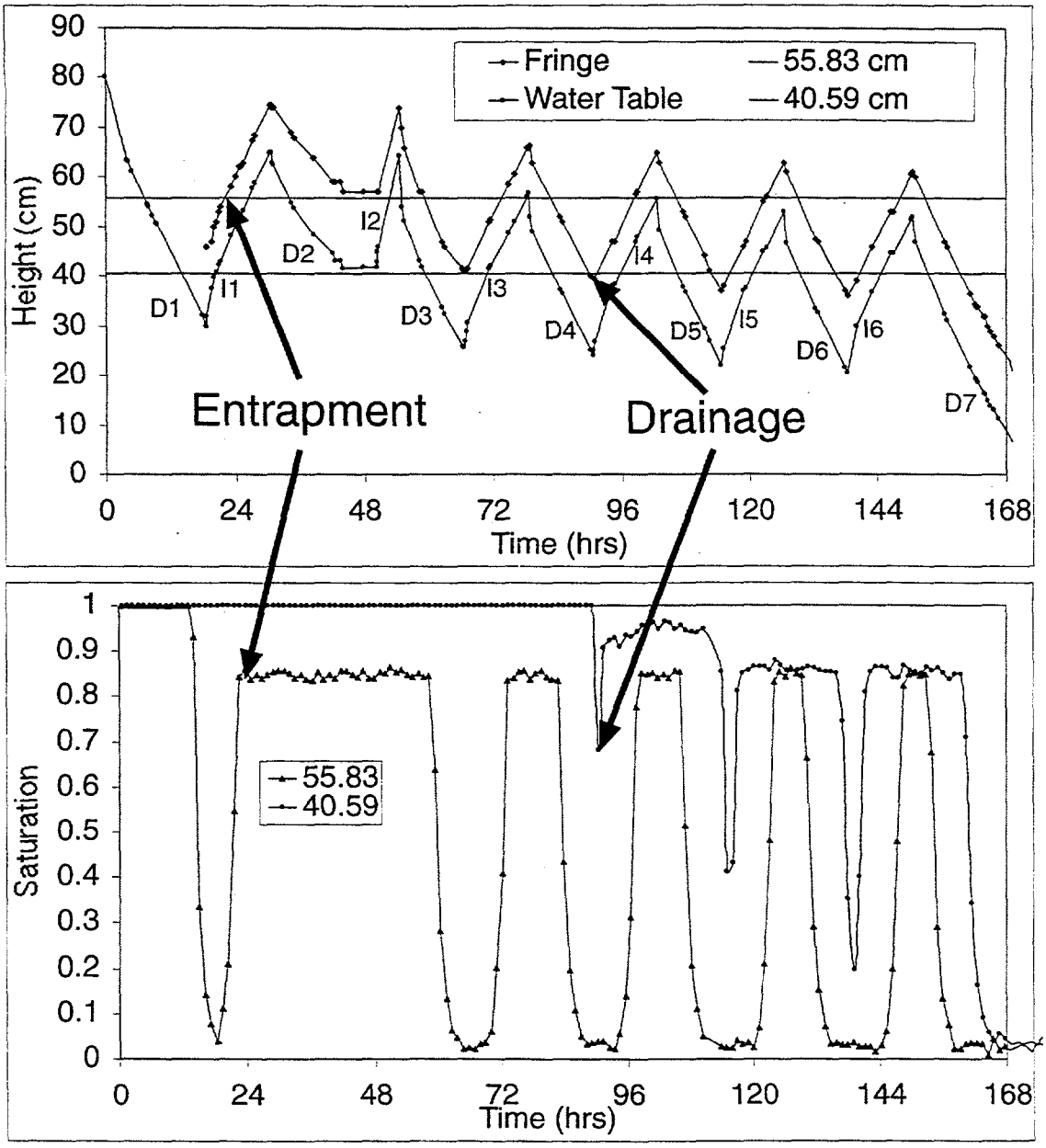


**Figure 3.4.** Water-Level Fluctuations During Experiment with Accusand During Drainage (D) and Inbibition (I). Gamma measurements of saturation are also shown in the lower figure.

During the experiment, the gamma system continuously scanned the 39 calibrated locations (Figure 3.2). The measurement time for each location was 60 seconds, resulting in a maximum relative error in the obtained water saturation of 2 percent (Oostrom et al. 1995). Aqueous samples for dissolved oxygen determinations were obtained approximately every four hours at locations with an apparent water saturation of 1.0 (Figure 3.5). These conditions include situations where all the air present is in entrapped form. No aqueous samples were taken at locations with free, continuous air.

## 3.3 Numerical Simulations

A numerical simulation of the experiment was conducted using the hysteretic water-air mode of the STOMP (Subsurface Transport over Multiple Phases) simulator (White and Oostrom 1999). This fully implicit, integrated finite difference code has simulated a variety of multifluid systems (e.g., Oostrom and Lenhard 1998; Schroth et al. 1998). In this mode, the following mass balance equations for the components water (superscript w) and air (superscript a), respectively, are solved for movement in the aqueous (subscript l) and gas phase (subscript g):

$$\frac{\partial}{\partial t}\left[\sum_{\gamma=l,g}\left(n_D\omega_\gamma^\omega\rho_\gamma s_\gamma\right)\right]=-\sum_{\gamma=l,g}\left(\nabla\mathbf{F}_\gamma^\omega+\nabla\mathbf{J}_\gamma^\omega\right) \tag{1}$$

$$\frac{\partial}{\partial t}\left[\sum_{\gamma=l,g}\left(n_D\omega_\gamma^a\rho_\gamma s_\gamma\right)\right]=-\sum_{\gamma=l,g}\left(\nabla\mathbf{F}_\gamma^a+\nabla\mathbf{J}_\gamma^a\right) \tag{2}$$

where

$$\mathbf{F}_\gamma^i=-\frac{\omega_\gamma^i\rho_l k_{r\gamma}\mathbf{k}}{\mu_\gamma}\left(\nabla P_\gamma+\rho_\gamma g\mathbf{z}_g\right)\quad\text{for i = w, a} \tag{3}$$

$$\mathbf{J}_\gamma^i=-\tau_\gamma n_D\rho_\gamma s_\gamma\frac{M^i}{M_\gamma}D_\gamma^i\nabla\chi_\gamma^i\quad\text{for i = w, a} \tag{4}$$

and $n_D$ is the total porosity, $\omega$ is the mass fraction, $\rho$ is the density ($ML^{-3}$), s is the saturation, $\mathbf{F}$ is the advective flux ($ML^{-2}T^{-1}$), $\mathbf{J}$ is the dispersive flux ($ML^{-2}T^{-1}$), $k_r$ is the relative permeability, $\mathbf{k}$ is the permeability ($L^2$), $\mu$ is the viscosity ($(ML^{-1}T^{-1})$, $P$ is the pressure, $g$ is the gravitational acceleration ($LT^{-2}$), $\mathbf{z}$ is the direction (L), $\tau$ is the tortuosity, $M$ is the molecular weight (M), $D$ is the hydrodynamic dispersion coefficient ($L^2T$), and $\chi$ the mole fraction. The simulator assumes equilibrium partitioning of the air component between the aqueous and gas phases, according to Henry's Law:

$$H=\frac{P_g^a}{\chi_l^a} \tag{5}$$

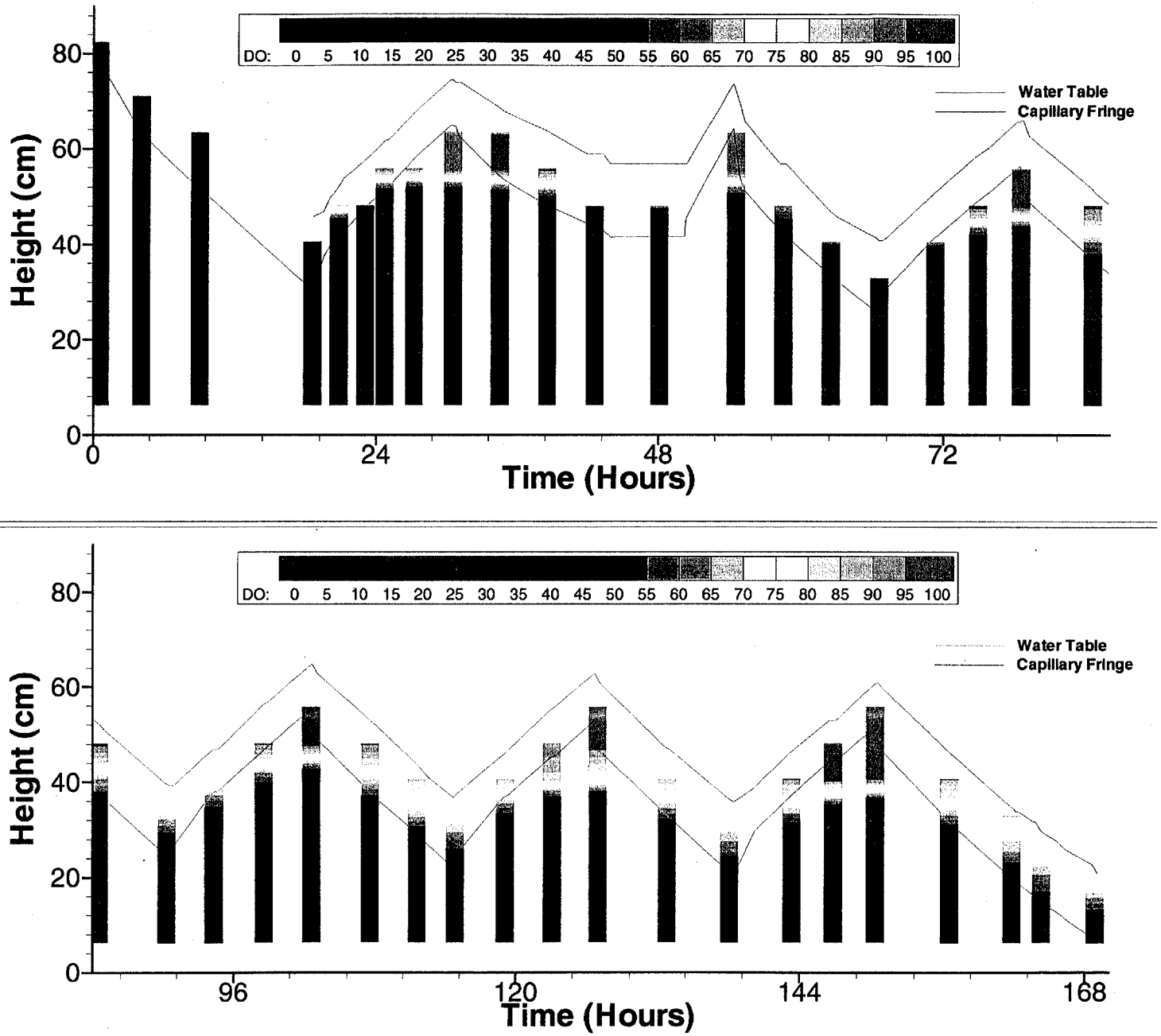


**Figure 3.5.** Dissolved Oxygen Concentrations (shown as percent saturation) from Accusand Test. Also shown are the water table and capillary fringe measurements for the duration of the test.

Previous implementations of the STOMP simulator have incorporated fully hysteretic relations to express the relative permeability-saturation-capillary pressure (k-s-P) relations for multiphase systems (White and Oostrom 1999). Experience has shown that this approach requires considerable computational effort and typically limits simulations to computational grids of one or two dimensions. The current formulation implemented in the water-air mode uses simplified two-phase k-s-P relations, which accounts for the effects of gas entrapment but ignores pore-geometry hysteresis and the associated complex tracking of multiple wetting and drainage scanning curves. The simplified hysteretic formulation has been extensively tested for two- and three-phase systems (Lenhard et al. 1995; Oostrom et al. 1997). The formulations follow procedures outlined by Kaluarachchi and Parker (1992), based on the fully hysteretic multifluid model by Lenhard and Parker (1987) and Parker and Lenhard (1987). Two-phase relations between the scaled capillary heads and apparent liquid saturations using the Brooks and Corey (1964) expressions describe the system of phase saturations. Entrapped gas saturations are computed as

$$\bar{S}_{gt} = \min\left[\left\{\frac{1-\bar{S}_l^{\min}}{1+R\left(1-\bar{S}_l^{\min}\right)}\right\} - \left\{\frac{1-\bar{\bar{S}}_l}{1+R\left(1-\bar{\bar{S}}_l\right)}\right\}, \bar{S}_g\right] \tag{6}$$

where $\bar{S}_{gt}$ is the effective entrapped gas saturation, $\bar{S}_l^{\min}$ is the minimum effective aqueous saturation, $\bar{\bar{S}}_l$ is the apparent aqueous phase saturation ($\bar{\bar{S}}_l = \bar{S}_l + \bar{S}_{nt}$), and $\bar{S}_g$ is the effective gas saturation. The effective saturation $\bar{S}_l = (S - S_{ir})/(1 - S_{ir})$, where $S$ is the actual saturation and $S_{ir}$ is the irreducible saturation. The Land's parameter, $R$ (Land 1968), is given by

$$R = \frac{1}{\bar{S}_{gr}^{\max}} - 1 \tag{7}$$

where $\bar{S}_{gr}^{\max}$ is the maximum effective residual gas saturation, obtained on the main imbibition branch. For the fine-grained 30/40-mesh Accusand, a value of 0.155 has been determined for $\bar{S}_{gr}^{\max}$ using a method described by Lenhard (1992). Compared to nonhysteretic simulations, this saturation is the only additional parameter to be determined experimentally. The relative permeability-saturation relations in the model are based on the on the Burdine pore size distribution model (Burdine1953), analogous to relations based the Mualem model (Mualem 1976), as used by Kaluarachchi and Parker (1992). Entrapped gas affects the aqueous-phase permeability by displacing water into larger pore spaces. The studies of Kaluarachchi and Parker (1992), for instance, have shown these effects to be relatively small and were neglected in the development of the relative permeability functions. (Refer to White and Oostrom [1999] for an overview of these functions.)

In the simulation, the 90-cm-long flow cell was discretized into a one-dimensional uniform grid using 1-cm-long cells. For the gas phase, a dirichlet-type constant-pressure boundary was prescribed at the top and a zero-flux boundary at the bottom of the domain. Oxygen concentrations in the inflowing gas phase at the top were set to atmospheric concentrations. For the aqueous phase, a zero-flux boundary was used at the top and a Neumann-type boundary was used at the bottom based on the flow rates used in the experiment. Incoming water was assumed

to be free of air and oxygen. Most input parameters were determined independently in the laboratory (Table 3.1). In the simulation, a time-step increment factor of 1.25 was used after convergence. The maximum number of Newton iterations was eight, with a convergence factor of $10^{-6}$. Upwind interfacial averaging was used for gas and aqueous phase relative permeabilities. Harmonic averages were used for all other flux components.

## 3.4 Results and Discussion

To illustrate the effect of the water table fluctuations on water and entrapped air saturations, measured and simulated water saturations at selected locations are shown in Figures 3.6 and 3.7. The top four locations (from z = 71 to 48 cm) were drained during the initial drainage period (period D1; Figure 3.4). The locations below $z$ = 36 cm remained fully saturated until the final drainage period (period D7; Fig. 3-4), when we attempted to fully drain the flow cell. Altering water saturations were observed as a result of water table fluctuations during the periods I1 through D6 at GLs 5 through 24 (GL locations are indicated in Figure 3.2).

At GL 7 (z = 71.07 cm in Figure 3.6), water saturation during the first and second imbibition period increased from almost 0 to 0.84. During these periods, the top of the capillary fringe moved above GL 7 to $z$ = 74 cm. At those times, the porous medium at that location was apparently fully saturated, indicating that the entrapped air saturation was approximately 0.16. The term "apparent saturation" is used to indicate the sum of the water saturation plus the entrapped air saturation (Parker and Lenhard 1987). This number corresponds well to the independently obtained maximum entrapped saturation of 0.155 using Lenhard's (1992) method (Table 3.1). During the later imbibition periods, the observed saturation peaks decreased as a result of the gradual downward shift of the maximum position of the water table (Figure 3.4). At GL 11 (z = 63.45 cm in Figure 3.6), maximum water saturations of 0.84 and entrapped air saturations of 0.16 were obtained during the first four imbibition periods. The fact that the entrapped air saturation reached a constant value of 0.16 every time the porous medium became apparently fully saturated (after a drainage period, when water saturations came close to the irreducible water saturation) suggests that the hysteretic entrapment and release of air was a reversible process. Similar patterns are shown for other locations in Figures 3.6 and 3.7. The water saturation maxima at location GL11 decreased during the last two imbibition periods as a result of the gradual lowering of the maximum water table positions over time (Figure 3.4). This lowering trend is also manifested in the decreasing width of the maximum saturation plateaus over time.

The difficulties with the pump and the resulting relatively high water table minimum at the end of the second drainage period caused the porous medium below GL 8 to remain apparently fully saturated during that period. For this location, near-irreducible water saturations were obtained during all other drainage periods, and maximum entrapped air saturations were obtained during the imbibition periods. The lower the location, the less the water table fluctuations affected the water saturation. The porous medium at GL 19 (z = 48.21 cm in Figure 3.7) only partially drained during the first drainage period, resulting in reduced air entrapment during the subsequent imbibition period. At GL 23 (z = 40.59 cm in Figure 3.7), reduced saturations were only observed starting with the fourth drainage period (see annotated drainage in Figure 3.4). Lower locations remained fully saturated during the experiment.

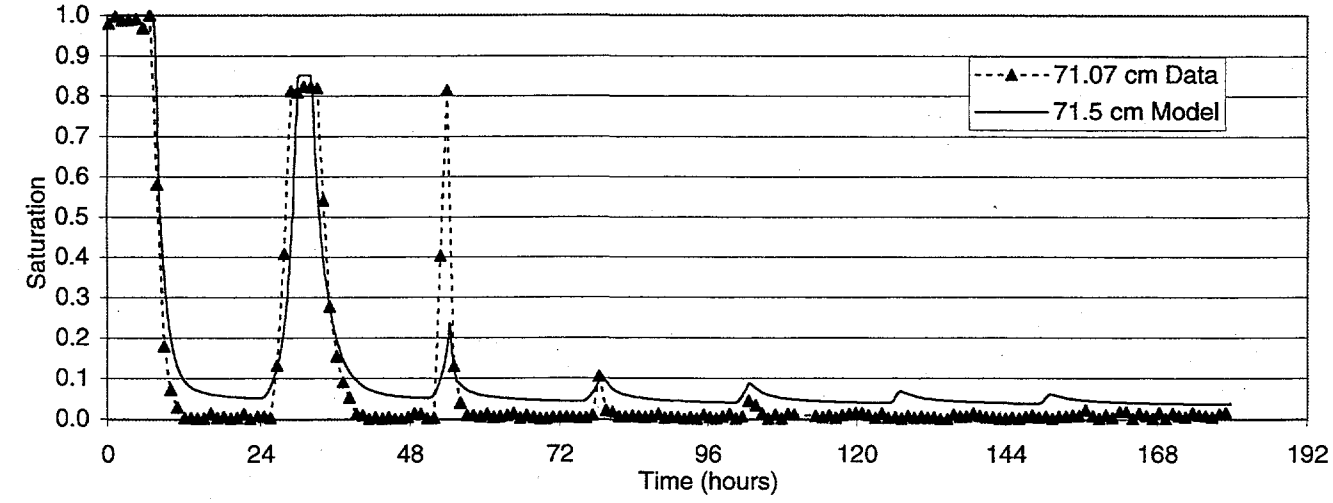


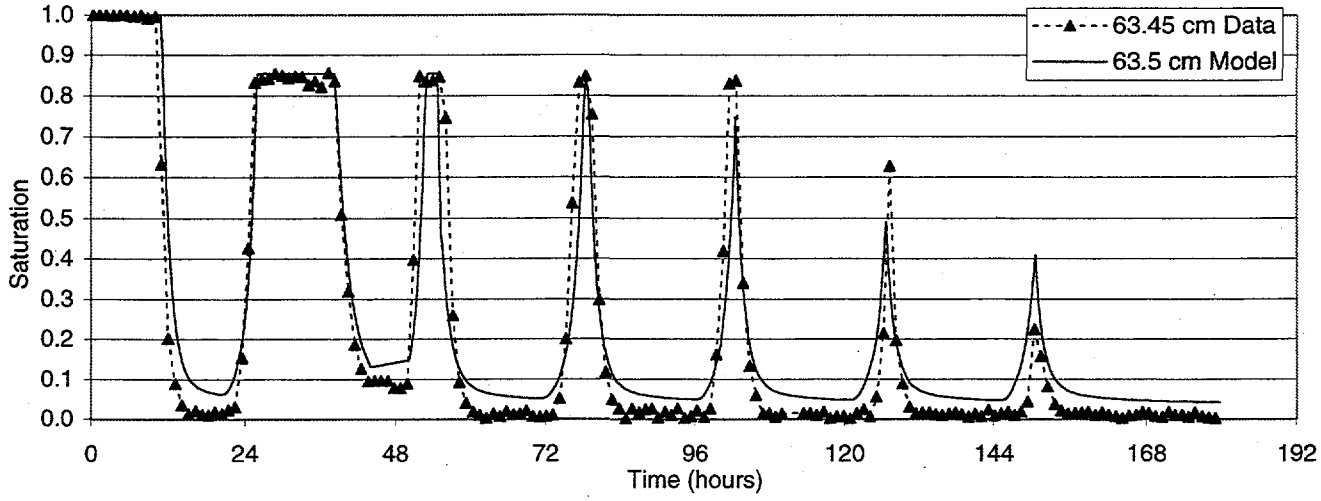


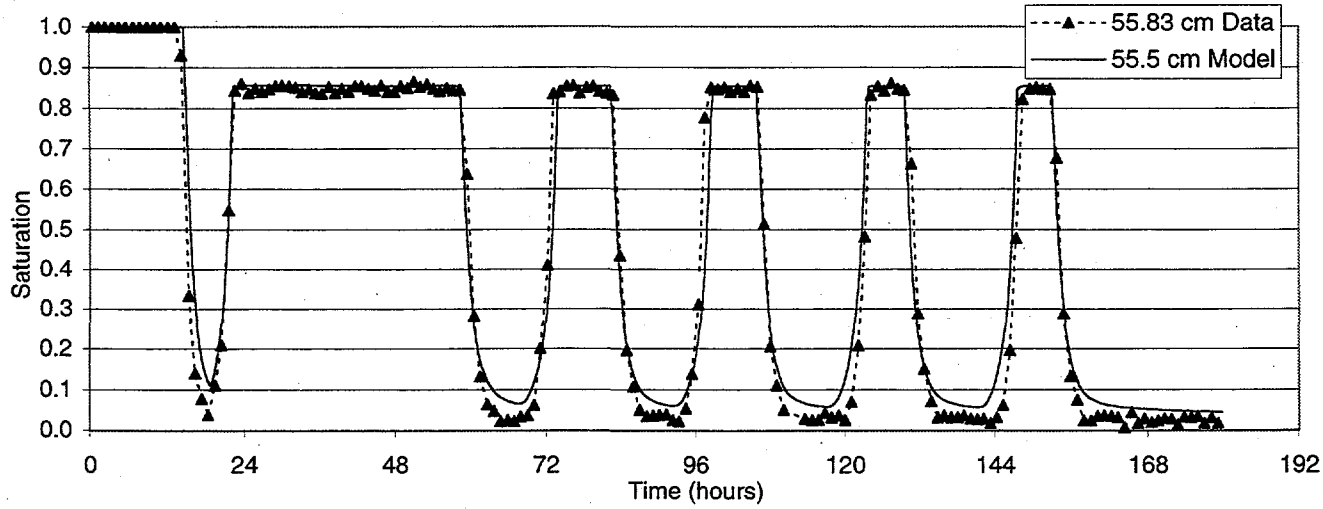


**Figure 3.6.** Water Saturation Measurements from Dual-Gamma System for Locations in Upper Portion of the Flow Cell (refer to Figure 3.2). Results of STOMP model are also shown.

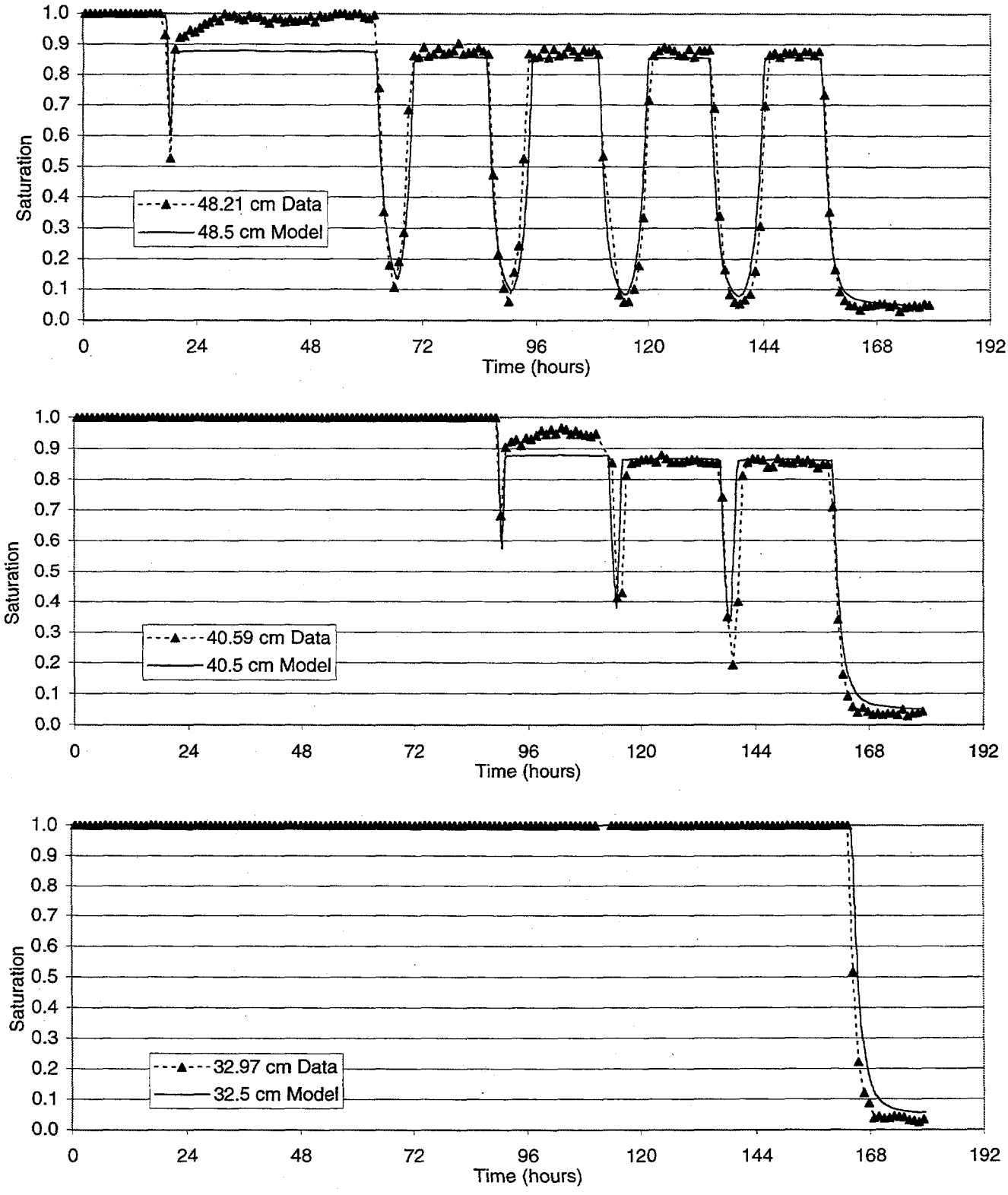


**Figure 3.7.** Water Saturation Measurements from Dual-Gamma System for Locations in Lower Portion of the Flow Cell (refer to Figure 3.2). Results of STOMP model are also shown.

The agreement between predicted and measured water saturations was generally good. In the upper location shown, GL 7 (e.g., z = 71.07 cm in Figure 3.6), the simulator over predicted water saturations during the later imbibition periods. An analysis showed that the predicted water saturations during these imbibition periods are very sensitive to the Brooks and Corey (1964) retention parameters. Because the sand used was quite uniform, indicated by the large $\lambda$-parameter value of 5.0 (Table 3.1), small discrepancies in the air-entry pressure head result in substantial differences in the maximum water saturation during the imbibition periods. For example, the lower observed water saturations during the last four imbibition periods for GL 7 (Figure 3.6) could be simulated more accurately using a air-entry pressure of 12.0 cm for that location instead of the independently obtained value of 13.0 cm. However, it should be noted that using different air-entry pressure-head values to more accurately simulate the water movement in the flow cell reduces the modeling effort to mere curve fitting. The sensitivity of the water saturations to the air-entry pressure value demonstrates that, despite considerable efforts to pack the flow cell as uniformly as possible, it is practically impossible to achieve a level of homogeneity so that the same air-entry pressure head value is applicable at all locations.

Height-interpolated DO concentrations for all measurement periods are shown in Figure 3.5 along with the locations of the water table and the top of the capillary fringe. This figure shows that over time the amount of oxygen below the water table increased substantially. This becomes more obvious when the vertical bars are compared at the end of the first six imbibition or drainage periods. For example, at the end of the first drainage period ($t$ = 18.75 hr), all measured concentrations were zero; whereas at the end of the sixth drainage period ($t$ = 138 hr), DO concentrations from 0 to 80 percent were observed. The fairly rapid oxygenation of the water below the water table was largely a result of air entrapment during the imbibition periods. During imbibition periods, a distinct, apparently fully saturated zone developed where about 15 percent of the pore space consisted of entrapped air. During these periods, oxygen partitioning from entrapped air into the aqueous phase continued, even when no 'free' air was present. Some of this oxygen was transported downward during the subsequent drainage periods. Without the air entrapment phenomenon, considerable DO concentrations would be found only at relatively higher elevations, and the reoxygenation process would be slower.

The observed and simulated DO concentrations at the dissolved-oxygen ports E–J are shown in Figure 3.8. The gaps in the measured DO concentration line at locations E and F (see top of Figure 3.8; DO locations are indicated on Figure 3.2) are the result of the presence of free air during some measurement periods. When free air was present, the sampling mechanism was not able to produce a representative aqueous sample. In general at a sampling port, DO concentrations decreased during imbibition periods, when oxygen-free water was injected in the flow cell, and increased during drainage periods, when oxygen-rich water moved downward. At all locations, a gradual increase of the maximum dissolved DO concentration was observed during drainage periods. At locations E and F, where free air was present during parts of the experiment, the concentration reached 100 percent after a few fluctuations. At locations G, H, and I, where no free air was ever present (Figure 3.8), DO concentrations increased to 80, 60 and 18 percent, respectively, after the sixth drainage period. The last (seventh) drainage period is not considered in this discussion because that period was not part of the fluctuating cycle. The goal during that period was to drain the flow cell as much as possible and to observe how quickly, if ever, fully oxygenated water would reach a sampling port. In that respect, it was surprising to see that at locations G–I the DO concentrations never reached 100 percent before free air entered the porous medium, although fully oxygen-saturated water was present in the system when the

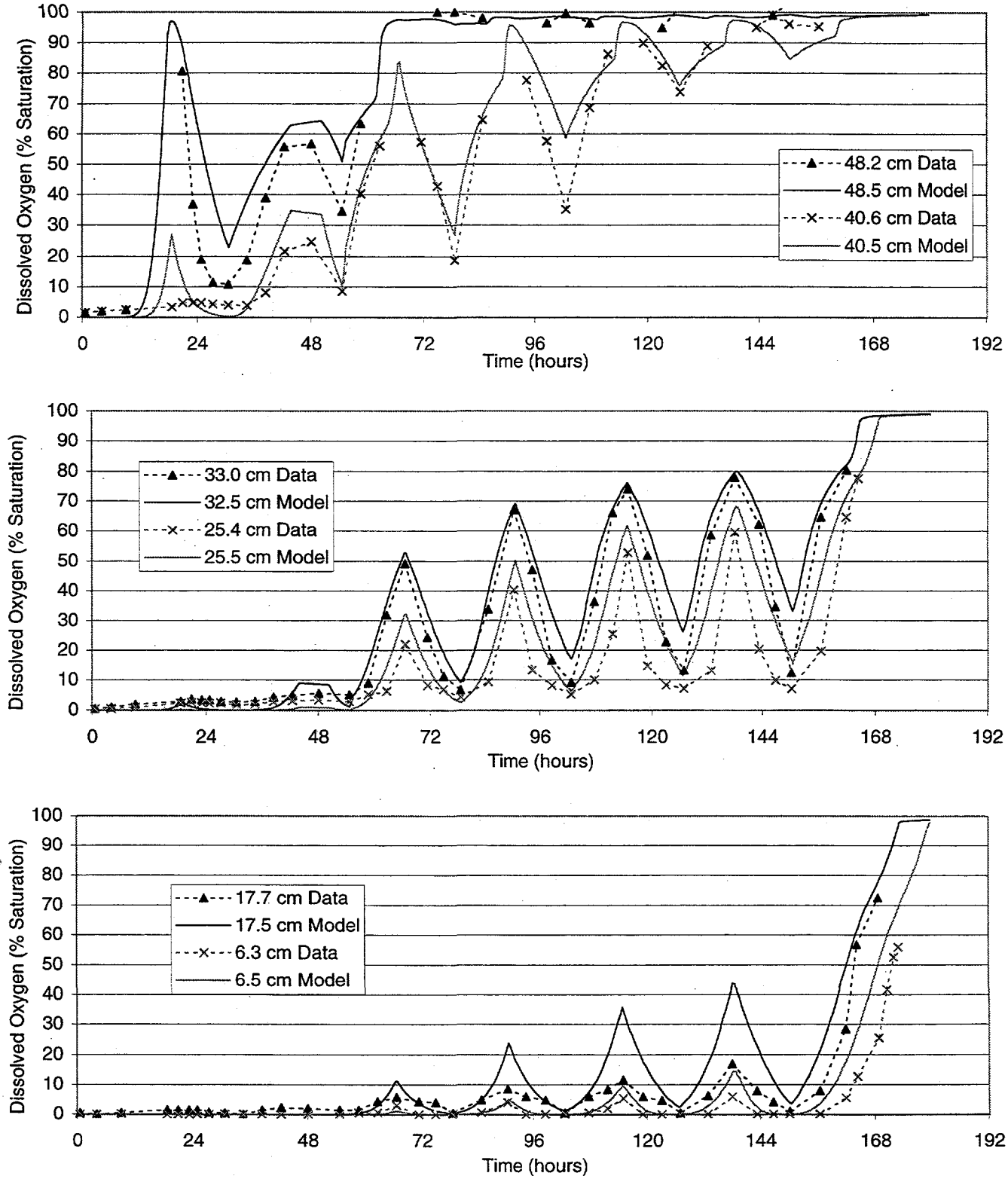


**Figure 3.8.** Dissolved Oxygen Measurements in the Flow Cell (refer to Figure 3.2). STOMP model results are also shown.

final drainage period began. It is hypothesized that some of the oxygen transported downward partitioned back into oxygen-depleted entrapped-air bubbles, created during the previous imbibition periods, gradually reducing the DO concentration of the downward moving water. This process is illustrated at the bottom of Figure 3.3. A comparison of DO concentrations at the end of the drainage period with those at the beginning of the drainage period clearly shows a reduction in concentrations during each drainage in Figure 3-5. Calculations of the total DO mass in the system throughout the experiment showed as much as 50 percent decrease in mass between the start and the end of each drainage period, with no loss of DO out the bottom of the flow cell. Even with these DO losses back to the gas phase during drainage, the system oxygenated rapidly—just not as rapidly as would be estimated from concentrations at the end of each imbibition period.

A comparison of the measured and simulated dissolved oxygen concentrations (Figure 3.7) shows that they are in good agreement. The largest discrepancies were in the peak concentrations at the bottom of the flow cell (i.e., 17.7 cm in Figure 3.7), although the two sampling ports above and below this location both show a much better match.

Earlier model results from this experiment did not agree with the DO data as well; the earlier results consistently overpredicted the dissolved oxygen concentrations. These results did show that the profiles of the simulated results were similar to the data, but model results from deeper in the flow cell matched data from higher locations (e.g., model results at location z = 40.5 cm matched laboratory data at 48.2 cm). In addition, the simulated results predicted much higher concentrations of dissolved oxygen at the end of the main drainage (D1) prior to any imbibition. The experimental data (Figure 3.5 at 20 hours) showed that the water was anoxic after the main drainage. Good agreement was achieved between model results and laboratory data by lowering the gas-phase molecular diffusion coefficient to a value between the molecular diffusion coefficients of oxygen's gas and aqueous phases (Table 3.1) and applying the Millington and Quirk (1960) diffusion model available in the STOMP code. The justification for this change is that the gas phase molecular diffusion coefficient for oxygen is four orders of magnitude greater than that for the aqueous phase. Although gas phase diffusion is not simulated within the zone of trapped air, it is simulated in the partially saturated zone above it. The selection of a value for a diffusion coefficient in this partially saturated zone between the gas and aqueous phases depends on whether there is a film of water blocking some of the pore spaces connecting the gas and thus limiting the diffusive flux, as discussed in Nielson et al. (1984). Nielson et al. showed that diffusion coefficients varied by the four orders of magnitude spanning the water and gas diffusion rates on various soils between dry and differing amounts of water saturation. They also developed a model for determining the effective molecular diffusion coefficient as a function of the pore size distribution of the sediment and water saturation. Although these more complex models have not been implemented in the STOMP code, adequate results were achieved by using the simple Millington and Quirk (1960) model, which calculates the diffusive flux tortuosity as a function of soil moisture, with a smaller gas phase diffusion coefficient.

Combined profiles for the laboratory data and model results for two selected times are shown in Figure 3.9. The water saturation measurements were taken over an approximate one-hour period during these times; all other data are from the end of the third drainage and imbibition periods (D3 and I3). These plots also show that there was overall good agreement between the measurements and model results. The water saturation measurements and model results both

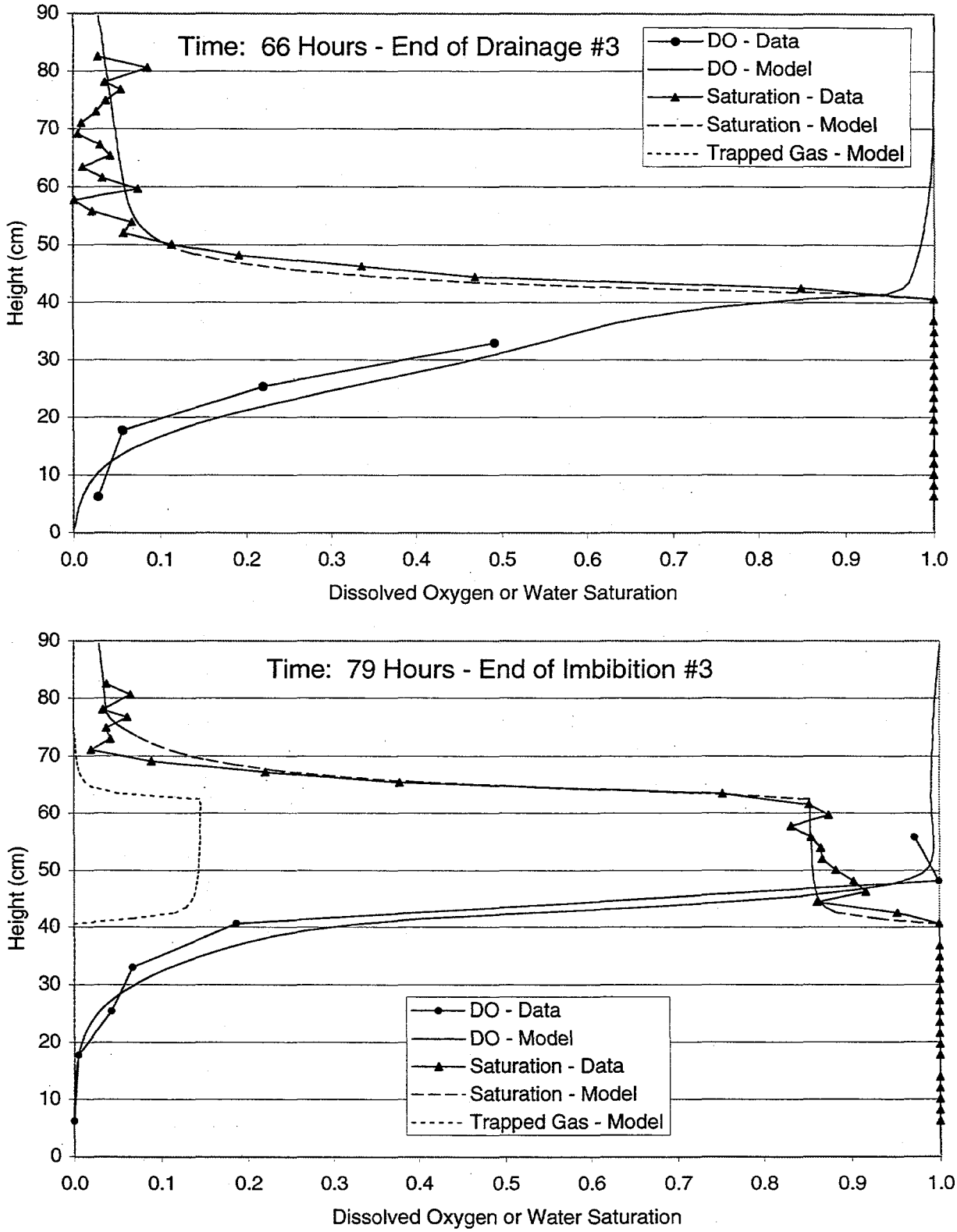


**Figure 3.9.** Dissolved Oxygen and Water Saturation Profiles Through Flow Cell During Drainage and Imbibition 3. Both data and STOMP model results are shown.

indicate the presence of an approximately 20-cm zone of trapped gas at the end of the imbibition period. Because the water table and the top of capillary fringe dropped lower during D3 than during previous drainage periods, no trapped gas was seen in the system at the end of D3.

In the profiles of Figure 3.9, the dissolved oxygen measurements indicate some oxygen depletion within the gas phase (since the aqueous and gas phases are in equilibrium) above the capillary fringe at the end of the drainage period and within the trapped gas at the end of the imbibition period.

## 3.5 Summary and Conclusions

The hypothesis that water table fluctuations increase oxygen transfer from air to water through enhanced exchange from entrapped air is tested in an intermediate-scale flow cell experiment with a fluctuating water table. In the experiment, the homogeneous porous medium was subjected to several water table fluctuations. Water saturations were measured with a dual-energy gamma radiation system, and microelectrodes were used to measure dissolved oxygen concentrations. The multifluid simulator STOMP was used to test whether observed DO concentrations could be predicted assuming equilibrium partitioning between the gas and the aqueous phases. For the simulation, the hysteretic two-phase mode of the simulator was used.

The results show that zones with entrapped air saturations of up to 16 percent are formed during the imbibition parts of the experiments. The entrapped air served as a source for oxygen transfer from air into the aqueous phase. The creation of such a zone within the capillary fringe caused considerable amounts of DO to migrate relatively deep into the flow system. Water in the zone of fluctuation (20 cm) became significantly reoxygenated (50 to 100 percent) within six imbibition/ drainage cycles over a one week period. The decrease in dissolved oxygen concentrations during drainage (relative to the previous imbibition peak) indicates that some dissolved oxygen gained during imbibition is transferring back into oxygen-depleted entrapped air at the bottom of the zone of entrapment.

The hysteretic air-water mode of the STOMP simulator was able to predict water, entrapped air saturations, and dissolved oxygen concentrations reasonably well. The comparison between experimental and numerical results demonstrates that fluctuating water table systems can be modeled successfully where oxygen partitions between phases. Therefore, it has been demonstrated that the most important processes involved in this phenomenon have been adequately identified and quantified at this scale. This provides some confidence in the application of the STOMP simulator using these functions in the field-scale fluctuating water table simulations discussed in Section 5.

# 4.0 Dissolved Gas Tracer Tests

Dissolved gas tracer tests were conducted in March and April 1998 to identify and possibly quantify the presence of trapped gas bubbles in the aquifer below the water table. Previous studies have shown the importance of trapped gas bubbles on the transport of dissolved gases (Fry et al. 1995, 1996; Donaldson et al. 1997, 1998). The presence of trapped gas has been inferred from the behavior of numerous dissolved gas tracer tests (see Fry et al. 1995 for a review of literature on the presence of trapped gas). While water table fluctuations induced from the Columbia River and near pumping wells can introduce trapped gas into the upper portion of the aquifer, the genesis of trapped gas in the deeper portions of an aquifer is not well understood.

In the presence of trapped gas bubbles, concentrations of dissolved gases are controlled by the volume of trapped gas and the concentrations of the gas within the bubbles (see Figure 4.1). When the trapped gas and dissolved gas are in equilibrium, the relative concentration in each of the phases is defined as the Henry's Law constant for that gas (e.g., solubility). Assuming equilibrium between the gas and aqueous phases and a gas phase uniformly distributed in the pore space, the following equation can be used to derive a retardation factor for the gas (in a manner similar to that used for distribution coefficients for the transport of sorbing species):

$$R = 1 + H * V_g/V_w \qquad (4.1)$$

where

R = retardation factor, ratio of groundwater velocity to dissolved gas velocity
H = dimensionless Henry's Law constant, [mass of gas/gas phase volume/mass of dissolved gas/water volume]
$V_g$ = volume of gas
$V_w$ = volume of water.

To use a gas tracer test for identification of the presence of trapped gas, the apparent retardation of a dissolved gas is measured relative to a conservative tracer (bromide). Equation 4.1 can then be used with the Henry's Law constant for the specific gas to determine the relative volume of gas in the aquifer ($V_g/V_w$). Using a number of dissolved gas tracers with differing Henry's Law constants provides for a test that is sensitive to a wide range of trapped gas volumes and for some cross-checking between results. It should be noted that this type of test assumes that that retardation of the test gas is affected only by gas phase partitioning. Because physical adsorption or chemical reactivity would produce a similar result, gases were chosen to minimize those potential effects.

Two dissolved gas tracer tests were conducted at the 100-D Area ISRM site, a small-scale push-pull test on a single well, and a larger well-to-well test with both an injection and an observation well. The dissolved gases used in the test and the Henry's Law coefficient are shown in Tables 4.1 and 4.2.

Air rotary drilling (ODEX) was used to install the wells at the ISRM site used in the dissolved gas tracer test. Observations in existing monitoring wells during the drilling of additional site wells indicated that the air rotary method was influencing water levels and

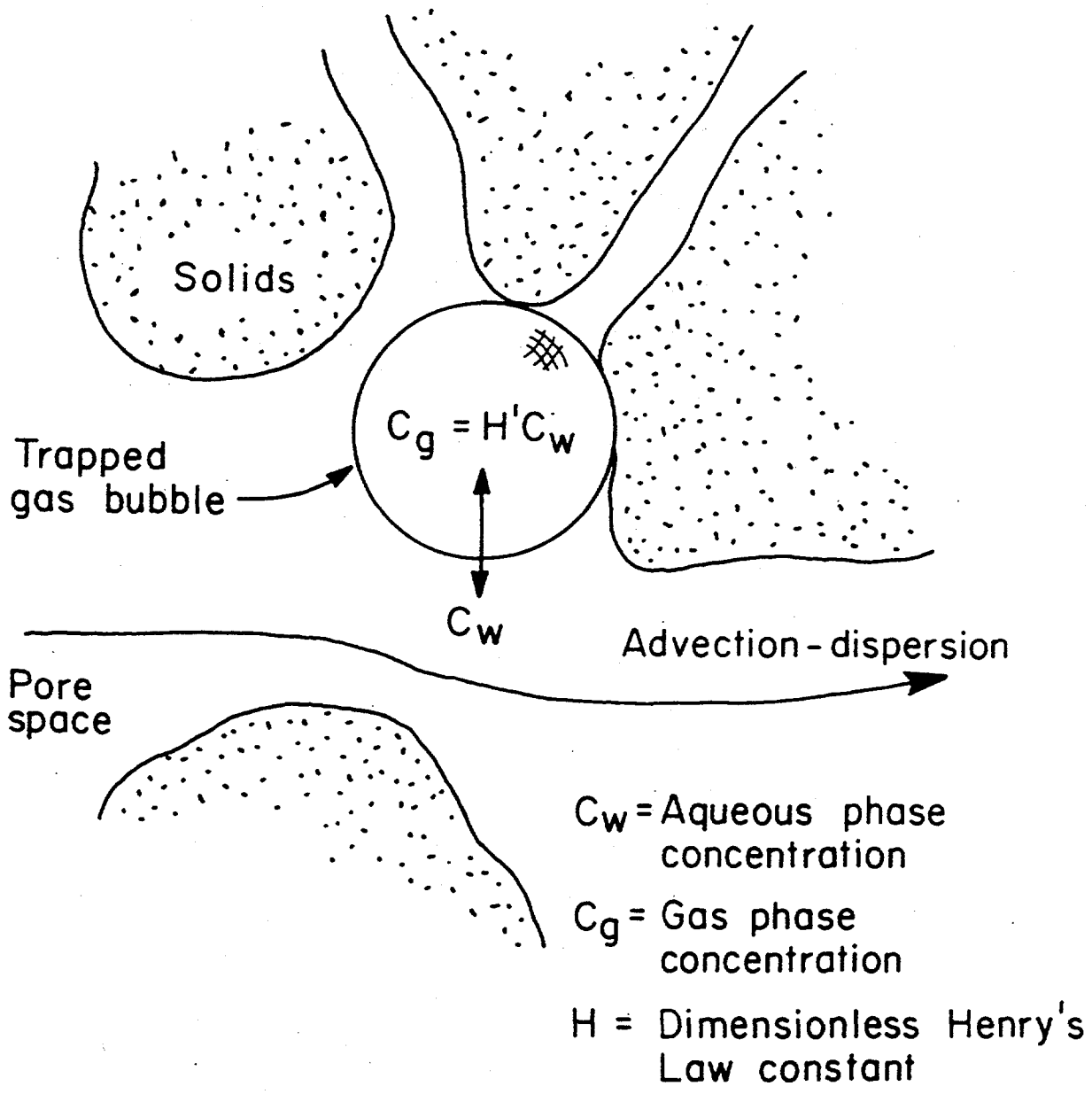


**Figure 4.1.** Conceptual Model of Dissolved Gas Transport in the Presence of a Trapped Gas Phase (from Frye et al. 1995, Figure 1)

dissolved oxygen concentrations at the site and potentially introduced some trapped air. It is recommended that additional dissolved gas tracer tests be conducted in wells that were installed at different locations with drilling methods other than air rotary (e.g., cable tool or resonant sonic). This will help verify the results obtained from this test and provide information on spatial variability of trapped gases at Hanford (far from the influence of the Columbia River). Although trapped gas is important for the behavior of dissolved oxygen transport in the aquifer, the results of these tests were not used to predict the fate of the anoxic plume. Neglecting the presence of trapped gas would result in a conservative estimate for the predictions.

**Table 4.1.** Properties and Concentrations of Gases Used in Push-Pull Test (3/26/98)

| Gas | Henry's Law Constant at 25°C | Percent/Cylinder Pressure |
|---|---|---|
| Nitrous oxide ($N_2O$) | 1.6 | 3% (40 psi) |
| Neon (Ne) | 91 | 12% (150 psi) |
| Nitrogen ($N_2$) | 63 | 85% (1110 psi) |
| Radon | 4.4 | None – radon-free water |
| Oxygen ($O_2$) | 31 | None |
| Carbon dioxide ($CO_2$) | 1.2 | None |

**Table 4.2.** Properties of Concentrations of Gases Used in Large Injection Test (4/24/98)

| Gas | Henry's Law Constant at 25°C | Percent/Cylinder Pressure |
|---|---|---|
| Nitrous oxide ($N_2O$) | 1.6 | 1.7% (22 psi) |
| Neon (Ne) | 91 | 9.6% (125 psi) |
| Sulfur hexafluoride ($SF_6$) | 136 | 0.23% (3 psi) |
| Nitrogen ($N_2$) | 63 | 88.5% (1150 psi) |
| Radon | 4.4 | None – radon-free water |
| Oxygen ($O_2$) | 31 | None |
| Carbon dioxide ($CO_2$) | 1.2 | None |

## 4.1 Push-Pull Test

The primary objective of the push-pull dissolved gas tracer test was to test the efficacy of a small-scale test (compared with the larger-scale test described in Section 4.2) to characterize trapped gases in the aquifer. A secondary objective of this test was to gain experience working with dissolved gas tracer tests before conducting the larger-scale test. The test was conducted in well D4-5 on March 26, 1998 (see Figure 2.3 for well location). A 500-gallon plastic tank filled with site groundwater was used to prepare the injection solution on March 11, 1998; this two-week period allowed any radon present in the groundwater to decay/degas. The injection solution was sparged overnight prior to injection with the compressed gas mixture shown in Table 4.1. Potassium bromide was also added to the injection solution for a nominal 100-ppm $Br^-$ concentration to be used as a conservative tracer.

In the push-pull test, 450 gallons of the dissolved gas tracer were injected into the aquifer at a rate of 3.0 gpm. Following the injection, 1281 gallons of groundwater were extracted from the aquifer at a rate of 3.0 gpm (2.8 times the injection volume).

### 4.1.1 Sampling

Aqueous samples for dissolved gas measurements were collected in 40-mL VOA vials with no headspace. Twenty milliliters of ultrapure nitrogen gas was added to the sample with a

syringe through the VOA vial septum while removing 10 mL of liquid with a second syringe, leaving a pressurized vial with a 10-mL headspace. The vial was stirred for three minutes to equilibrate the gas and liquid in the VOA vial prior to removal of a 10 mL sample of the headspace for analysis, as discussed below.

### 4.1.2 Analysis

Analysis for neon and nitrous oxide was performed in the mobile laboratory at the ISRM site using an MTI field-portable capillary gas chromatograph (GC) equipped with integral thermal conductivity detectors (TCDs). The GC was equipped with two columns operated in parallel, each with its own TCD. Neon separations were performed using a 5A molecular sieve capillary packed column operated with argon as the carrier gas. A Poraplot Q capillary column with helium carrier was used for nitrous oxide determination. Carbon dioxide, nitrogen, and oxygen peak areas were also recorded with the Poraplot Q channel. This GC has been shown to exhibit a highly linear response over a very wide dynamic range. All determinations of Ne and $N_2O$ were done on a relative basis with samples collected from the injection tank used for normalization of relative amounts. Radon samples were collected in 20-mL vials and returned to Oregon State University (OSU) for analysis by liquid scintillation counting. Bromide determinations were initially performed in the field using an ion-selective electrode. Because of concerns over potential sulfate interference, archived aliquots of the extracted samples were rerun for bromide by ion chromatography (IC) at OSU. Only the IC data were used in the discussions that follow.

### 4.1.3 Results and Discussion

The push-pull test provided an excellent opportunity to refine the methodology for the planned well-to-well test; however, because of the nature of the well itself (199-D4-5), the efficacy of this approach was limited. Loss of dissolved gas (particularly the relatively insoluble neon) occurred in the injection stream (large-diameter pipe [1.5 in.] for 3 gpm), which contained some air space due to the low flow rates used in the test. Some loss may also have occurred in the well bore itself, which was screened above the water table. For the same reason, mounding during the injection may have caused additional losses to the unsaturated zone. Results of the push-pull test are shown graphically in Figure 4.2. All results for bromide, nitrous oxide, and neon were normalized to the average maximum concentrations measured in the injection tank. The radon measurements were normalized to the maximum observed value at the end of the test. These data show a very sharp injection profile for bromide and nitrous oxide, but unfortunately neon showed considerable loss during injection. Radon-free water was injected to measure pick-up of gas-phase radon from void space in the aquifer. The radon measurements are thus not sensitive to injection losses. Radium, the parent of radon, is typically present at undetectably low levels in Hanford groundwater. Figure 4.3 shows a plot of the cumulative relative concentrations plotted as a function of extraction time relative to injection time. Bromide is plotted both directly for comparison to nitrous oxide and as 1 minus the bromide concentration for comparison with radon. Figure 4.3 shows very good correspondence between the non-gaseous tracer, bromide, and the water-soluble gaseous tracer, nitrous oxide. Radon, by contrast, exhibits a time offset of almost one hour to reach 50 percent of equilibrium. That suggests a substantial residence in the aquifer. Unfortunately, these data are also difficult to interpret because of uncertainties in the relative roles of sorption on sediment versus gas phase accumulation in unfilled pore space.

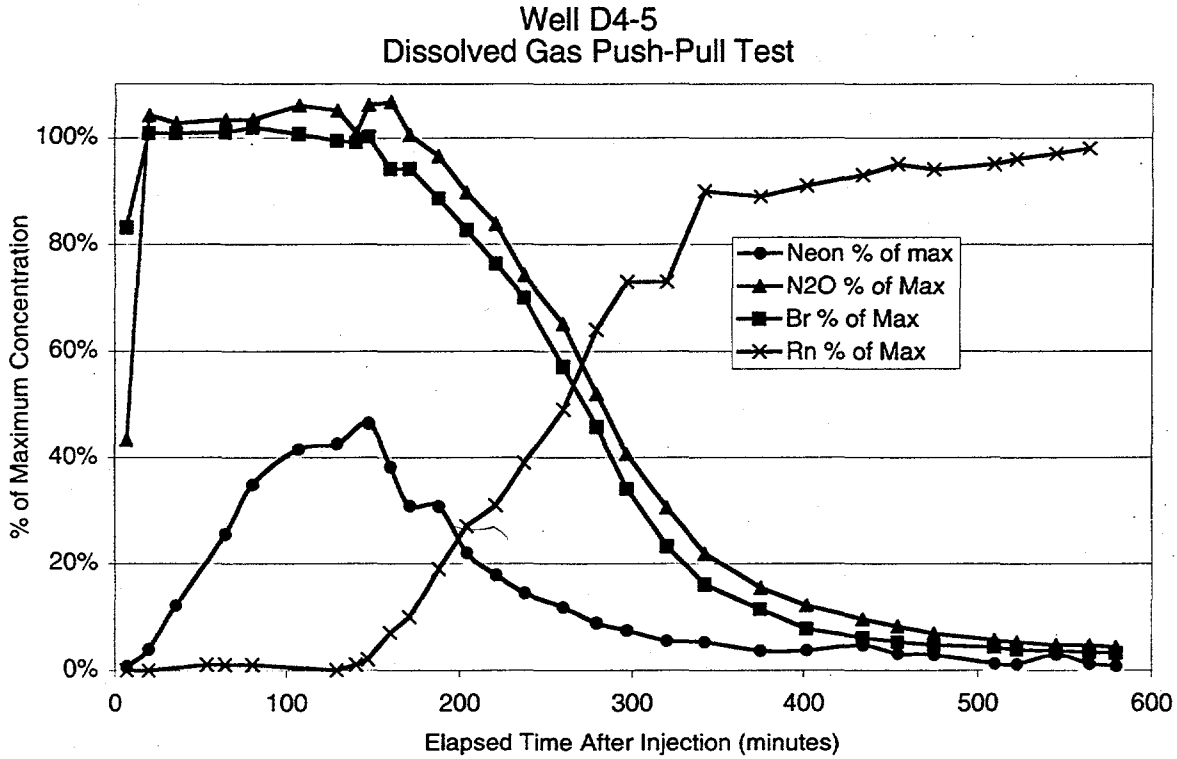


**Figure 4.2.** Dissolved Gas Push-Pull Tracer Test, Injection/Withdrawal Tracer Concentrations

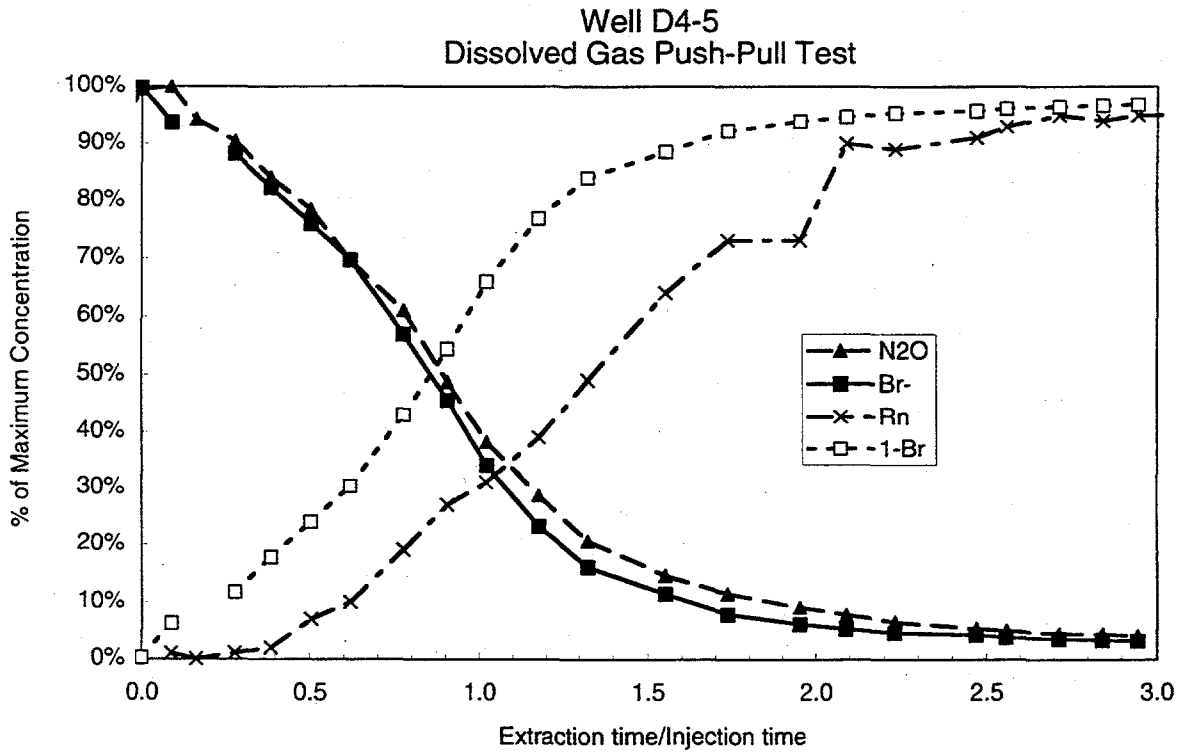


**Figure 4.3.** Dissolved Gas Push-Pull Tracer Test, Normalized Extraction Breakthrough Curves

## 4.2 Well-to-Well Injection Test

Twelve cylinders of compressed gas were prepared with the percentages and pressures of each gas tracer, as shown in Table 4.2. A 4,000-gallon mixing tank was filled with groundwater two weeks before the test to provide time for radon to decay/degas. Sparging stones were installed in an array along the tank bottom. The compressed gas cylinders and a headspace recirculation pump in the tank were connected to the sparging stones. Potassium bromide salts were added to the water as a conservative tracer. The injection solution was sparged the day before the injection at flow rates ranging from 5.7 to 1.25 cfm (cubic feet per minute) and sparged overnight at a rate of 0.6 cfm.

Well D4-5 was used for the injection well (same as the push-pull test), and Westbay well D4-17 was used as a multilevel observation well (see Figure 2.3 for well locations). These wells are separated by 3.05 m (10 ft). Well D4-5 screened over the entire unconfined aquifer from 78 to 98 ft bgs (below ground surface). Well D4-17 has three discrete vertical monitoring locations at 81 to 83 ft bgs (Zone 1), 87.5 to 89.5 ft bgs (Zone 2), and 95 to 96 ft bgs (Zone 3).

A pulse injection strategy was used where the gas tracer was injected first followed by a larger volume of groundwater. The gas tracer mixture was injected into well D4-5 at a flow rate of 40 gpm for 99 minutes (3,960 gallons total). The pulse of gas tracer was pushed out by 19,840 gallons of groundwater at a rate of 40 gpm for 496 additional minutes of injection.

### 4.2.1 Sampling

Aqueous samples for this test were collected directly into a 20-mL syringe using a luer-loc fitting. A 10-mL syringe with ultra high-purity nitrogen gas was connected to the water sample via a luer-loc coupling. The gas and water syringes were mixed together and stirred for three minutes prior to removing the gas sample in one syringe for measurement.

Samples were collected from a sampling port with a luer-loc fitting connected to the submersible pump installed in well D4-5. The Westbay sampler was more difficult for use with the highly insoluble gases (e.g., neon and $SF_6$), because these gases concentrate into the small headspace in the sampler. A vacuum pump was used to establish a hard vacuum in the sampler to minimize the headspace. For the Westbay well, D4-17, a luer-loc fitting and a 20-mL syringe were attached to the bottom of the Westbay sampler following sample collection. A syringe plunger was pushed into the top of the sampler to drive the water sample into the syringe. Given the discrepancies between samples measured from the submersible pump and the Westbay well, the Westbay sampler was also used in well D4-5 to establish values for normalization of the observation well measurements to the injection concentrations.

### 4.2.2 Analysis

Field analyses were performed in a manner similar to that described in Section 4.1.2. Initially, sulfur hexafluoride measurements were also made with the MTI system on the 5A molecular sieve channel using helium carrier flow instead of argon. Under those conditions, the instrument was transparent to helium, and $SF_6$ elutes very early, well in advance of neon.

However, sensitivity was marginal for $SF_6$ by this method so gas samples were archived in empty VOA vials for subsequent reanalysis by GC/MS (using an HP 5971 system with a 60 m DB-1 column). Only the GC/MS results were used for the final data analysis.

### 4.2.3 Results of Test

Results for the three zones sampled in the well-to-well test are displayed graphically in Figures 4.4, 4.5, and 4.6, respectively. The data are plotted as a fraction of the maximum concentration measured at the injection well using the Westbay sampler lowered into the well. An average of the three measurements taken during the injection period was used to calculate the normalizing factor. All plots are referenced against the number of minutes elapsed since injection began. The three plots show quite different behavior, reflecting the large differences in geologic conditions over those zones. Zone 1, the upper zone, shows significant loss of all four tracers including bromide due to dispersion effects over the 10-hour collection period. At the end of the collection time, bromide levels had returned to low values in Zone 1. Neon and nitrous oxide exhibited much larger losses to the formation and a significant amount of retardation. Transit time was much more rapid in Zone 2, the middle zone, for all four species. Bromide concentrations approached the full injection level, and all four species tailed out to very low levels within about four hours. Zone 3, the lower zone, has a relatively low permeability with correspondingly longer transit times between wells. Observed analyte loss was large for all

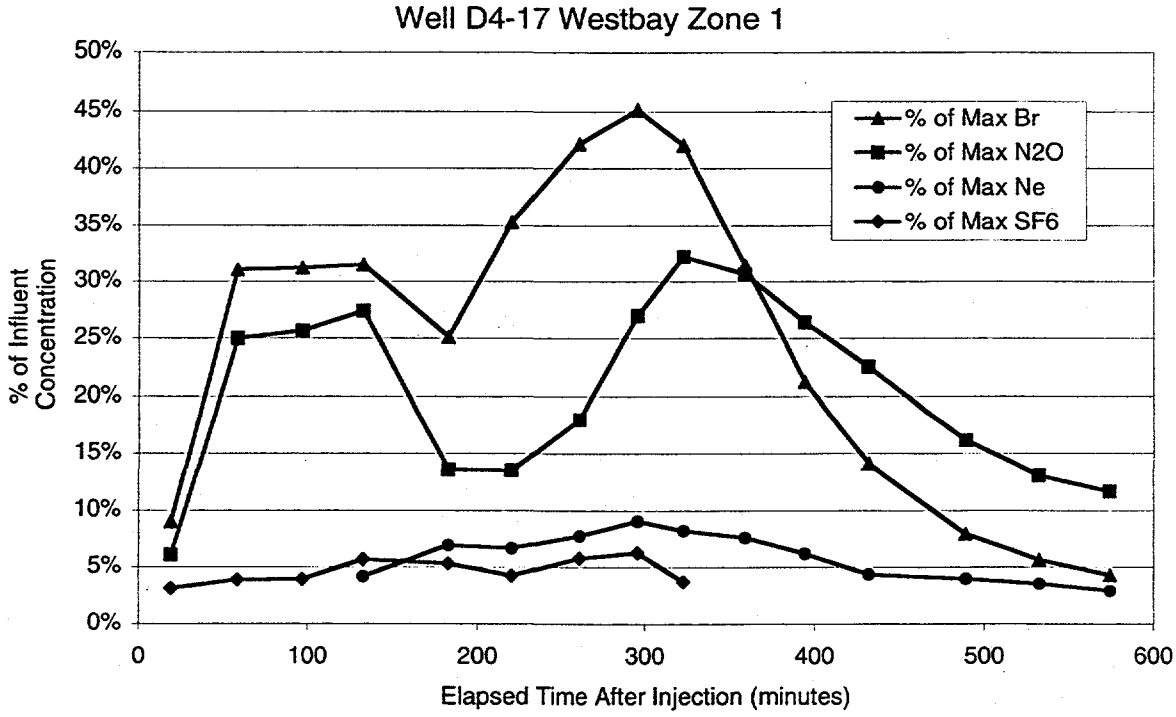


**Figure 4.4.** Dissolved Gas Tracer Test, Zone 1 Breakthrough Curves

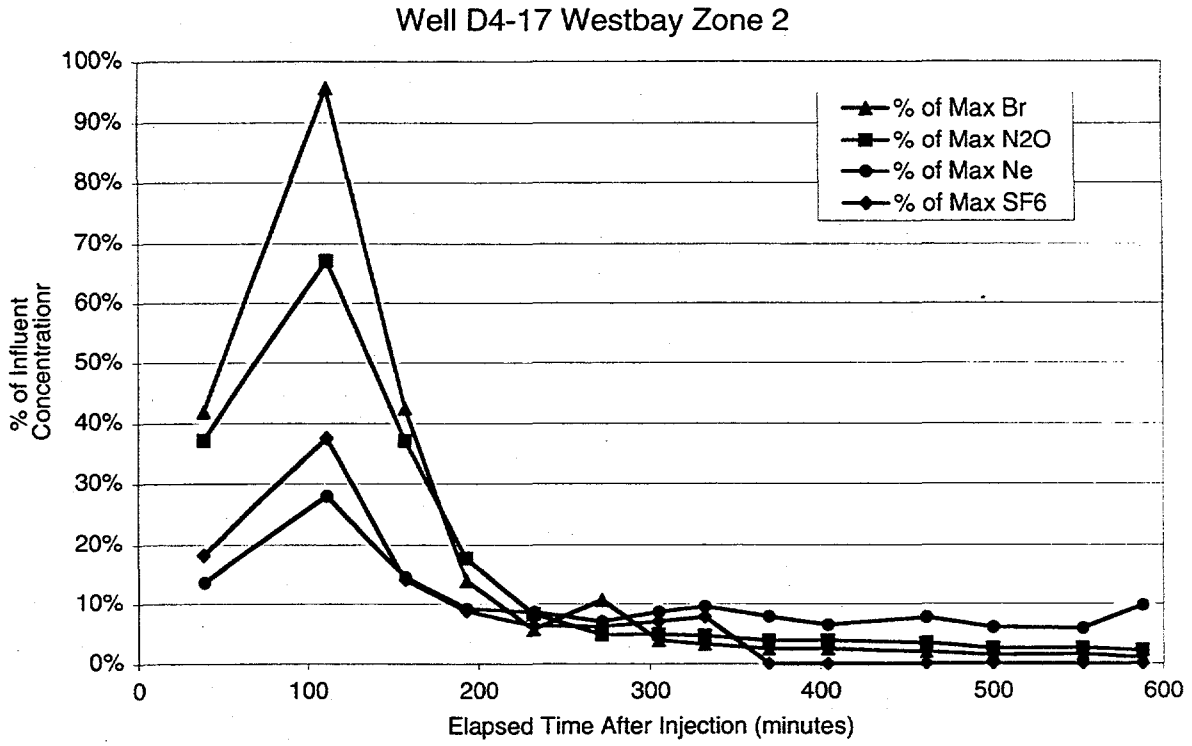


**Figure 4.5.** Dissolved Gas Tracer Test, Zone 2 Breakthrough Curves

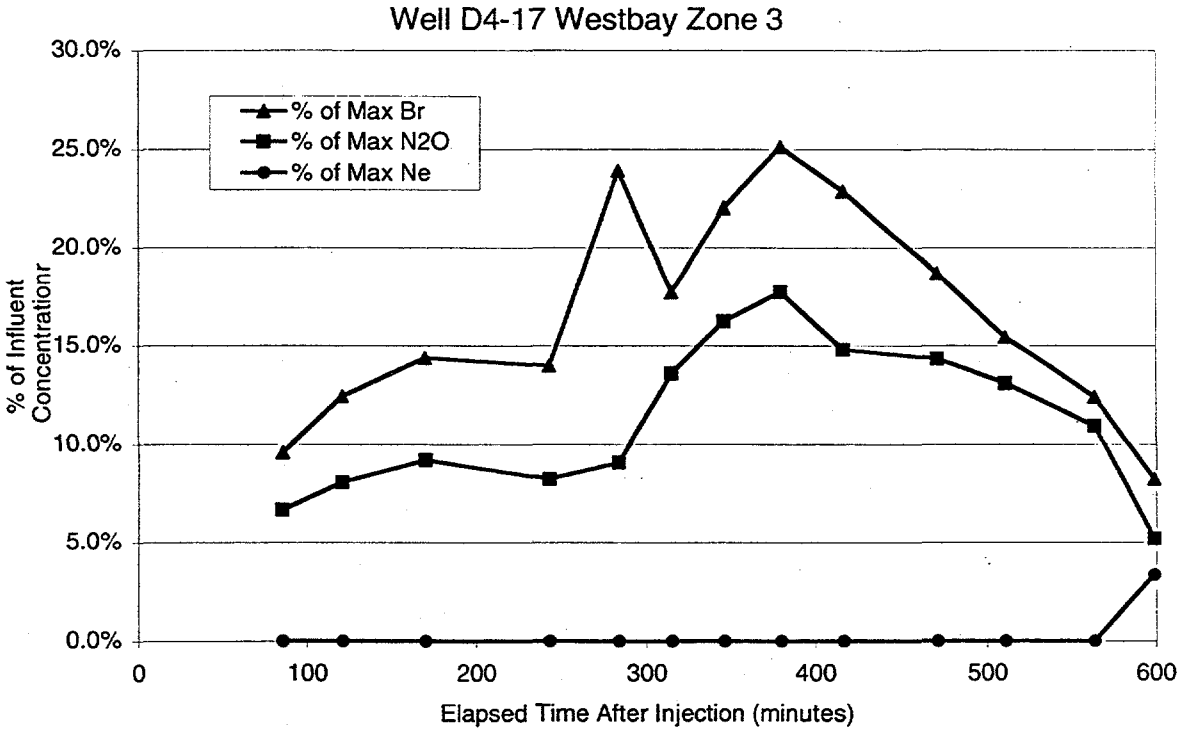


**Figure 4.6.** Dissolved Gas Tracer Test, Zone 3 Breakthrough Curves

four components, with the low-solubility species disappearing altogether. Recovery of bromide was still incomplete after 10 hours. Detectable neon appeared only in the last sample taken before the test was terminated.

To define the effect of retardation better, the same data were replotted as running totals or cumulative plots. The three cumulative plots are displayed in Figures 4.7, 4.8, and 4.9. To produce these plots, each data point was normalized to the time interval between measurements and the maximum concentration measured as discussed above. Running totals were then computed and a final renormalization performed to make the final bromide number equal to 100 percent in each zone. Retardation factors were then computed from these plots by calculating the 50 percent crossing time for each species. The crossing times are based on a linear regression calculation for the two or three data points spanning the 50 percent level. The results of that calculation are presented in Table 4.3. This procedure could be used only for species that reached 50 percent.

## 4.3 Discussion of Results

While the results of these tracer tests were highly variable and difficult to quantify, they strongly suggest that the presence of trapped gas within the aquifer at this site can influence the transport behavior of dissolved gases. Overall, the relative arrival times for the dissolved gas tracers in these wells follow the order of Henry's Law coefficients, with the relatively high

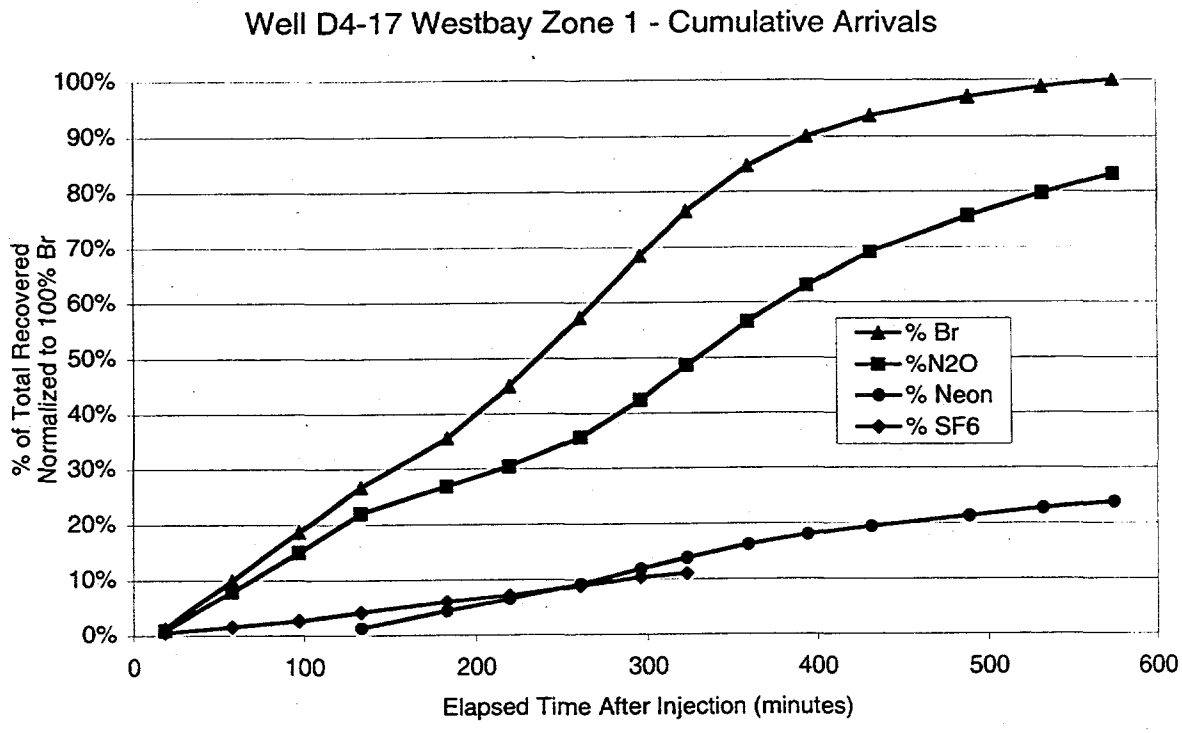


**Figure 4.7.** Dissolved Gas Tracer Test, Zone 1 Cumulative Arrival Curves

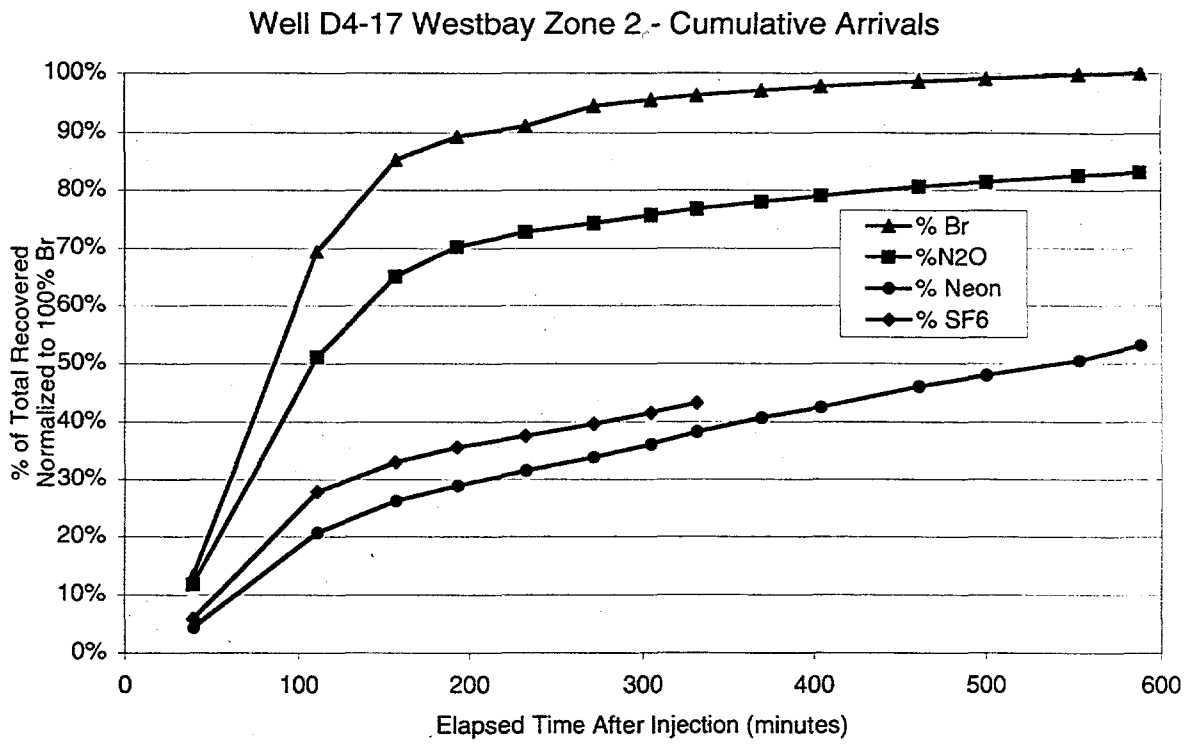


**Figure 4.8.** Dissolved Gas Tracer Test, Zone 2 Cumulative Arrival Curves

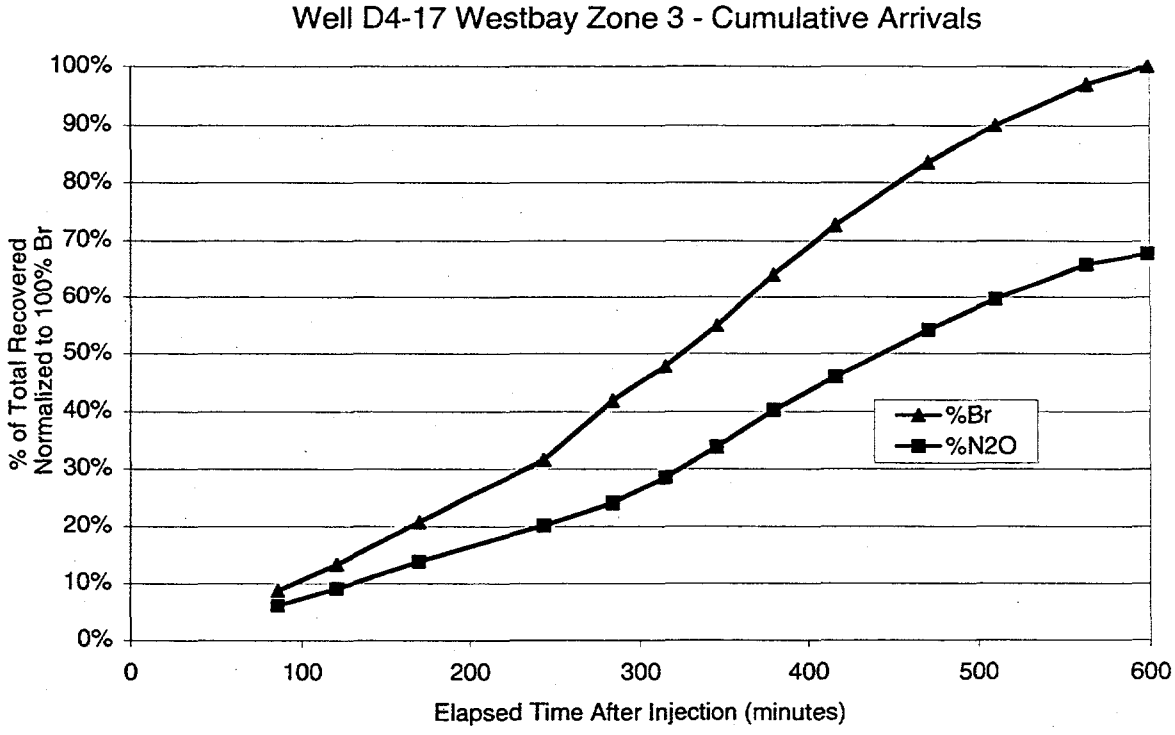


**Figure 4.9.** Dissolved Gas Tracer Test, Zone 3 Cumulative Arrival Curves

**Table 4.3.** Calculated Results from Well-to-Well Tracer Test

| Zone/Tracer | 50% Crossing Time (minutes) | Retardation Factor (R) | Unfilled Pore Volume Ratio ($V_g/V_w$) |
|---|---|---|---|
| **Zone 1** | | | |
| Bromide | 237 | ≡ 1 | |
| Nitrous oxide | 325 | 1.4 | 0.23 |
| **Zone 2** | | | |
| Bromide | 86 | ≡ 1 | |
| Nitrous oxide | 108 | 1.3 | 0.16 |
| Sulfur hexafluoride | 424 | 4.9 | 0.03 |
| Neon | 532 | 6.2 | 0.06 |
| **Zone 3** | | | |
| Bromide | 325 | ≡ 1 | |
| Nitrous oxide | 453 | 1.4 | 0.25 |

solubility tracers (low H, thus low R) arriving before the more insoluble tracers (high H, high R). The one exception to this trend was Well D4-17, Zone 2, where the $SF_6$ peak arrival was of a higher concentration than neon (though occurring at the same time). $N_2O$, the gas with the lowest H, tracked closely with $Br^-$ and was widely separated from the more insoluble neon and $SF_6$ in all the observation zones. Estimates of the percent trapped gas varied widely based on the gas tracers and zone (see Table 4.3), with a range of 16 to 25 percent pore space estimated for the three zones using $N_20$. Zone 2 was the only one in which sufficient concentrations were measured to enable retardation (thus trapped gas) estimates from the insoluble tracers. These resulted in much lower estimates (3 percent using $SF_6$; 6 percent using neon) than from $N_20$.

Although dissolved gases are challenging to sample and analyze, the variability in these tracer breakthrough curves for the well-to-well test are primarily due to heterogeneities in the aquifer, as evidenced by the highly variable bromide data measured both by ion-selective probes during the test and IC analysis on archive samples afterward. The vertical variability in bromide arrival times measured at the three depths of the observation well indicate that the permeability and/or porosity distribution of the aquifer at this location results in much faster velocities in the center of the aquifer (Zone 2) and much slower velocities in the top and bottom portions (Zones 1 and 3). The Zone 1 peak arrival times were earlier than Zone 3. The impact of these heterogeneities on the design of the test was that the injection rate (or duration) was too high for the middle zone but too low (or not of sufficient duration) for resolving the breakthrough curves in the upper and lower zones. In addition, the peak concentrations measured in Zones 1 and 3 were significantly dampened for the tracer pulse (less than 45 and 25 percent, respectively).

The results of these dissolved gas tracer tests were judged not quantifiable and have provided conclusive evidence of trapped gas within the aquifer. Larger volumes of gas tracers and longer duration injections at slower rates would help reduce the sensitivity of these tests to local heterogeneities. These results should help guide future tests, if needed, with the choice of suitable gases to use for tracers and the wide range of retardation factors that must be measured.

# 5.0 Numerical Modeling

A numerical model of the site was developed for predicting dissolved oxygen concentrations downgradient from the 100-D Area ISRM site. Two basic models were developed: a simple model for investigating the impact of oxygen diffusion from the vadose zone above the water table and a more complex model that also accounts for the dynamics of the fluctuating water table. The fluctuating water table model was developed based on previous work at N-Springs by Connelly et al. (1997).

The three simulations discussed in the following sections are presented to help quantify the effects of reoxygenation of an anoxic plume from some of the processes as outlined in Figure 1.3. A simple diffusion simulation across a static water table will help to provide a conservative estimate of the mass of oxygen that can diffuse across the water table during the transport of groundwater from the ISRM site to the river, 160 m downgradient. A conservative tracer simulation was run to establish the range of concentrations discharging to the river from mixing/dilution of river water entering and exiting the aquifer during fluctuating river stage (i.e., bank storage). The final simulation accounts for air entrapment and reoxygenation from a fluctuating water table and necessarily incorporates the effects of the first two simulations (diffusion and river water mixing from a fluctuating river stage). Based on the results of these three simulations, the relative importance of these processes can be estimated and compared.

Not all processes shown in Figure 1.3 were incorporated into these simulations. Those not modeled include trapped gas deep below the water table and upward oxygen diffusion from the underlying aquitard (i.e., Ringold mud). The omission of these reoxygenation mechanisms, due to uncertainties in the parameters, should yield a conservative estimate of the dissolved concentrations downgradient from the ISRM site.

These simulations used the STOMP numerical code (White and Oostrom 1999) as discussed in Section 3. The tracer simulation needed only the water mode with solute transport (STOMP1). The diffusion and fluctuating river stage simulations used the mode for water, air, and solute transport (STOMP2). Features common to the models are described below with specific details and results of each simulation discussed in the respective sections.

## 5.1 Common Model Features

### 5.1.1 Domain and Finite Difference Grid

The finite difference grid used in these simulations is shown in Figure 5.1. The simulations are two-dimensional (x-z) cross-sections representing the unconfined aquifer in the Ringold gravels and a portion of the vadose zone above (Figure 1.4). A 1-m width was specified in the y-direction, parallel to the Columbia River. The bottom of the grid, at an elevation of 113.7 m, was set at the bottom of the unconfined aquifer (top of the Ringold mud), as discussed in Section 2.1. The left portion of the model domain represents the unconfined aquifer at the river shoreline. The deep channel in the river near the bank at D-Area (depicted in Figure 1.4), in which the river channel may be incised into Ringold sediments of the upper unconfined aquifer

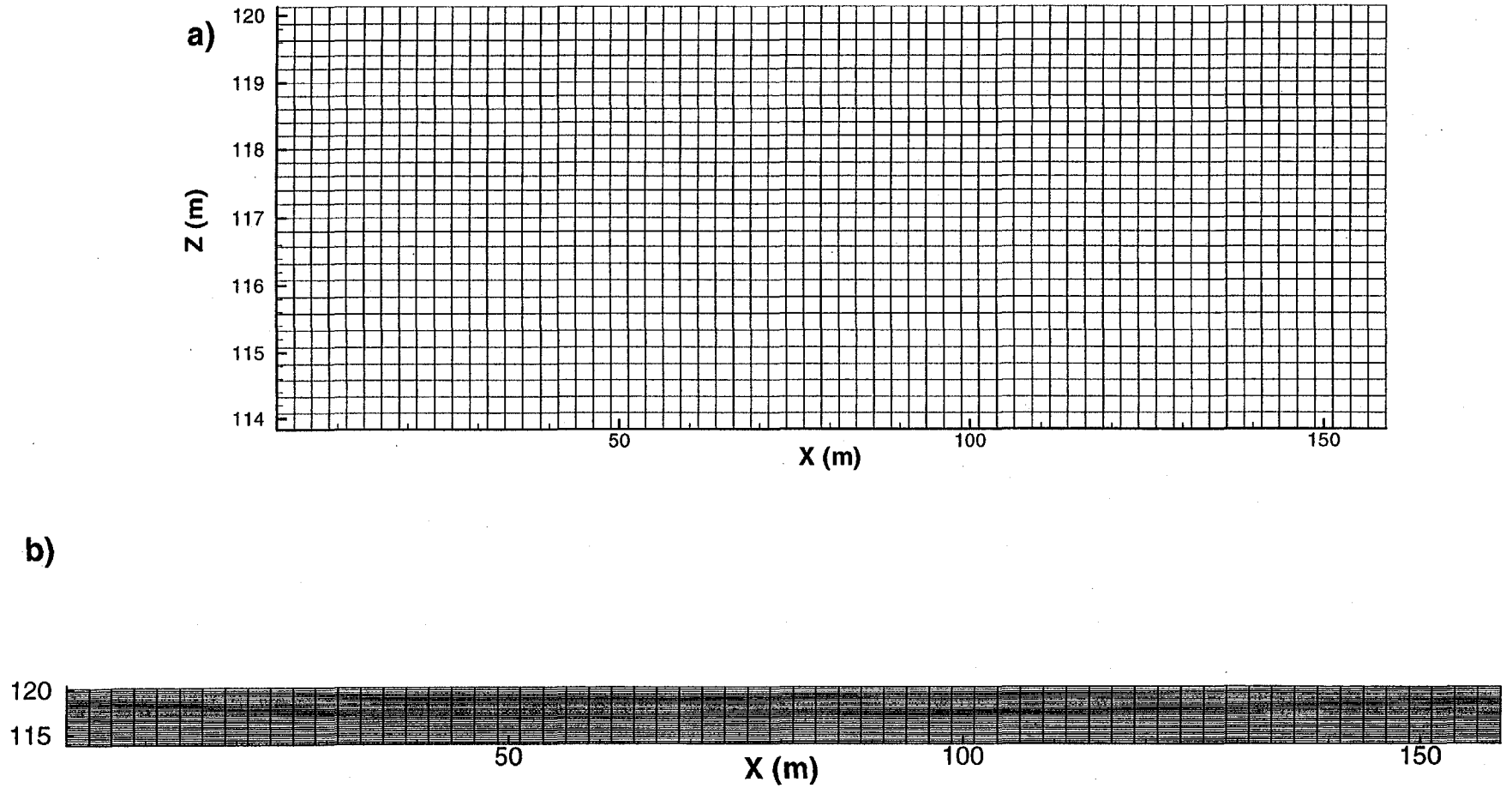


**Figure 5.1.** Finite Difference Grid Used in 100-D Area ISRM Simulations (shown with no vertical exaggeration in [b])

in this location, also justifies this simplified geometry. The exact Columbia River/upper aquifer interface (within a few meters of the river channel), incorporating the influence of turbulent flow and the Hyporeic zone, was not modeled.

The 160-m (525-ft) length (x-direction) is the distance between the 100-D Area ISRM site and the Columbia River. Although the Columbia River can still influence the water table elevation at that distance (see N-Springs example in Figure 2.10), the magnitude is small (<0.05 m on the daily cycle) and seems to respond more to seasonal trends and extreme events than most daily river fluctuations. Primarily, the domain was limited to this distance to minimize the simulation times, and it should not change the results significantly.

As shown in Figure 5.1, a constant 2.5-m horizontal grid spacing was used. Grid spacing in the vertical direction ranged from 0.2 to 0.25 m, with the finest grid spacing near the water table. Simulations run with a 0.1-m vertical grid spacing indicated that the coarser grid was adequate and provided for shorter execution times. The final grid comprised 64 nodes in the x-direction by 29 nodes in the z-direction (1856 nodes total).

### 5.1.2 Hydraulic Properties

A single homogeneous isotropic geologic unit was used for the unconfined aquifer in these simulations representing the Ringold E gravels, as shown in Figure 1.4. Table 5.1 summarizes the hydraulic properties specified for this unit. Hydraulic conductivity was determined through aquifer testing at the 100-D Area ISRM site (see Williams et al. 1999). The porosity was determined from the physical property measurements on six sediment samples collected during installation of wells at the ISRM site.

In situ unsaturated hydraulic properties of Ringold gravels are not well characterized or documented. A Brooks-Corey function with air entrapment was used to model the unsaturated zone. Published parameters of van Genuchten characteristic curves for Hanford and Ringold gravels (Rockhold 1993) measured on core samples were consulted to estimate the ranges in these parameters for local sediments (i.e., for deriving air entry pressure and lambda), but the saturated hydraulic conductivity values published with these data were substantially different than field measurements. The values for the Brooks-Corey function were also derived from laboratory soil moisture measurements of Ringold sediments (i.e., gas residual saturation) and

**Table 5.1.** Hydraulic Properties Used in 100-D Area Simulations

| Parameter | Value | Units |
|---|---|---|
| Hydraulic Conductivity (Kx) | 54 | feet/day |
| Anisotropy (Kz/Kx) | 0.1 | |
| Porosity | 0.14 | |
| Specific Storage | 1.0E-6 | $m^{-1}$ |
| Brooks/Corey (psi) | 18 | cm |
| Brooks/Corey (lambda) | 2 | |
| Gas Residual Saturation | 0.15 | |
| Residual Water Saturation | 0.02 | |

the resulting simulated water saturations. The Burdine relative permeability function was used for aqueous and gas relative permeabilities in the unsaturated zone, as described in Section 3.

### 5.1.3 Transport Parameters

These simulations use STOMP2, which simulates transport of both a water and air phase. Because air is mostly nitrogen (78 percent nitrogen, 21 percent oxygen), an oxygen solute was used that partitions into the aqueous and gas phases. Transport parameters used in the simulations are summarized in Table 5.2. Parameters for oxygen were taken from Donaldson et al. (1997) and Fry et al. (1995) at 20°C. Oxygen concentrations in air were set to 261 $g/m^3$, which results in a saturated dissolved oxygen concentration of 8.6 mg/L at 1 atm and 20°C using the Henry's Law coefficient for oxygen shown in Table 5.2.

The gas-phase molecular diffusion coefficient for oxygen selected for these simulations was the standard published gas phase value shown in Table 5.2 with the Millington and Quirk (1960) function for diffusion tortuosity in the STOMP code. Although a lower value was required for modeling the intermediate scale water table fluctuation experiment discussed in Section 3, this modification was to correct for predictions at a scale less than the 20-cm grid spacing used in these simulations.

Additional laboratory studies were conducted with a sieved portion of Ringold gravels collected from cores from the site in a fluctuating water table experiment (as described for the sand in Section 3). The dissolved oxygen measurements from this test were similar to the results of the sand tests discussed previously. This poorly sorted sediment made it difficult to achieve a uniform packing within the flow cell, resulting in heterogeneities. These heterogeneities make the interpretation of the experimental results less clear. Gamma measurements of water saturation during the Ringold test resulted in a wide range of entrapped air—from 20 to 40 percent. Porosity measurements of the flow cell packed with the Ringold sediments ranged from 10 to 24 percent. The average porosity determined from six core samples for the entire core was 14 percent (with a range from 5 to 18 percent). Because the large size fraction (>4 mm) of the

**Table 5.2.** Transport Parameters Used in 100-D Area ISRM Simulations

| Parameter | Value | Units |
|---|---|---|
| Longitudinal dispersivity | 0.2 | m |
| Transverse dispersivity | 0.02 | m |
| Oxygen: Henry's Law coefficient | 30.5 | Dimensionless (gas mass/gas volume)/ (dissolved gas mass/water volume) |
| Oxygen: Aqueous-phase molecular diffusion coefficient | $2.0 \times 10^{-9}$ | $cm^2/s$ |
| Oxygen: gas-phase molecular diffusion coefficient | $2.0 \times 10^{-5}$ | $cm^2/s$ |

sediment was not used in the flow cell, which made up as much s 60 percent of the total sediment samples, the average air entrapment percent measured during the test was reduced to 15 percent in these simulations to account for these larger particles (i.e., gas residual saturation 0.15).

Concentrations of oxygen within the gas of the vadose zone were set to atmospheric values based upon soil gas monitoring conducted at the 100-D Area ISRM site. Well D4-18 had a soil gas monitoring tube installed during drilling at a depth of 74.5 ft below ground surface (approximately 5 ft above the average water table). Analysis of gas samples collected from this tube showed atmospheric concentrations. The analysis methods and equipment used in the dissolved gas tracer test (discussed in Section 4 above) were used to measure these soil gas samples for $CO_2$ and $O_2$.

### 5.1.4 Boundary Conditions

Boundaries on the bottom and sides (y-direction) of the finite difference grid shown in Figure 5.1 were set to "no flow" for water or oxygen. The no-flow boundary on the sides represents a zone of infinite width parallel to the river (i.e., no oxygen fluxes are permitted from the sides). The bottom no-flow boundary ignores any upward movement of water into the unconfined aquifer from the Ringold mud below. This condition provides a conservative estimate for the predictions in these simulations given the uncertainty in the upward groundwater flow through the aquitard in this area.

For the upper boundary, gas pressures and oxygen concentrations were set to 1-atm values. A 2-mm/yr recharge rate was also specified along the upper boundary. A relatively low value for recharge (approximately an order of magnitude less than estimated values for the area) (see Fayer and Walters 1995) provides for conservative simulation results without adding more complexity and uncertainty.

The most complex portion of these simulations is the left boundary, representing the aquifer at the Columbia River shoreline. Figure 2.12 shows hourly Columbia River stage measurements made in the D-Area (at the pump house near the ISRM site) during 1998. To incorporate some natural complexity into the model, hourly river levels from the first quarter of 1998 were used to specify the water table elevations in the fluctuating water table simulations. This 90-day river stage cycle was then repeated for the duration of the simulation. This time period was selected because it included a wide range of daily and weekly cycles without being an extreme case in range and elevation. River levels are highly dependent on operation of the dams. Spring levels are generally the highest of the year, from flooding (see Figure 2.12b), and the average river stage drops during the summer. River stage is the lowest in the fall and has a wide daily range. Thus the results of the simulations from a more "normal" period would not make long-term predication dependent on extreme events and are easier to implement numerically. The mean river stage during the first quarter of 1998 was 118.1 m. This value was used to maintain a constant river level for the diffusion-only simulation with a static water table.

Water entering the aquifer from the left boundary (when the river level is high relative to the aquifer) is saturated with dissolved oxygen. Above the water table on the left boundary, the gas pressures and oxygen concentrations were set to atmospheric values.

On the right boundary, representing the ISRM site, a dirichlet boundary condition was imposed, resulting in a constant water table elevation of 118.4 m (from measurements of wells at the ISRM site on January 28, 1998). Although the water table at the site does vary, particularly during the spring and summer of 1997 when water levels at the site were up to 1.5 m higher from the flooding in the Columbia River, hourly water table fluctuations were small for most typical periods. In addition, hourly water level data were not available for the site during the simulation period of interest. For most of the simulations, water entering the system from the right boundary is anoxic (0 mg/L dissolved oxygen), representing the dissolved oxygen concentrations immediately downgradient of the ISRM site. Above the water table on the right boundary, the gas pressures and oxygen concentrations were set to atmospheric values.

### 5.1.5 Initial Conditions

Before these simulations began, the entire system was initially saturated and then slowly drained. During the initial saturation period, oxygen- and air-saturated water was flushed upward through the aquifer to achieve uniform concentrations. The system was drained to 0.2 m below the starting water table value and then raised to the required level. A static water level was then maintained for a period of seven years to achieve quasi-steady state conditions for the water saturations in the vadose zone. The air and aqueous pressure boundary conditions were applied to the top and sides of the model domain during this seven-year period to allow gas pressures to equilibrate.

## 5.2 Oxygen Diffusion Across A Static Water Table

The purpose of this simulation is to quantify the diffusive fluxes of dissolved oxygen into the anoxic aquifer across a static water table from the vadose zone above, as shown in the conceptual diagram in Figure 1.3. The water table on the right boundary (i.e., ISRM site) was held constant at an elevation of 118.4 m (measured at the site in January 1998). The water table elevation at the left boundary (i.e., river) was held constant at 118.1 m, the mean Columbia River stage measured at 100-D Area during the first quarter of 1998. This hydraulic gradient results in a porewater velocity of 0.23 m/day (0.74 ft/day) for the 4.6-m (15-ft) average aquifer thickness.

For initial conditions, the entire system was set to dissolved oxygen saturation (8.6 mg/L). At the start of the simulation, water entering the system from the right boundary was anoxic (0 mg/L DO). Figure 5.2 shows the development of the anoxic plume as it migrates toward the left river boundary. This shows that by thee years the anoxic plume has reached the river; then only relatively small changes occur in dissolved oxygen concentrations during the next 22 years. After 25 years, water entering the system from the right boundary was set back to dissolved oxygen saturation, as shown in Figure 5.3 representing the average longevity estimated for the reducing conditions for the 100-D Area ISRM site. The aquifer had returned to mostly oxic conditions within another three years. The slow reoxygenation shown in Figure 5.3 near the water table is due to trapped air bubbles in this zone that have been depleted in oxygen. Although the water table was static in these simulations, some air entrapment occurred from the establishment of the initial water table conditions and soil moisture profile, as discussed in Section 5.1.4. This trapped gas remained for the entire simulation and was included to provide comparable results for the fluctuating water table simulations.

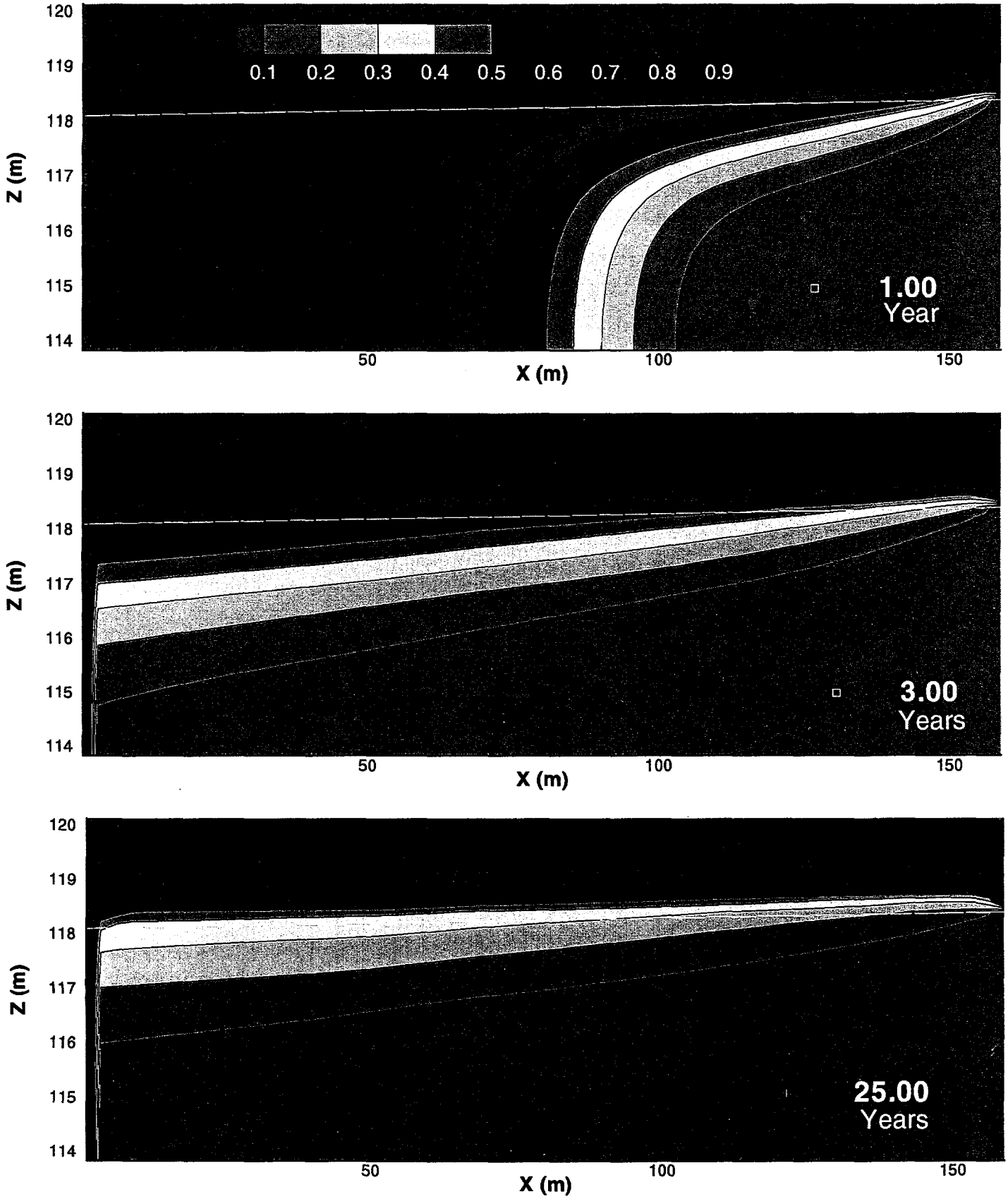


**Figure 5.2.** Oxygen Diffusion Across a Static Water Table Simulation Results. Anoxic water enters the right boundary from 0 to 25 years.

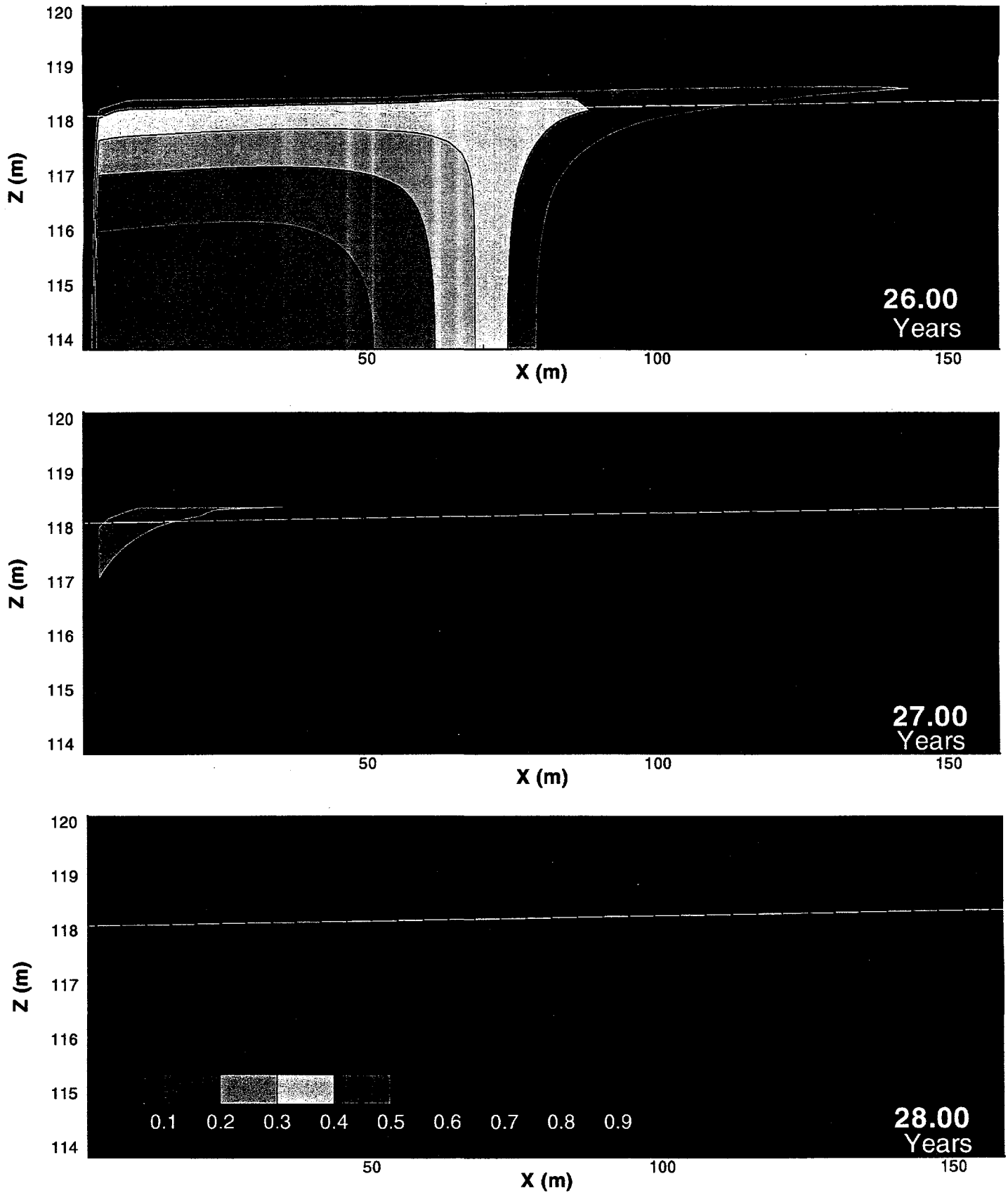


**Figure 5.3**. Oxygen Diffusion Across a Static Water Table Simulation. Anoxic water enters the right boundary from 0 to 25 years. Oxygen-saturated water then enters from 25 to 30 years.

Dissolved oxygen fluxes in the simulation are summarized in Figure 5.4. This figure plots the oxygen fluxes at various vertical planes in the aquifer along the cross-sectional model. Figure 5.4 also includes the oxygen flux across a horizontal plane at the top of the aquifer. The dissolved oxygen fluxes are a product of the groundwater flux for the aquifer and the dissolved oxygen concentrations. These data were normalized to the oxygen flux at the river under saturated dissolved oxygen concentrations. The oxygen fluxes for the first six years of the simulation, including the initial development of the anoxic plume, are shown in Figure 5.4a. The dissolved oxygen fluxes drop first at distances closest to the ISRM site (160 m). At the river boundary, dissolved oxygen fluxes dropped rapidly between the second and third year to less than 30 percent of the saturated values and then decreased much more slowly to 20 percent saturation after six years. The oxygen flux at the top of the aquifer, representing the oxygen mass diffusing into the aquifer from above the water table, matches the flux of dissolved oxygen to the river by six years.

Figure 5.4b shows the oxygen fluxes for the final six years of simulation time when oxygenated water was reintroduced into the system at 25 years. The recovery again illustrates that oxygen concentrations are mostly recovered at the river boundary after three years to 90 percent saturation. The oxygen fluxes at the top of the aquifer show a negative flux (out of the aquifer), which is driven out of the aquifer by the lower oxygen concentrations above the water table in the lower portion of the vadose zone.

An additional diffusive flux of oxygen is expected from the Ringold mud unit aquitard below the unconfined aquifer. This flux was not accounted for in the simulations due to the uncertainties in hydraulic properties and the water flux from this layer. For very low permeabilities and fluxes, the long-term diffusive flux from this unit may be negligible once the oxygen is depleted in the upper portion. Results from this simulation are very conservative and should be interpreted as the minimum predicted oxygen flux to the river because they neglect oxygen flux from below, mixing of river water within the aquifer, and reoxygenation in a fluctuating water table.

## 5.3 Behavior of a Tracer in a Fluctuating Water Table

Simulations were conducted for a conservative, nonreacting tracer that is released at the right boundary (ISRM site) to investigate the effects of dilution and mixing of the tracer as it migrates downgradient from the ISRM site and discharges into the river. This process is shown in the conceptual diagram in Figure 1.3. As mentioned previously for the fluctuating water table simulations, pressures on the left boundary (i.e., river) were specified hourly and taken from the Columbia River stage measured at 100-D Area during the first quarter of 1998 (Figure 2.12a). This 90-day cycle was repeated for the duration of the simulation. Tracer behavior would be similar to chromate migrating from this distance to the river prior to the installation of the ISRM barrier.

### 5.3.1 Simulated Water Table Response

The hydraulic head results for the simulation at selected distances from the river boundary are shown in Figure 5.5 for the second 90-day cycle. These data show that simulated hydraulic heads within a 25-m distance respond rapidly to hourly river-stage changes, although the magnitude of the response is damped. The water table 50 m from the river still responds to most daily

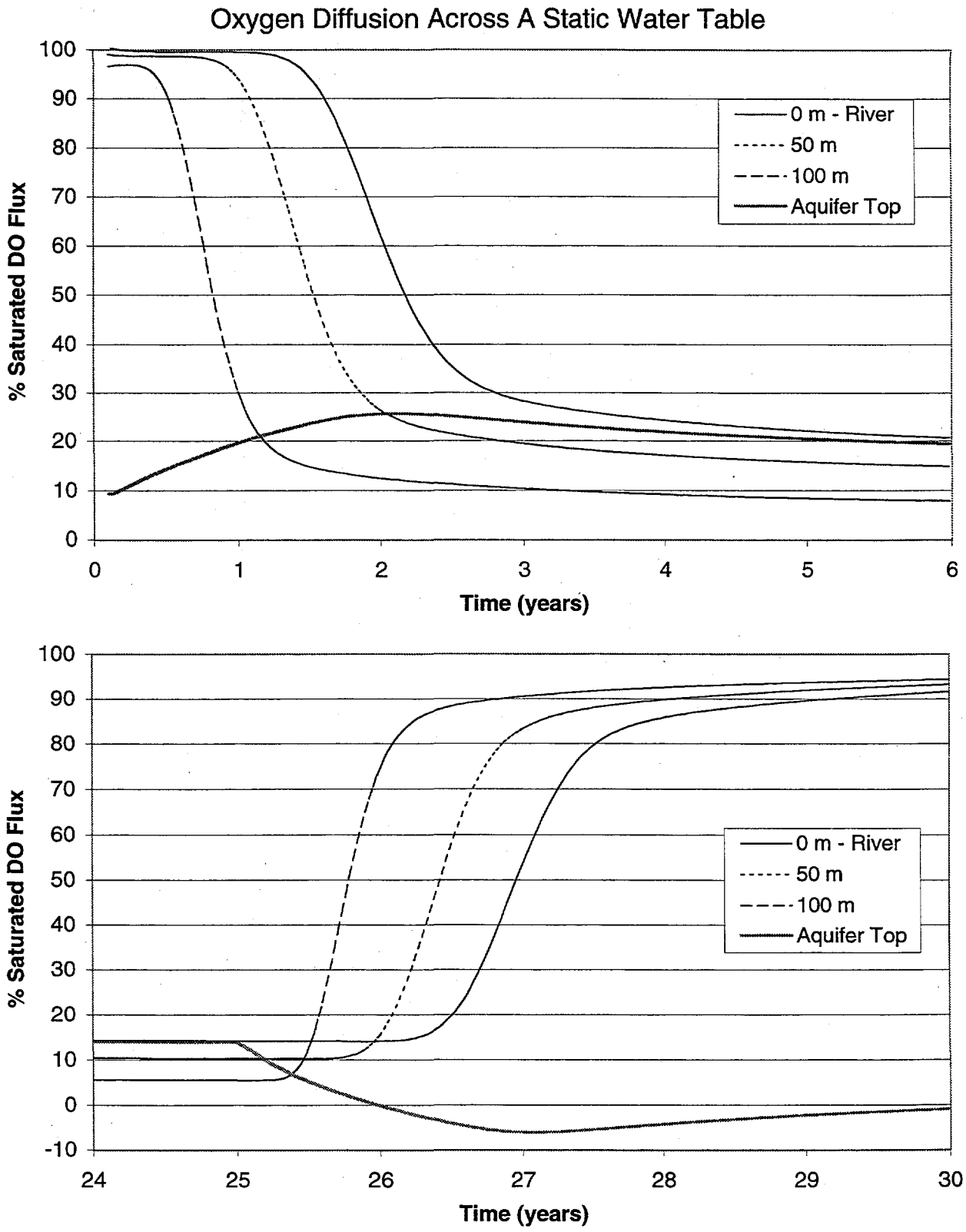


**Figure 5.4.** Oxygen Diffusion Across a Static Water Table. Anoxic water entered the system at the right boundary (160 m) from 0 to 25 years.

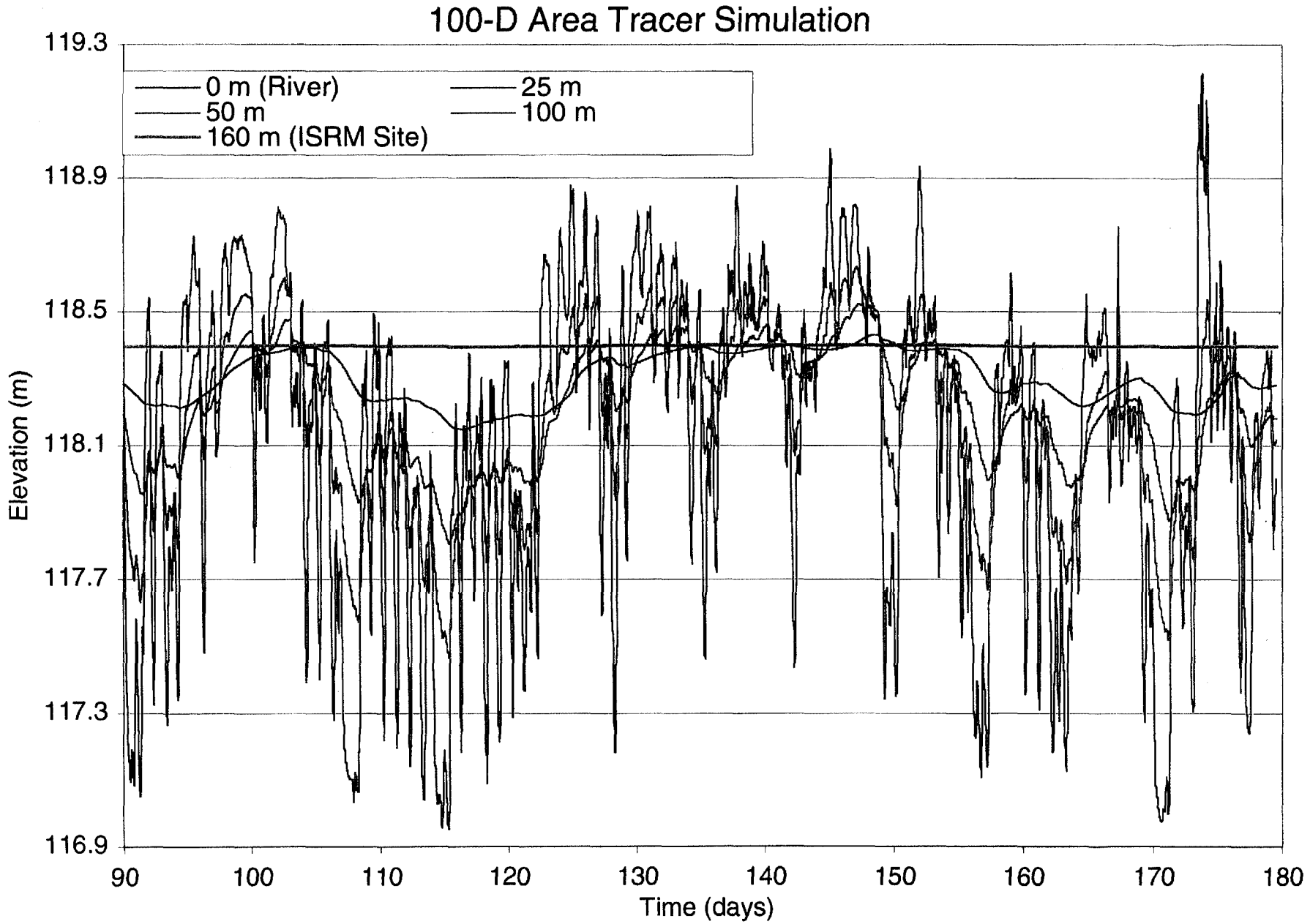


**Figure 5.5.** Tracer Simulation Hydraulic Head Results for the Second 90-Day Period

fluctuations in river stage. Distances of 75 m or greater respond to longer-term changes in the average daily high or low river stages. No changes occurred at the 160-m distance because the hydraulic heads were held constant at the right boundary.

While there are no wells close to the river at the 100-D Area ISRM site for validating or calibrating these simulation results, data from the N-Springs well network (as discussed in Section 2) can be used to determine whether the results are within the bounds of measured water level responses along the Hanford Reach. The hydrogeology of the unconfined aquifer at N-springs is different than that at D-Area. The upper aquifer at N-Springs is in the more permeable Hanford Formation gravels rather than the less permeable Ringold Formation gravels between the river and the 100-D Area ISRM site. Given the availability and variability of these data, selecting periods with the same water stage fluctuations for comparison was not possible. The responses are also complicated by the influence of earlier river stage changes on the water table response. With these qualifications, comparing the simulated water elevations for a four-week period (Figure 5.6) with the water level measurements in Figure 5.7 shows that overall the magnitude of water table responses in the simulations was less than those measured at N-Springs for a similar range in river stage. For a 1.2-m daily river stage fluctuation at a 25-m distance, the D-Area simulations showed an approximate 0.3-m change in water table elevation (around day 20); measured changes at N-Springs were about 0.4 to 0.5 m. Seventy-five meters from the river, the N-Springs data still respond to the daily river fluctuation with a magnitude of up to 0.2 m for daily river stage fluctuations from 1 to 1.4 m. The simulated hydraulic heads at the 75-m distance were less responsive than the N-Springs wells to most daily water level changes and of smaller magnitude. Both the N-Springs wells and simulated hydraulic heads at a distance of 100 m show only a small delayed response to most daily river stage changes. These differences between the simulated results and N-Area water level responses are expected due to the higher permeability of the N-Area aquifer.

### 5.3.2 Groundwater Fluxes

Groundwater fluxes at various vertical planes in the aquifer were calculated from the simulation results (see Figure 5.8). Because this was a two-dimensional simulation, these fluxes are per 1-m width of aquifer measured parallel to the river shoreline. Darcy fluxes can be derived by dividing these fluxes by the aquifer thickness (4.6 m) and the 1-m width. Groundwater velocities are calculated by dividing the darcy flux by the porosity (0.14).

Figure 5.8 shows a very large range in groundwater fluxes between the river and distances farther into the model. Negative fluxes in the figure are in the negative x-direction or toward the left of the model domain (i.e., toward or into the river). Positive values represent water moving into the aquifer from the river or away from the river toward the right boundary (ISRM site). The results for the simulated period show frequent reversals of groundwater flow direction for distances within 50 m of the river boundary. During most daily high-river stages, river water enters the aquifer (positive flux). At most daily low-river stages, groundwater discharges into the river (negative flux). Near the river boundary, maximum fluxes ranged from ±180 L/hr (6.7 m or 22 ft/day groundwater velocity) with one peak up to 320 L/hr into the aquifer during the peak river stage of 119.25 m in the simulated period. Calculated fluxes (Figure 5.8a) at the river were up to five times greater than at 25 m from the river (Figure 5.8b) for the time period simulated. Thus, large quantities of river water are entering and leaving the aquifer daily.

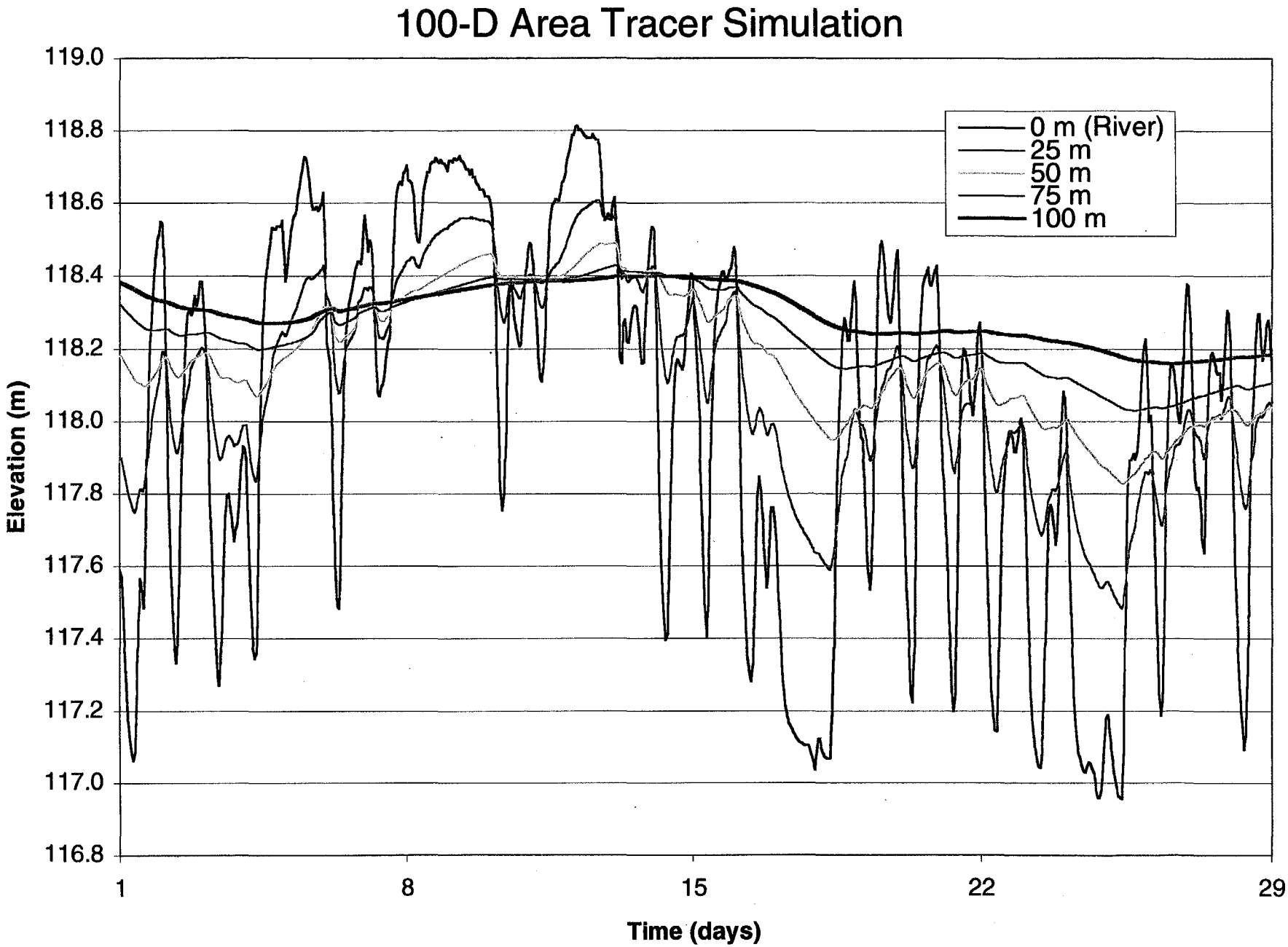


**Figure 5.6.** Tracer Simulation Hydraulic Head Results for a Four-Week Period

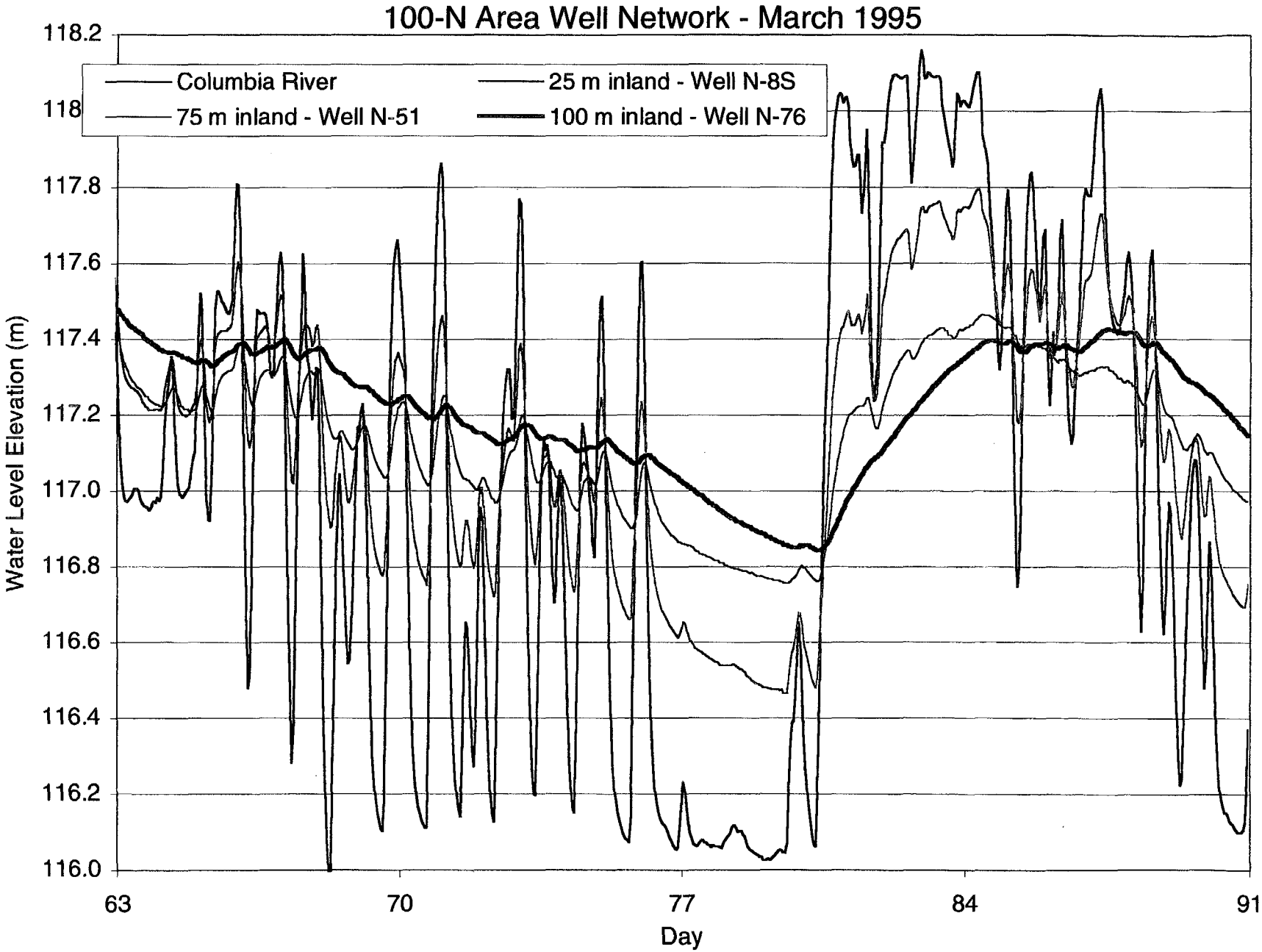


**Figure 5.7.** N-Area Columbia River and Monitoring Well Water Elevations, March 1995

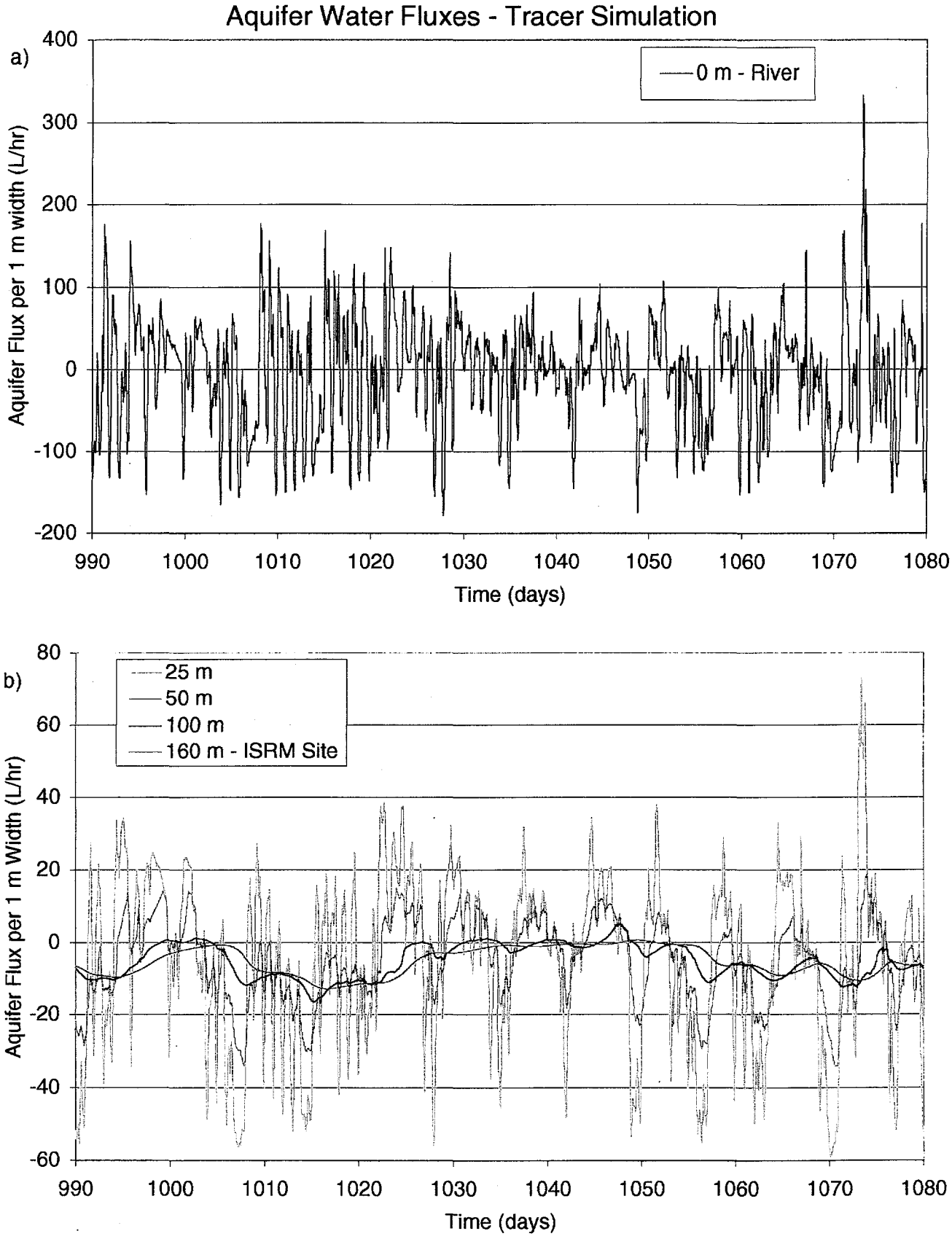


**Figure 5.8.** Tracer Simulation Aquifer Water Fluxes

With greater distance from the river (e.g., 100, 160 m), groundwater flow directions are mostly toward the river with a few periods of reversal (Figure 5.8b). Flux ranges from 0 to -10 L/hr (groundwater velocities from 0 to 0.37 m or 1.2 ft/day). Groundwater flow was slower and even reversed direction at these distances during periods when the maximum daily river stage was greater than 118.5 m for a few days. Groundwater flow direction reversals have been measured at the ISRM site, as shown in Figure 2.5. These results should be expected because a dirichlet condition is used for the hydraulic heads on the right boundary at elevation 118.4 m.

The cumulative aquifer water flux per 1-m width for a 90-day portion of the simulation is shown in Figure 5.9. This shows a running total of the net water flux (as mentioned previously, negative numbers are fluxes toward the river) from the beginning of the selected period at selected distances from the river boundary. Although there is a large variation in the total flux near the river due to daily variations, the long-term rate tracks the total flux from the greater distances. This simply shows that the net flux to the river over a long period of time is supplied by the groundwater flow from the regional aquifer, with daily fluctuations superimposed.

### 5.3.3 Predicted Tracer Migration

Tracer plumes at the end of each year for the first three years of simulation time are shown in Figure 5.10. Tracer breakthrough curves at selected distances are shown in Figure 5.11; groundwater velocities estimated from the 50 percent arrival times of the tracer at distances greater than 50 m from the river are 0.18 to 0.19 m/day (0.61 ft/day). Based on these results, a 50 percent arrival time of 2.3 years was predicted at the river. Although there is a large variability in the tracer breakthrough curves at distances near the river (i.e., 5, 15, and 25 m), increases in the peak concentrations for each 90-day cycle have leveled off by the end of the three-year simulation period.

Animation sequences of the tracer plume (color-shaded contour plots from Figure 5.10) over a period of days toward the end of the simulation period shows the entire front of the plume shifting back and forth toward the river. Concentrations as high as 50 percent were observed adjacent to the river, as shown in Figure 5.11.

The plateaus during tracer increase in the breakthrough curves shown in Figure 5.11 for distances 50 m or greater occur during relatively high river stage when groundwater flow toward the river is stalled or reversed. These occur mostly in the middle of the 90-day river stage cycle and correspond to the zero of positive fluxes calculated for 100 m distance in Figure 5.8b at periods when the high river stage was greater than 118.5 for a few consecutive days.

Based on these results, concentrations at a 25-m distance during the last 90-day cycle show a range between 85 and 90 percent of the maximum tracer concentration due to dilution and mixing with river water entering the aquifer (10 to 15 percent dilution). At a 15-m distance from the river, concentration ranges between 50 and 70 percent of the maximum tracer concentration (30 to 50 percent dilution). At a 5-m distance, concentrations ranged from 5 to 60 percent (40 to 95 percent dilution). The maximum concentrations corresponded to the low river stage around day 20 in the cycle. These data show that, although the average concentrations are lower toward the river, the range in variability is also greater.

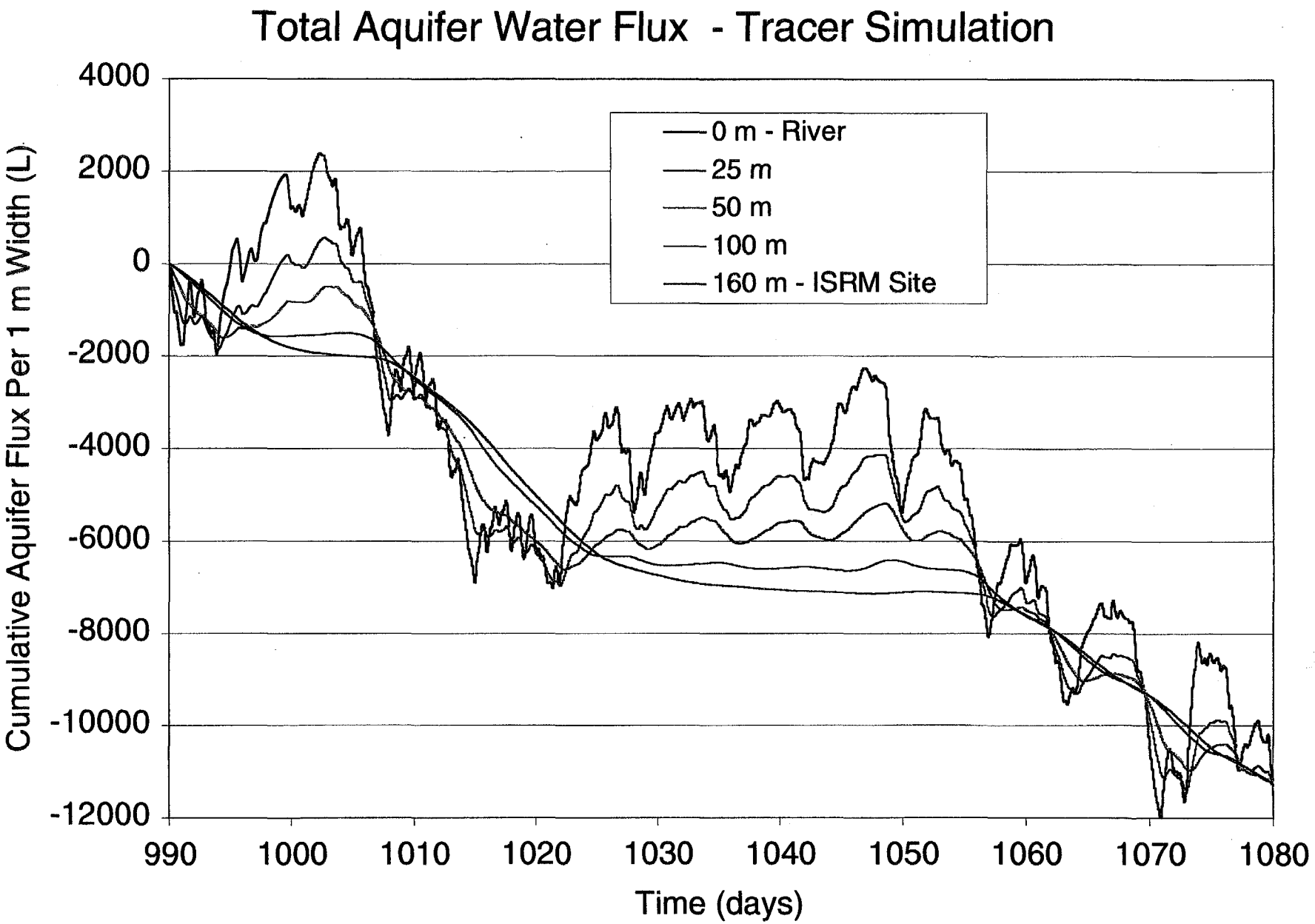


**Figure 5.9.** Tracer Simulation total Water Flux per Meter of Aquifer Width

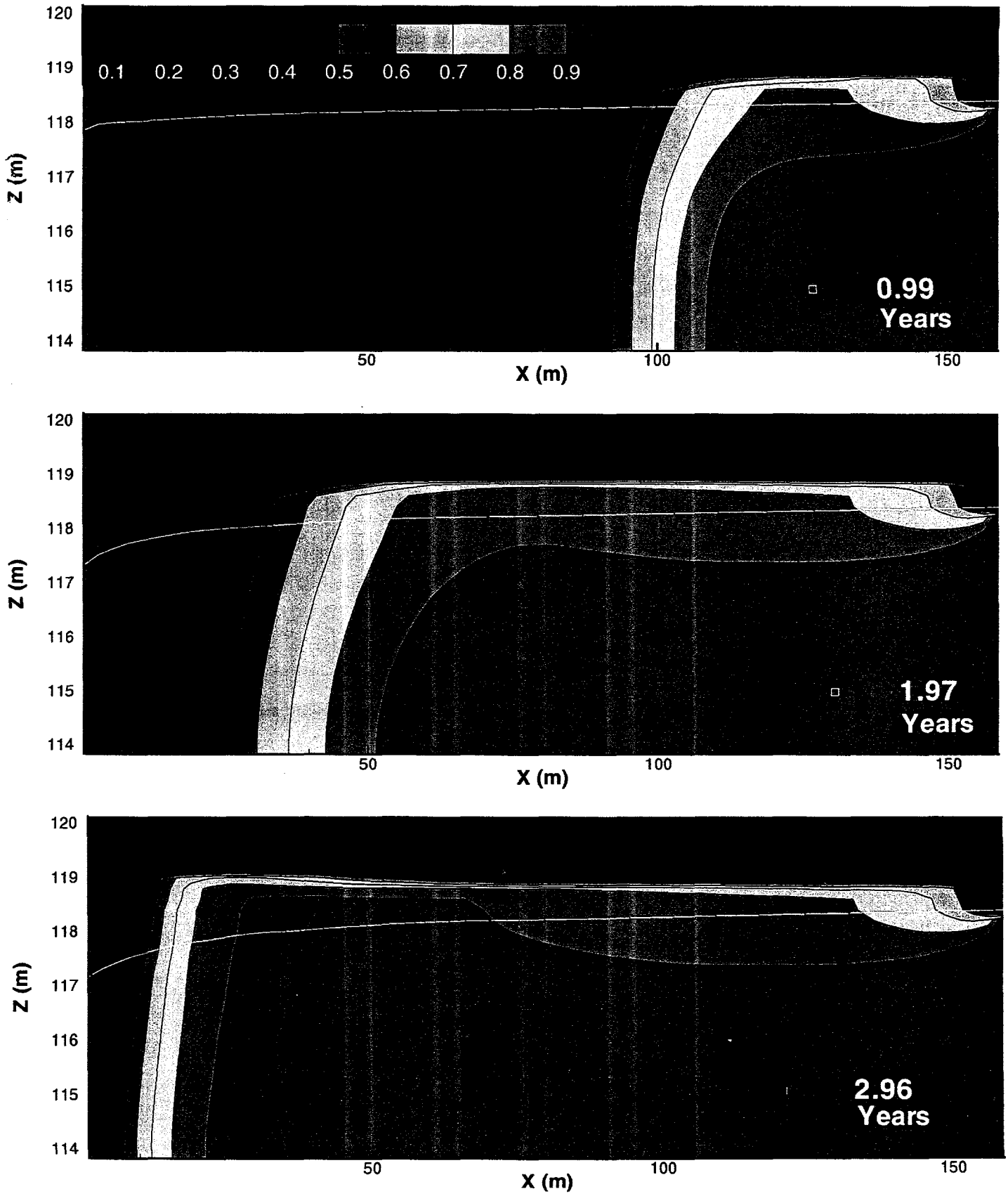


**Figure 5.10.** 100-D Area Tracer Simulation Plume Results

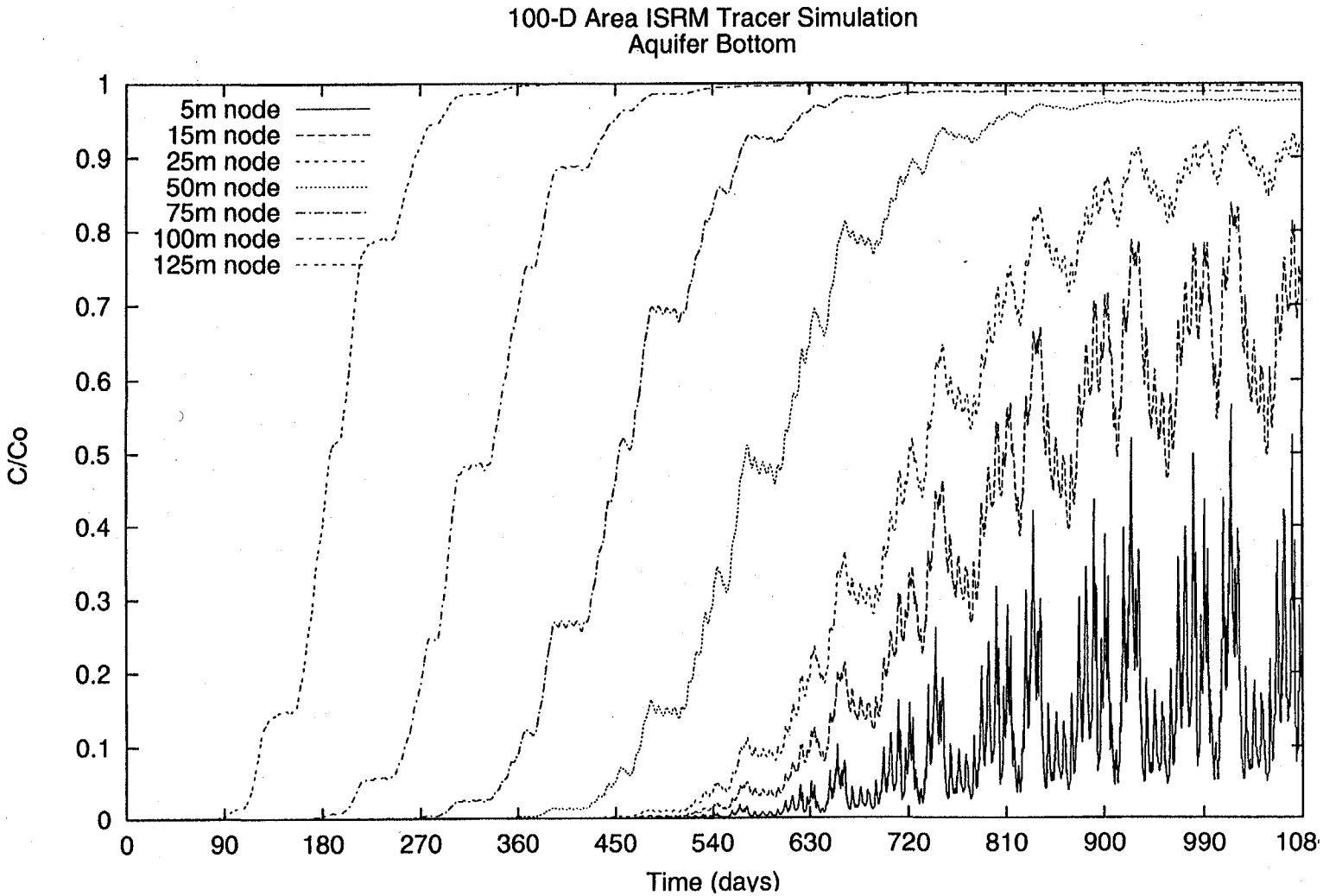


**Figure 5.11.** 100-D Area ISRM Tracer Simulation Breakthrough Curves

The hydrodynamic dispersivities selected for these simulations were relatively low (see Table 5.2). Larger values would lower predicted concentrations in the mixing zone and at the river. Some numerical dispersion is also expected in the results due to the large variation in courant numbers resulting from a wide range in spatial and temporal velocities with a fixed horizontal grid spacing. Overall, the fronts of the plumes (shown in Figure 5.10) are relatively sharp and uniform, indicating that numerical dispersion was minimal.

The tracer concentration results are similar to the hydraulic head and water flux results in that the impact of the river stage fluctuations is most pronounced within 50 m from the river. Although the mixing zone does substantially reduce the average tracer concentrations within 25 m of the river, high-percentage concentration peaks do occur. This corresponds to the wide range in electrical conductivity and chromate concentrations measured from the river substrate sampling tubes at the site, as discussed in Section 2 (Figure 2.9). Some measurements showed as high as 90 percent of aquifer concentrations in the samples collected from the Columbia River substrate sampling tubes.

The dependence of the aquifer discharge concentrations on the river stage, which cannot be adequately predicted (e.g., future hydroelectric dam operations), means that a certain percentage of dilution from the mixing cannot always be depended on. The mixing/dilution effect within the aquifer may be reliable to maintain some average aquifer discharge concentration that would be significantly lower than the aquifer concentrations measured at distances greater than 50 m inland. This could be accomplished by conducting simulations similar to this tracer simulation using longer-term river stage conditions (e.g., years instead of 90 days) and knowing that this mean concentration will occasionally be violated. Additional data and effort would also be required to adequately validate or calibrate a numerical model for this purpose.

## 5.4 Reoxygenation in a Fluctuating Water Table

The differences between the reoxygenation in a fluctuating water table simulation and the tracer simulation discussed in the previous section is that oxygen is simulated as a species that partitions in both the gas and aqueous phases. This problem used the STOMP2 code, which simulates gas, water, and solute transport, as discussed in Section 3. Oxygen was treated as a solute that partitions into the air and water based on the Henry's Law coefficient in Table 5.2. Water pressure boundaries were the same as the tracer simulation discussed in the previous section. Air pressures were also specified on the left and right boundaries to establish a static pressure profile for water-saturated air ($\rho$ = 1.195 kg/m$^3$). Atmospheric air pressure and oxygen composition were specified at the top of the system.

Hydraulic heads and water fluxes were the same for this simulation as for the tracer simulation discussed in the previous section. The discussion here will focus on the dissolved oxygen concentration results. The tracer simulation is also helpful in determining the relative importance of the effects of mixing river water in the aquifer and the reoxygenation in the fluctuating water table on the predicted dissolved oxygen concentrations. Diffusion from the vadose zone is also incorporated in this simulation. Because the water table is dynamic, enhancing gas exchange in the vadose zone and replenishing oxygen, the diffusive flux into the aquifer would be greater than shown in the static water table diffusion simulation discussed in Section 5.2.

### 5.4.1 Simulated Dissolved Oxygen Concentrations

Figure 5.12 shows the dissolved oxygen plumes at the end of each of the three years of simulation time. The largest differences between these results and the tracer simulation results (Figure 5.10) for the same time periods are the large vertical concentration gradients for dissolved oxygen in the aquifer and the much lower relative dissolved oxygen concentration within 50 m of the river. The vertical gradients in dissolved oxygen concentration are from reoxygenation at the water table from air entrapment and diffusion. Figure 5.13 shows the movement of the plume toward the end of the simulation on three different days during a high-low-high river stage change period. The front of the plume is displaced by about 5 m of river water during the high river stage. Slightly anoxic water (>80 percent oxygen saturation) is shown discharging into the river during low river stage.

Arrival curves of anoxic water (Figures 5.14 to 5.16) are inverted from the arrival curves shown in the tracer simulation because these are expressed as percent oxygen saturation (e.g., a negative tracer). The arrival times for the 50 percent oxygen-depleted water at the bottom of the aquifer for distances of 50 m and greater in Figure 5.14 are similar to the tracer arrival curves. Groundwater flow rates based on these arrival times are 0.18 m/day. Dissolved oxygen arrival curves for distances 50 m and closer are shown in Figures 5.15 and 5.16 for the third year of simulation time. These results are much different than the tracer arrival curves at these distances.

Dissolved oxygen concentrations at the 15 m distance at the aquifer bottom show a range of 40 to 70 percent oxygen saturation. Taking the inverse of this range, these values would correspond to 30 to 60 percent tracer, compared with the 50 to 80 percent seen in the tracer simulation results (a 20 percent reduction in the predicted concentration range at this distance). At a 5-m distance, dissolved oxygen concentrations ranged from 70 to 95 percent oxygen saturation at the bottom of the aquifer. This compares with 5 to 30 percent tracer with the tracer simulations showing a range of 5 to 55 percent.

Given the vertical concentration gradients shown in Figures 5.12 and 5.13, dissolved oxygen concentrations in the middle of the aquifer are higher than at the bottom of the aquifer and the variation in concentrations is much narrower. At a 15-m distance, dissolved oxygen concentrations are from 65 to 85 percent saturation during the last 90-day cycle of the simulation. At a 5-m distance, dissolved oxygen concentrations are from 85 to 95 percent saturation in the middle of the aquifer. Dissolved oxygen concentrations at the top of the aquifer would be even greater.

Depth-averaged concentrations of dissolved oxygen discharging to the river was up to 95 percent dissolved oxygen saturation and was always greater than 75 percent oxygen saturation during this 90-day river stage period. The 75 percent minimum would be equivalent to values of 6.9 mg/L dissolved oxygen at 20°C.

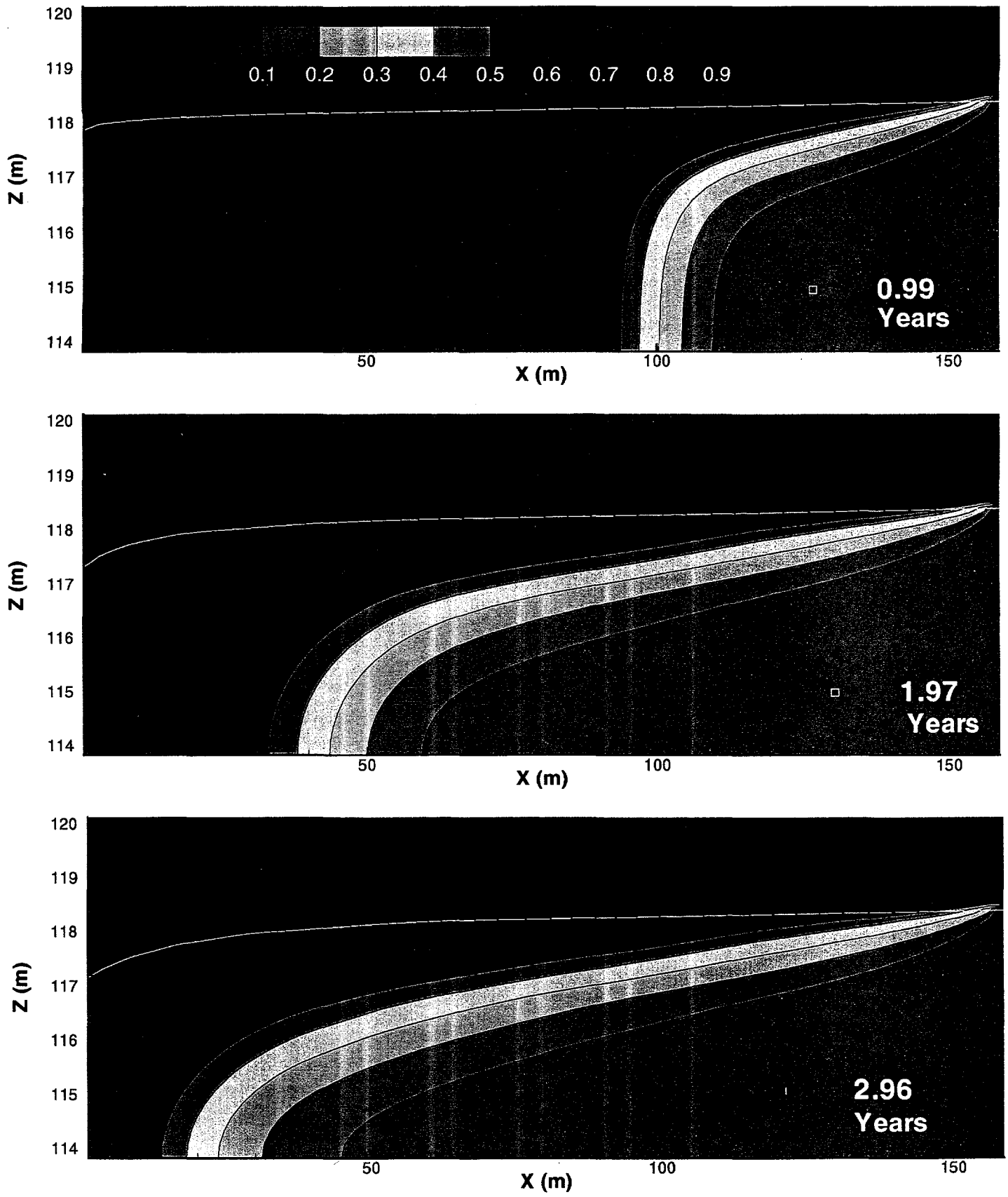


**Figure 5.12.** 100-D Area ISRM Fluctuating Water Table Simulation—Dissolved Oxygen Concentrations (oxygen saturation ratio)

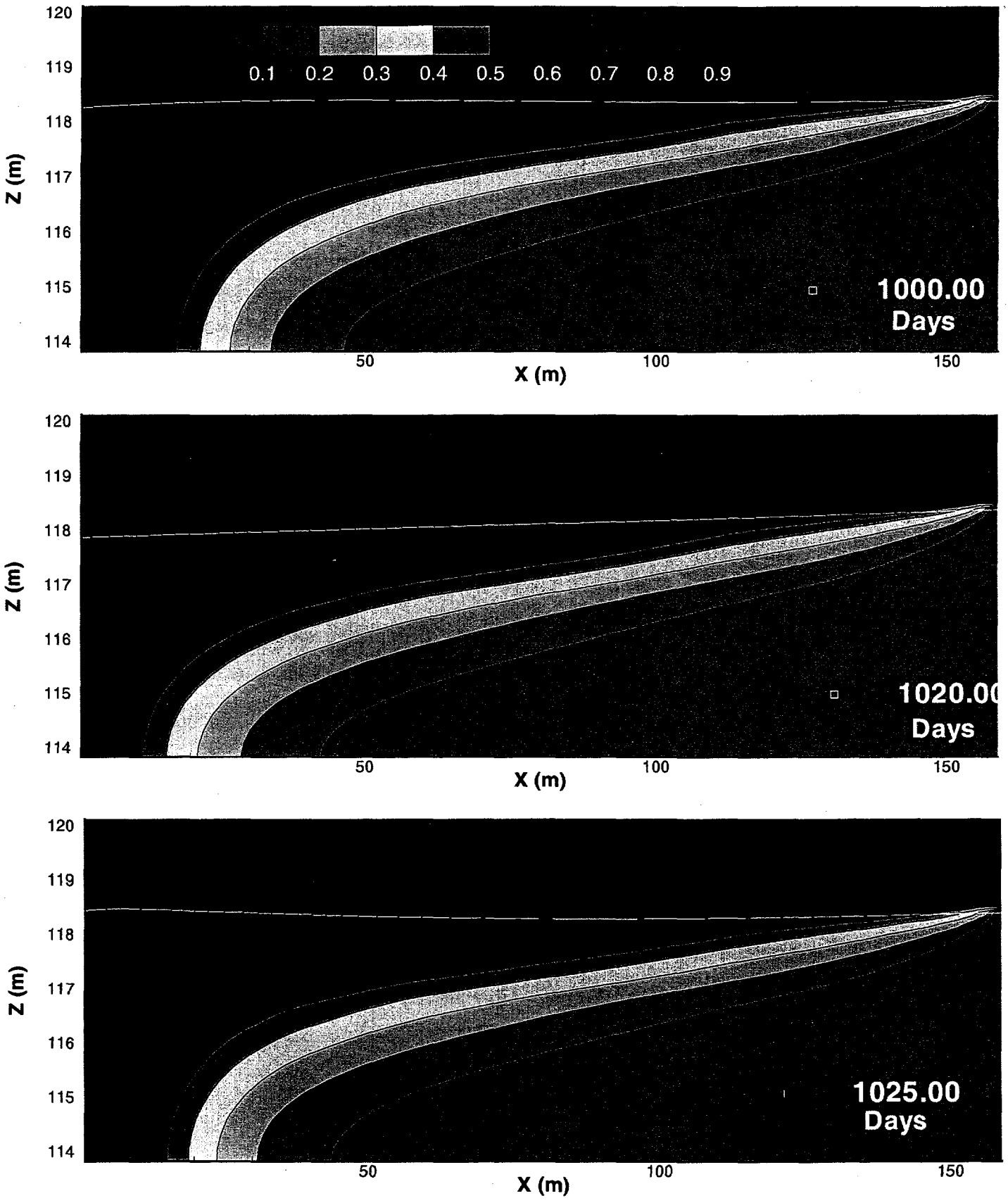


**Figure 5.13.** 100-D Area ISRM Fluctuating Water Table Simulation—Dissolved Oxygen Concentrations (oxygen saturation ratio) During High-Low-High River Stage

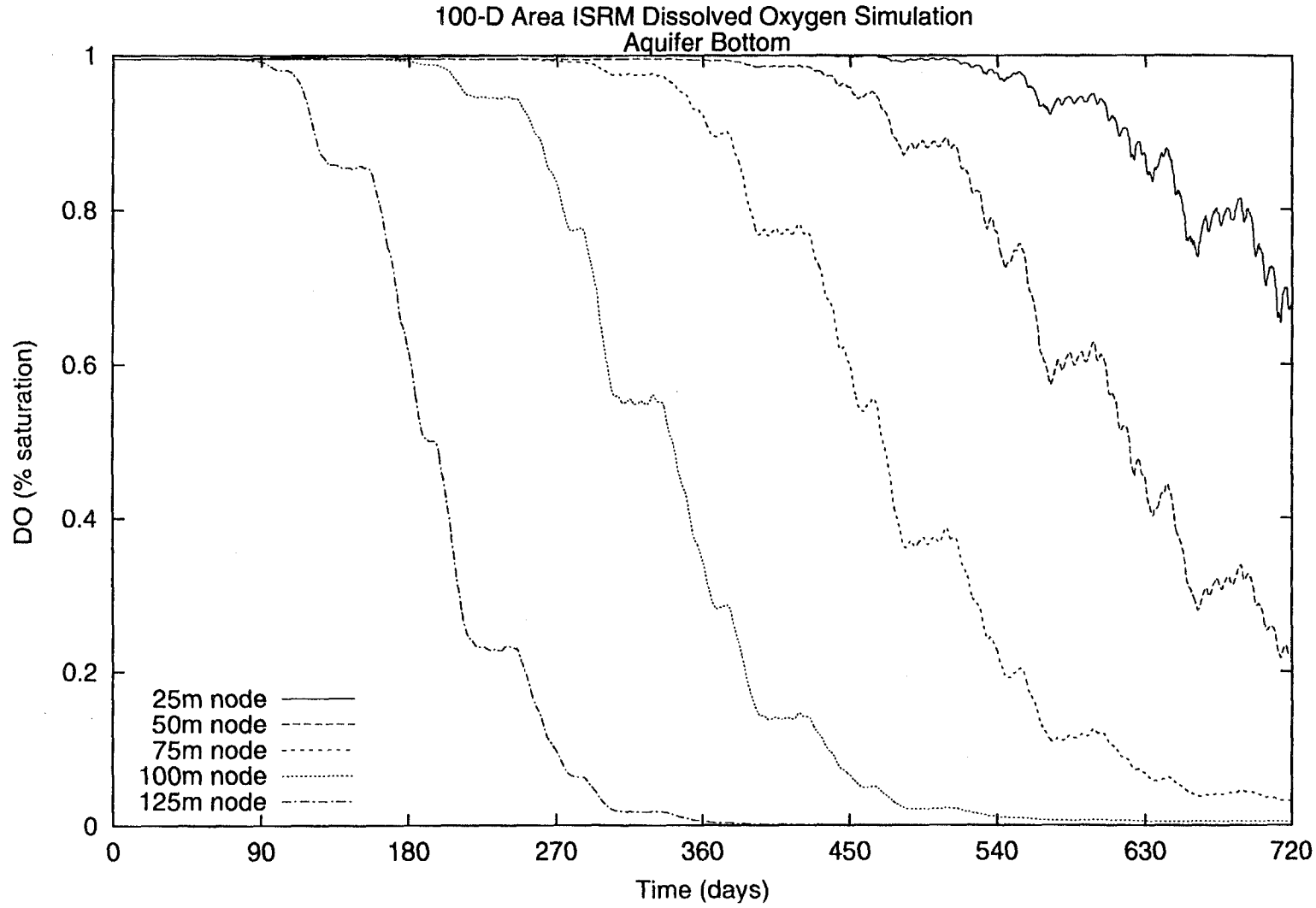


**Figure 5.14.** 100-D Area ISRM Fluctuating Water Table Simulation—Dissolved Oxygen Breakthrough Curves for Years 0 to 2 at Aquifer Bottom

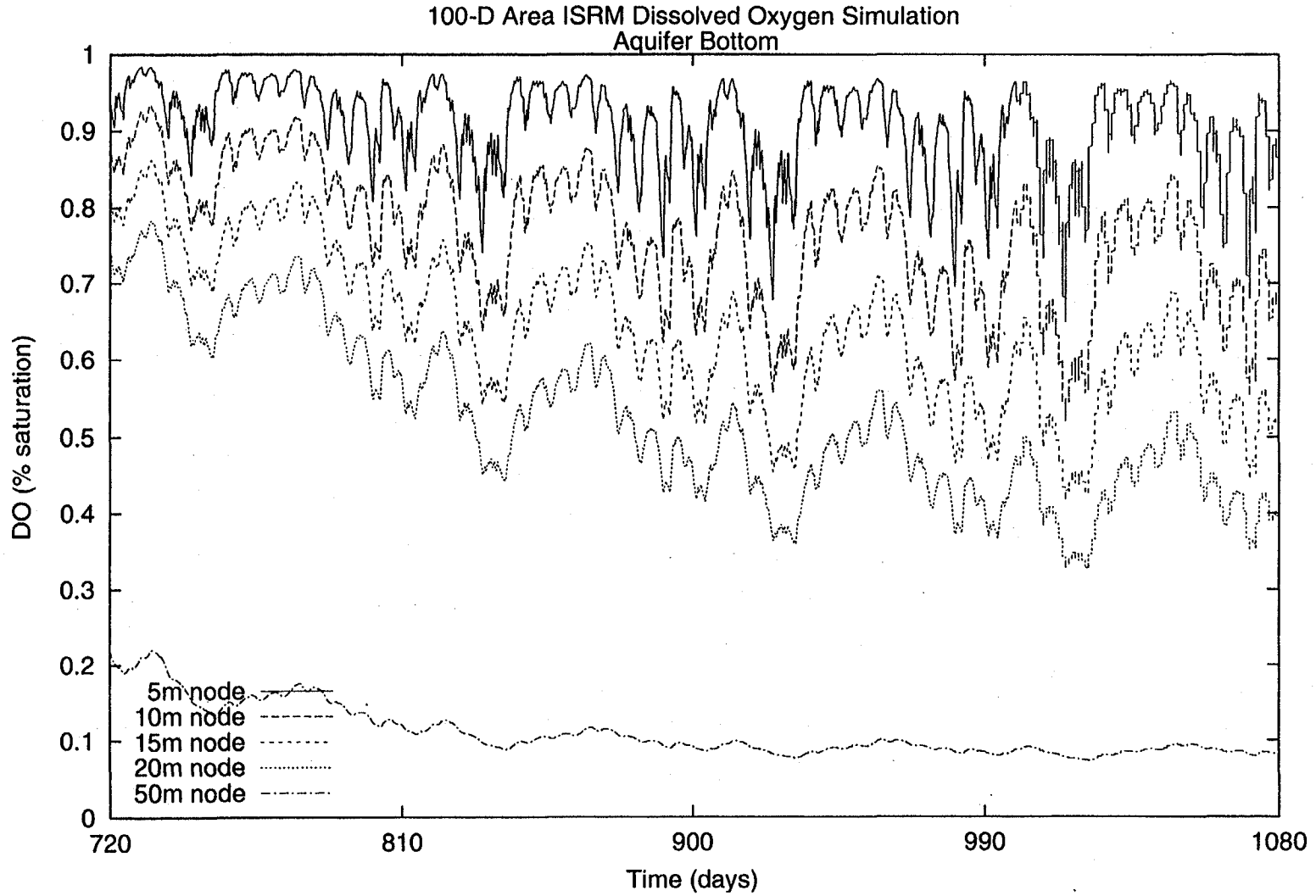


**Figure 5.15.** 100-D Area Fluctuating Water Table Simulation—Dissolved Oxygen Breakthrough Curves for Years 2 to 3 at Aquifer Bottom

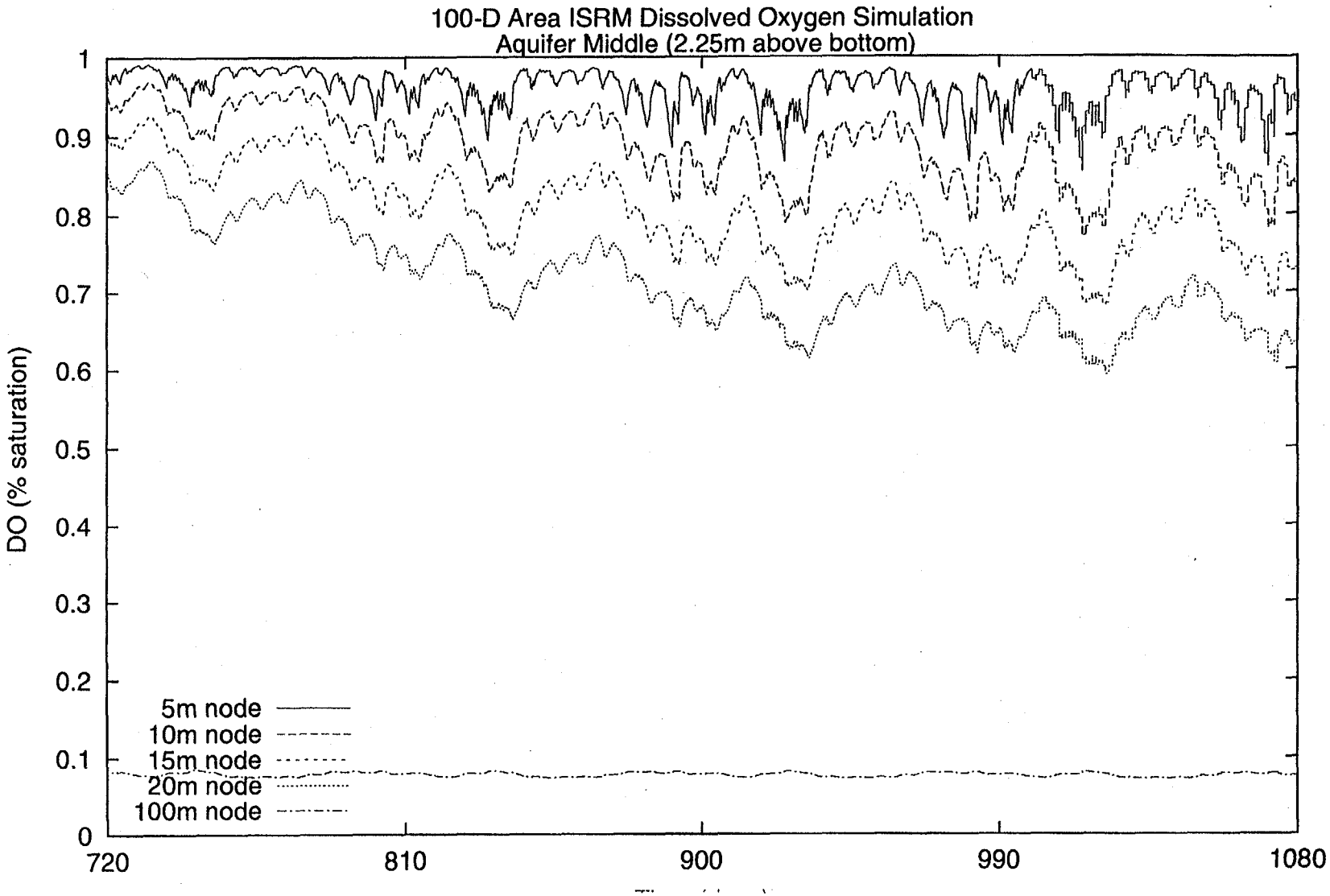


**Figure 5.16.** 100-D Area ISRM Fluctuating Water Table Simulation—Dissolved Oxygen Breakthrough Curves for Years 2 to 3 at Aquifer Middle

### 5.4.2 Saturations, Pressures, and Hydraulic Heads

Figures 5.17 and 5.18 show water saturations, aqueous pressures, and hydraulic heads for two periods in the simulation at low and high river stage. The water saturations highlight the area near the left boundary, where the river stage-induced water table fluctuations occur. This zone extends up to 50 m inland and corresponds to previous discussions on the extent of aquifer that is greatly impacted by river stage changes in the model. During the low river stage period shown, the aquifer is mostly 100 percent water saturated below the water table (Figure 5.17). During high river stage (Figure 5.18), a large area of 15 percent air entrapment (85 percent saturation) occurs below the water table up to 50 m from the river boundary. The air entrapment zone is 1.2 m tall near the river and tapers to approximately 0.2 m 50 m away. The air in this zone contains oxygen at concentrations up to atmospheric composition. In addition to reoxygenation with entrapped air below the water table, saturations increase in the vadose zone above the water table, which is also in direct contact with air containing oxygen. This oxygenated water drains back toward the aquifer during subsequent periods of low river stage.

Pressures and hydraulic heads are also shown in Figures 5.17 and 5.18. During low river stage, the hydraulic gradient steepens toward the river, as shown by the decreasing distances between contour lines in Figure 5.17c. During a period of high river stage (Figure 5.18c), groundwater is flowing toward the midpoint of the simulation domain from both the left (river) and the right (ISRM site) boundaries. This causes groundwater at around a 90 m distance to stop flowing during this river stage period.

## 5.5 Modeling Discussion and Conclusions

Overall, the most important mechanism demonstrated for the attenuation of the anoxic plume emanating from the ISRM site at 100-D Area is air entrapment and reoxygenation in a fluctuating water table induced by changes in the stage of the Columbia River. Numerical simulations that include these processes indicate a maximum aquifer discharge of 95 percent oxygen saturated water (using atmospheric air composition) under favorable conditions. Even under less favorable conditions, the minimum percentage of oxygen saturation discharged from the aquifer in these simulations was 75 percent. Laboratory studies have also demonstrated that this mechanism can significantly reoxygenate water in the zone of water table fluctuations within a week (although these experiments did not investigate the vertical movement of water deeper into the aquifer). The selection of river stage period for use in the simulation attempted to select the most conservative period (winter 1998) without extreme events. Water table fluctuations in other quarters of 1998 had much greater ranges of river stage fluctuation and much higher average river levels (see Figure 2.12). These greater ranges would result in a greater amount of reoxygenation by this process, and the higher river stages would also have resulted in smaller aquifer discharge. It could be reasonably assumed that these types of river stage and water table fluctuations selected for the simulation period (i.e., first quarter 1998) would occur as long as the hydroelectric dams are operating on the Columbia River.

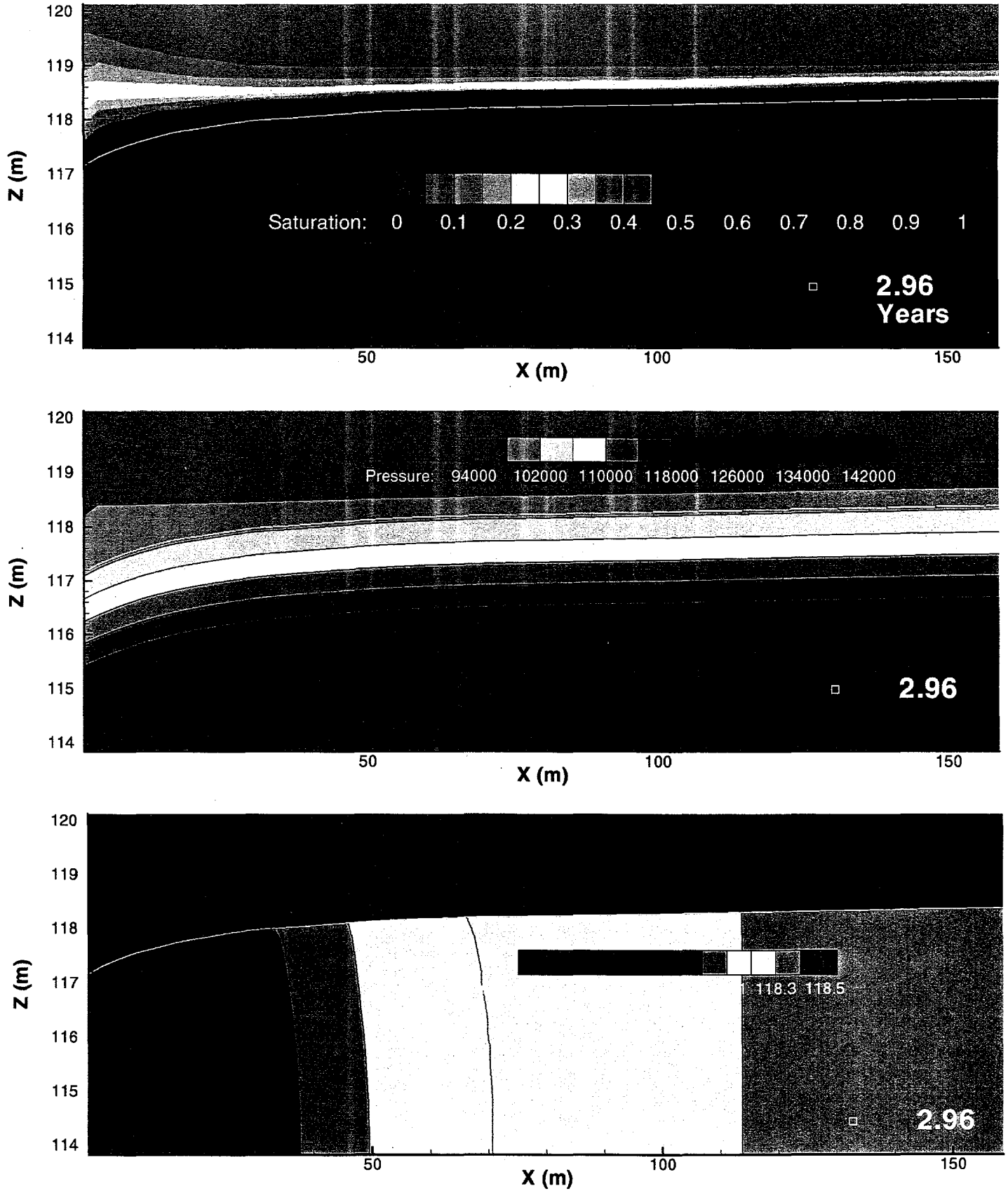


**Figure 5.17.** 100-D Area ISRM Fluctuating Water Table Simulation—Water Saturation, Pressure (Pa), and Hydraulic Heads (m) During Low River Stage

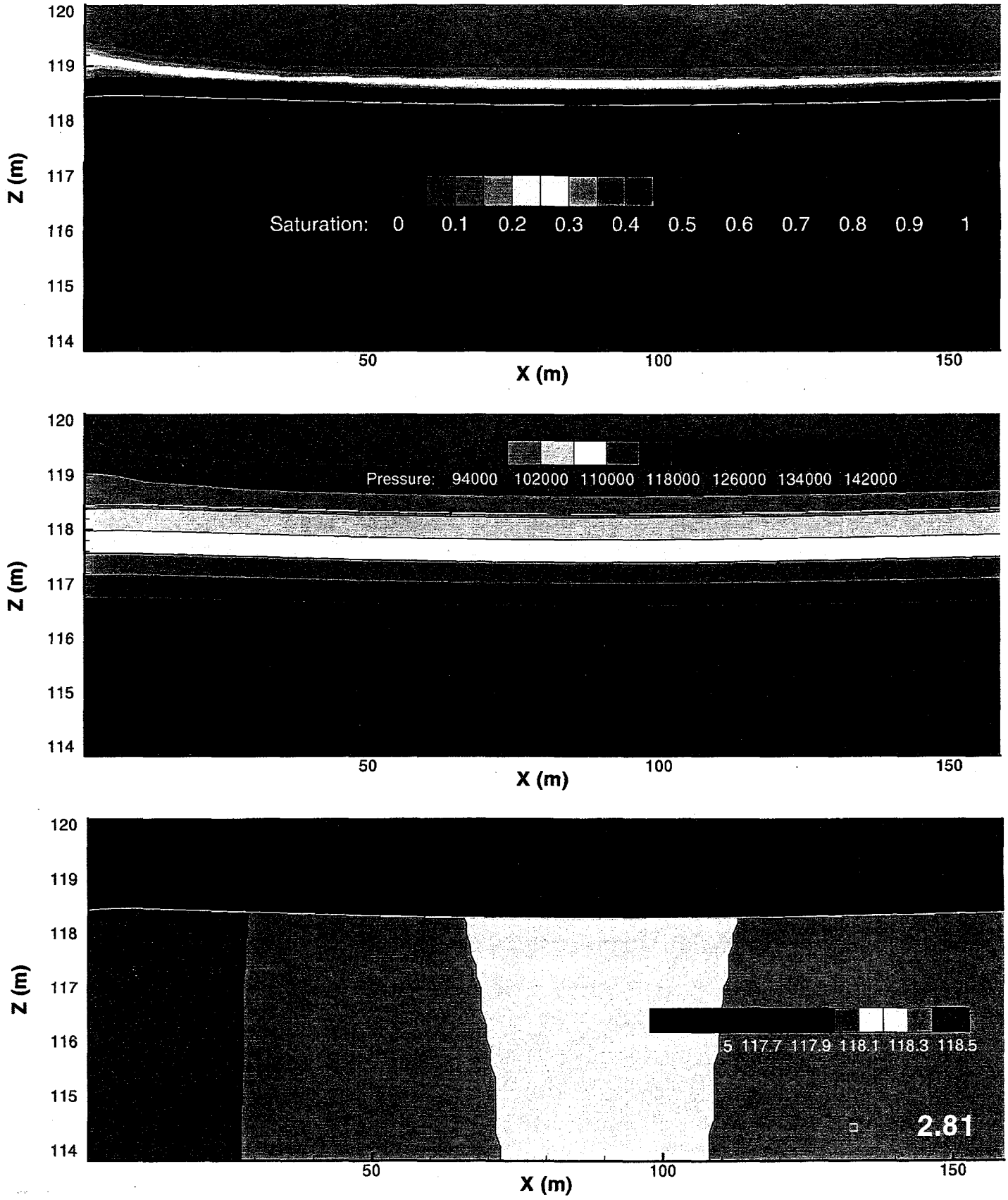


**Figure 5.18.** 100-D Area ISRM Fluctuating Water Table Simulation—Water Saturation, Pressure (Pa), and Hydraulic Heads (m) During High River Stage

# 6.0 Conclusions

Prior to the ISRM treatability test at the 100-D Area, dissolved oxygen concentration measurements indicated that the groundwater was saturated with oxygen (7 to 9 mg/L). Following the emplacement of the 56-m (150-ft)-long test section, dissolved oxygen concentrations decreased to nearly 0 mg/L in wells within the treated area. Dissolved oxygen concentrations in the downgradient wells have been decreasing since the test. Well D4-6, the farthest downgradient well (27 m [90 ft] distance from the treatment zone) was at 20 percent oxygen saturation during the latest sampling round (1.68 mg/L in April 1999).

While an anoxic plume forms downgradient from an ISRM zone, numerous processes (as shown in Figure 1.3) exist in a normally oxidizing aquifer to attenuate the anoxic plume as it migrates downgradient from the reduced zone to the Columbia River. Because adequate time has not elapsed for sufficient monitoring since the start of the ISRM treatability study at 100-D Area, this study uses a combination of applied laboratory experiments and numerical modeling to predict downgradient dissolved oxygen concentrations from the site. Modeling can also be used to identify important processes and can guide future data collection. The numerical modeling and predictions were based on processes within the aquifer and vadose zone only. Other effects, such as mixing of river water with discharging groundwater within the upper 1 m of sediments in the river bottom (hyporheic zone) were outside the scope of this study and thus were not investigated.

The intermediate-scale laboratory experiments on reoxygenation in a fluctuating water table showed that anoxic water can be rapidly reoxygenated from water table fluctuations due to the entrapment of air bubbles containing atmospheric concentrations of oxygen. These rates were much greater than oxygen diffusion alone. The water within the zone of fluctuation was significantly reoxygenated within one week of daily water table raising and lowering. The results of the dissolved gas tracer tests were not quantifiable and were not used in this analysis.

The numerical model incorporated a fluctuating water table induced by the Columbia River along with air entrapment in the zone of fluctuation. The model also incorporated the effects of the groundwater mixing with river water (bank storage) near the river's edge. This model predicted dissolved oxygen concentrations of 75 to 95 percent oxygen saturation at the river. Air entrapment caused by water table fluctuations had the greatest impact of those tested on the attenuation of the dissolved oxygen concentrations discharging from the aquifer and should be reliable over a wide range of river stage fluctuations. For comparison, a simpler model, which incorporated only molecular diffusion of dissolved oxygen from above across a static water table, predicted 20 percent dissolved oxygen saturation by the time the treated water from the ISRM site reached the river, 160 m downgradient, after approximately two years of travel time. However, this simpler model is not considered realistic. In either case, mixing processes in the riverbed will further increase the oxygen saturation.

A newly installed well in the spring of 1999 will provide additional downgradient water quality monitoring (including dissolved oxygen) and water table fluctuations between the ISRM site and the Columbia River to test some of the predictions, parameters, and assumptions in these

simulations. Columbia River substrate porewater sampling tubes installed along the river shoreline downgradient of the site will provide additional monitoring data in the future with the predicted arrival of groundwater from the ISRM site later in 1999 and 2000.

# 7.0 References


Brooks RH and AT Corey. 1964. "Hydraulic properties of porous media." Hydrol. Pap. 3, Civ. Eng. Dept., Colo. State Univ., Fort Collins.

Burdine NT. 1953. "Relative permeability calculations from pore-size distribution data." *Petr. Trans.*, Am. Inst. Mining Metal. Eng., 198:71-77.

Connelly MP, CR Cole, and MD Williams. 1997. *Bank Storage Modeling at the 100-N Area.* CH2MHill, Richland, Washington.

Donaldson JD, JD Istok, MD Humphrey, KT O'Reilly, CA Hawelka, and DH Mohr. 1997. "Development and Testing of a Kinetic Model for Oxygen Transport in Porous Media in the Presence of Trapped Gas." *Groundwater*, 35(2):270-279.

Donaldson JD, JD Istok, and KT O'Reilly. 1998. "Dissolved Gas Transport in the Presence of a Trapped Gas Phase: Experimental Evaluation of a Two-Dimensional Kinetic Model." *Groundwater*, 36(1):133-142.

Fayer MJ and TB Walters. 1995. *Estimated Recharge Rates at the Hanford Site.* PNNL-10285, Pacific Northwest Laboratory, Richland, Washington.

Fruchter JS, JM Zachara, JK Fredrickson, CR Cole, JE Amonette, TO Stevens, DJ Holford, LE Eary, GD Black, and VR Vermeul. 1992. "Manipulation of Natural Subsurface Processes: Field Research and Validation." *Pacific Northwest Laboratory Annual Report for 1991 to the DOE Office of Energy Research, Part 2: Environmental Sciences.* PNL-8000, Pacific Northwest Laboratory, Richland, Washington, pp. 88-106.

Fruchter JS, FA Spane, JK Fredrickson, CR Cole, JE Amonette, JC Templeton, TO Stevens, DJ Holford, LE Eary, BN Bjornstad, GD Black, JM Zachara, and VR Vermeul. 1994. *Manipulation of Natural Subsurface Processes: Field Research and Validation.* PNL-10123, Pacific Northwest National Laboratory, Richland, Washington.

Fruchter JS, JE Amonette, CR Cole, YA Gorby, JE Szecsody, SS Teel, VR Vermeul, MD Williams, and SB Yabusaki. 1995. *Test Plan for the 100-H Area In Situ REDOX Manipulation Experiment.* Pacific Northwest National Laboratory, Richland, Washington.

Fruchter JS, JE Amonette, CR Cole, YA Gorby, MD Humphrey, JD Istok, FA Spane, JE Szecsody, SS Teel, VR Vermeul, MD Williams, and SB Yabusaki. 1996. *In Situ Redox Manipulation Field Injection Test Report - Hanford 100-H Area.* PNNL-11372, Pacific Northwest National Laboratory, Richland, Washington.

Fruchter JS, MD Williams, VR Vermeul, CR Cole, and SS Teel. 1997. *Treatability Test Plan for In Situ Redox Manipulation in the 100-HR-3 Operable Unit, D-Area, Hanford Site, Washington.* Pacific Northwest National Laboratory, Richland, Washington.

Fry VA, JD Istok, L Semprini, KT O'Reilly, and TE Buscheck. 1995. "Retardation of Dissolved Oxygen Due to a Trapped Gas Phase in Porous Media." *Groundwater,* 33(3):391-398.

Fry VA, JD Istok, and KT O'Reilly. 1996. "Effect of Trapped Gas on Dissolved Oxygen Transport–Implications for In Situ Bioremediation." *Groundwater*, 34(2):200-210.

Hope SK and RE Peterson. 1996. *Chromium in the River Substrate Porewater and Adjacent Groundwater: 100-D/DR Area, Hanford Site, Washington.* BHI-00778 Rev.0, Bechtel Hanford Co., Richland, Washington.

Istok JD, JE Amonette, CR Cole, JS Fruchter, MD Humphrey, JE Szecsody, SS Teel, VR Vermeul, MD Williams, and SB Yabusaki. 1998. "In Situ Redox Manipulation by Dithionite Injection: Intermediate-Scale Laboratory Experiments." Submitted for publication in *Groundwater.*

Kaluarachchi JJ and JC Parker. 1992. "Multiple flow with a simplified model for oil entrapment." *Transp. in Porous Media,* 7:1-14.

Klute A and C Dirksen. 1986. "Hydraulic conductivity and diffusivity: Laboratory Methods." *Methods of soil analysis Part 1-Physical and mineralogical methods.* Soil Science Society of America, Madison, Wisconsin, pp. 687-734.

Land CS. 1968. "Calculations of imbibition relative permeability for two- and three phase flow from rock properties." *Trans. Am. Inst. Min. Metal. Pet. Eng.,* 207:149-156.

Lenhard RJ. 1992. "Measurement and modeling of three-phase saturation pressure hysteresis." *J. Contam. Hydrol.*, 9:243-269.

Lenhard RJ, M Oostrom, and MD White. 1995. "Modeling fluid flow and transport in variably saturated porous media with the STOMP simulator. 2. Verification and validation exercises." *Adv. in Water Resour.,* 18:365-373.

Lenhard RJ and JC Parker. 1987. "A model for hysteretic constitutive relations governing multiphase flow. 2. Permeability-saturation relations." *Water Resour. Res.*, 23:2197-2206.

Lindsey KA. 1991. *Revised Stratigraphy for the Ringold Formation, Hanford Site, South Central Washington.* WHC-SD-EN-EE-004 Rev. 0, Westinghouse Hanford Company, Richland, Washington.

Lindsey KA and GK Jaeger. 1993. *Geologic Setting of the 100-HR-3 Operable Unit, Hanford Site, South-Central Washington.* WHC-SD-EN-TI-132 Rev. 0, Westinghouse Hanford Company, Richland, Washington.

Luttrell S, M Chamness, D Dauble, R Dirkes, and T Walters. 1995. Letter Report-100-HR-3, *Groundwater and Riverbank Springs Information and Fall Chinook Spawning Habitat of the Hanford Reach, Columbia River.* Pacific Northwest Laboratory. Richland, Washington.

Millington RJ and JP Quirk. 1960. "Transport in porous media." *Trans. 7th Int. Congr. Soil Sci.*, Madison, Wisconsin, 1:97-106.

Mualem Y. 1976. "A new model for predicting the hydraulic conductivity of unsaturated porous media." *Water Resour. Res.*, 12:513-522.

Mueller RP and DR Geist. 1998. *Evaluation of Fall Chinook Salmon Spawning Adjacent to the In-Situ Redox Manipulation Treatability Test Site, Hanford Site, Washington.* PNNL-12025, Pacific Northwest National Laboratory, Richland, Washington.

Nielson KK, VG Rogers, and GW Gee. 1984. "Diffusion of Radon Through Soils: A Pore Distribution Model." *Soil Science Society of America Journal*, 48(3):482-487.

Oostrom M and JH Dane. 1990. "Calibration and automation of a dual-energy gamma system for applications in soil science." *Agronomy and Soils Dep. Ser.* 145. Alabama Agriculture Experimental Station, Auburn.

Oostrom M, JH Dane, BC Missildine, and RJ Lenhard. 1995. " Error analysis of dual-energy gamma radiation measurements." *Soil Science,* 160:28-42.

Oostrom M, C Hofstee, and JH Dane. 1997. "Light nonaqueous-phase liquid movement in a variably saturated sand." *Soil Sci. Soc. Am. J.*, 61:1547-1554.

Oostrom M, C Hofstee, JH Dane, and RJ Lenhard. 1998. "Single-source gamma radiation procedures for improved calibration and measurements in porous medium systems." *Soil Science* 163:646-656.

Oostrom M and RJ Lenhard. 1998. "Comparison of relative permeability-saturation pressure parametric models for infiltration and redistribution of a light nonaqueous phase liquid in sandy porous media." *Adv. in Water Resour.*, 21:145-157.

Parker JC and RJ Lenhard. 1987. A model for hysteretic constitutive relations governing multiphase flow 1. Saturation-Pressure Relations. *Water Resour. Res.*, 23:2187-2196.

Peterson RE, JV Borghese, and DB Erb. 1998. *Aquifer Sampling Tube Completion Report: 100 Area and Hanford Townsite Shoreline.* BHI-01153 Rev. 0, Bechtel Hanford Co., Richland, Washington.

Puls RW, RM Powell, and CJ Paul. 1995. "In situ remediation of groundwater contaminated with chromate and chlorinated solvents." *Proceedings of the 209th Am. Chem. Soc. National Meeting*, Anaheim, California, pp. 788-791.

Roberts AL, LA Totten, WA Arnold, DR Burris, and TJ Campbell. 1996. "Reductive elimination of chlorinated ethylenes by zero-valent metals." *Environ. Sci. Technol.*, 30:2654-2659.

Rockhold ML et al. 1993. *Physical and Hydraulic Properties of Grout Materials.* PNL-8813, Pacific Northwest National Laboratory, Richland, Washington.

Schroth MH, SJ Ahearn, JS Selker, and JD Istok. 1996. "Characterization of Miller-similar silica sands for laboratory subsurface hydrologic studies." *Soil Sci. Soc. Am. J.* 60:1331-1339.

Schroth MH, JD Istok, JS Selker, M Oostrom, and MD White. 1998. "Multifluid flow in bedded porous media: Laboratory experiments and numerical simulations." *Adv. in Water Resour.*, 22:169-183.

White MD and M Oostrom. 1999. *STOMP 2.0: Subsurface Transport Over Multiple Phases, Theory Guide.* PNNL-12030, Pacific Northwest National Laboratory, Richland, Washington.

Williams MD, SB Yabusaki, CR Cole, and VR Vermeul. 1994. "In situ redox manipulation field experiment: Design analysis." *Proceeding of the 33rd Hanford Symposium on Health and the Environment.* Battelle Press, Columbus, Ohio.

Williams MD, VR Vermeul, JE Szecsody, JS Fruchter, and CR Cole. 1999. *100-D Area In Situ Redox Treatability Test for Chromate-Contaminated Groundwater: FY-1998 Year-End Report.* PNNL-12153, Pacific Northwest National Laboratory, Richland, Washington.

# Distribution

**No. of Copies**

**Offsite**

2 Office of Scientific and Technical Information

Grover Chamberlain, EM-54
U.S. Department of Energy
Office of Science and Technology
Cloverleaf Building
2400 Century Blvd.
Germantown, MD 20874

Dr. Randal J. Charbeneau
Pickle Research Campus #119
University of Texas
Austin, TX 78712

Tom Engle, HAB
Department of Civil Engineering
University of Washington
Seattle, WA 98185

Dr. Joseph P. Gould
Georgia Institute of Technology
School of Civil and Environmental Engineering
790 Atlantic Drive
Atlanta, GA 30332

Barbara Harper
Yakama Indian Nation
P.O. Box 151
Toppenish, WA 98984

Stuart Harris
Confederated Tribes of the Umatilla Indian Reservation
P.O. Box 638
Pendleton, OR 97801

**No. of Copies**

Dr. Alan Moghissi
Institute for Regulatory Science
5457 Twin Knolls Road Ste 312
Columbia, MD 21045

Donna L. Powaukee
Nez Perce Tribe
ERWM Manager
P.O. Box 365
Lapwai, ID 83540-0365

Dr. Vernon C Rogers
Rogers and Associates
P.O. Box 330
Salt Lake City, UT 84110-0330

Philip Washer, DOE-SR
U.S. Department of Energy
Savannah River Operations Office
RFD #1, Bldg. 703A, Rm E208 North
P.O. Box A
Aiken, SC 29802

James A. Wright, DOE-SR
U.S. Department of Energy
Savannah River Operations Office
RFD #1, Bldg. 703A, Rm E208 North
P.O. Box A
Aiken, SC 29802

**Onsite**

7 DOE Richland Operations Office

| | |
|---|---|
| D.L. Biancosino | K8-50 |
| J.P. Hanson | K8-50 |
| R.M. Rosselli | K8-50 |

**No. of Copies**

| | | |
|---|---|---|
| | K.M. Thompson | H0-12 |
| | A.C. Tortoso | H0-12 |
| | F.R. Serier | H0-12 |
| | J.P. Neath | K8-50 |
| 5 | PHMC Team | |
| | G.C. Henckel | H0-09 |
| | M.A. Buckmaster | H0-19 |
| | J.G. April | H0-05 |
| | M.J. Graham | H0-21 |
| | V.J. Rohay | H9-02 |
| 3 | U.S. EPA | |
| | D.A. Faulk | B5-01 |
| | L.E. Gadbois | B5-01 |
| | D.R. Sherwood | B5-01 |
| 3 | Washington State Department of Ecology | |
| | D.N. Goswami | B5-18 |
| | W.W. Soper | B5-18 |
| | N.H. Uziemblo | B5-18 |
| | Washington Department of Fish and Wildlife | |
| | J.L. McConnaughey | B5-18 |

**No. of Copies**

| | | |
|---|---|---|
| 54 | Pacific Northwest National Laboratory | |
| | S.Q. Bennett | K7-90 |
| | C.L. Blair | K9-14 |
| | W.F. Bonner | K9-14 |
| | A. Chilakapati | K9-36 |
| | C.R. Cole | K9-36 |
| | J.L. Devary | K6-96 |
| | R.M. Ecker | K6-91 |
| | J.C. Evans | K6-96 |
| | M.D. Freshley | K9-36 |
| | J.S. Fruchter (10) | K6-96 |
| | D. C. Lanigan | K6-81 |
| | W.J. Martin | K9-14 |
| | M. Oostrom | K9-33 |
| | C.S. Simmons | K9-36 |
| | J.E. Szecsody | K3-61 |
| | V.R. Vermeul | K6-96 |
| | M.D. White | K9-36 |
| | T.W. Wietsma | K8-96 |
| | R.E. Wildung | P7-54 |
| | M.D. Williams (20) | K9-36 |
| | J.M. Zachara | K8-96 |
| | Information Release (5) | K1-06 |